IMPLICATIONS OF DIFFERENT NITROGEN INPUT SOURCES FOR PRIMARY PRODUCTION AND CARBON FLUX ESTIMATES IN COASTAL WATERS

A Dissertation

by

JONGSUN KIM

Submitted to the Office of Graduate and Professional Studies of
Texas A&M University
in partial fulfillment of the requirements for the degree of

DOCTOR OF PHILOSOPHY

Chair of Committee,	Piers Chapman
Committee Members,	Gilbert T Rowe
	Steven F DiMarco
	Daniel Thorton
Head of Department,	Shari Yvon-Lewis

August 2018

Major Subject: Oceanography

ABSTRACT

The coastal Gulf of Mexico (GOM) and Coastal Sea off Korea (CSK) both suffer from eutrophication and/or hypoxia, both of which are driven mainly by humans. We compared two different regions with different nitrogen input sources to estimate organic carbon fluxes and predict future carbon fluxes based on our model scenarios. This research focuses on how we take advantage of carbon-nitrogen cycling and ecological consequences to estimate the effects of future nutrient inputs.

We tested the Rowe and Chapman (RC02) three-zone hypothesis of hypoxia using two different methods. We found that RC02 applied only in certain seasons and that a major nutrient input source is necessary. We used both nutrient/salinity relationships and a N-mass balance model to identify three different zones, each with different productivity and carbon fluxes. We define the brown zone as having a linear nutrient/salinity relationship, where physical forcing (river flow) dominates over local production, and defined the blue zone as having nutrient (N or Si) concentrations < 1 μM. The green zone, with variable nutrient concentrations, occurs between them. Based on our N-mass balance model results, we could set the potential primary production rate in the brown zone of the GOM and CSK, respectively, as over 2 (GOM) and over 1.5 gC m^{-2} day^{-1} (CSK). In the green zone, production was between 0.1 to 2 (GOM) and 0.3 to 1.5 gC m^{-2} day^{-1} (CSK) and in the blue zone less than 0.1and 0.3 gC m^{-2} day^{-1}, respectively. From our results, we have estimated the fluxes of nitrogen via the atmosphere, groundwater, and river to the ocean, based on observational and literature data.

The coastal Gulf of Mexico receives nitrogen predominantly from the Mississippi and Atchafalaya Rivers and AN-D is only a minor component in this region. However, in the coastal sea off Korea, either groundwater or atmospheric nitrogen deposition is more important controlling

factors of our model results. In the future, we need to consider collecting data on both groundwater and AN-D inputs in investigations of chemical cycling in the coastal ocean.

ACKNOWLEDGEMENTS

During my time at Texas A & M University, I have learned so much, and I would like to thank my advisor Professor Piers Chapman, for his excellent assistance and guidance in my research, for all the other support in the last four and half years to finish my Ph.D. program. Mainly I would like to thank for making me think more for my research and keep standing in this academic field.

I also want to say thanks to my other committee members: Professor Gilbert Rowe, for his assistance in the model study and constructive advice in my research idea; Professor Steven DiMarco, for his memorable word (“Love your data") and helpful information during my grad school life; Professor Daniel Thorton, for his useful comments and invaluable suggestions on my research.

I also want to express my thanks to Dr. Matt Howard and Dr. Marion Stossel for their assistance in the data management. Moreover, I truly appreciate to Professor Chrissy Wiederwohl and Professor David Brooks for their advice for teaching OCNG 251 and 252 classes and thanks to having had the opportunity to get teaching experience with such a great student.

Thanks also go to my friends and colleagues and the department faculty and staff for making my time at Texas A&M University a great experience. Finally, thanks to my family for their encouragement and their patience and love.

CONTRIBUTORS AND FUNDING SOURCES

This work was supported by a dissertation committee consisting of Professor Piers Chapman (Chair), Professor Steven DiMarco, and associate Professor Daniel Thornton of the Department of Oceanography at Texas A & M University and Professor Gilbert Rowe of the Department of Marine Biology at Texas A & M University Galveston campus. All work for the dissertation was completed independently by the student.

Graduate study was supported partially by the award of a Graduate Teaching Assistantship and a Graduate Assistant Lectureship from the Department of Oceanography, and by Dr. Chapman's R-IDC account.

NOMENCLATURE

AN-D	Atmospheric Nitrogen Deposition
AR	Atchafalaya River
C	Carbon
CBWM	Cheonsu Bay Water Mass
CDOM	Colored Dissolved Organic Matter
CSK	Costal Sea off Korea
CTD	Conductivity, Temperature, Depth
DIN	Dissolved Inorganic Nitrogen
DO	Dissolved Oxygen
GBWM	Gyunggi Bay-influenced Water Mass
GOM	Gulf of Mexico
IPP	Integrated Primary Production
KRWM	Keum River-influenced Water Mass
LATEX	The Louisiana-Texas Shelf Physical Oceanography Program
LUMCON	Louisiana Universities Marine Consortium
MARS	Mississippi Atchafalaya River Systems
MCH	Mechanisms Controlling Hypoxia
MCK	Mid-western Coastal Sea off Korea
MR	Mississippi River
N	Nitrogen
NEGOM	North Eastern Gulf of Mexico
OC	Organic Carbon

P	Phosphorus
PAR	Photosynthetically Active Radiation
PP	Primary Production
PPP	Potential Primary Production
QA/QC	Quality Assurance and Quality Control
RC02	Rowe and Chapman 2002
SCK	Southern Coastal of Korea
SeaWiFs	Sea-viewing Wide Field-of-view Sensor
SGD	Submarine Groundwater Discharge
Si	Silicate
SRE	Seomjin River Estuary
T	Temperature
TN	Total Nitrogen
TAMU	Texas A & M University
USGS	United States Geological Survey
YSBCWM	Yellow Sea Bottom Cold Water Mass

TABLE OF CONTENTS

LIST OF FIGURES

LIST OF TABLES

CHAPTER I

INTRODUCTION

1.1 Background

Nutrient concentrations and their distribution in the ocean are important tracers of chemical cycling (Nixon, 1981). The cycling of nutrients, such as Nitrogen (N), Phosphorus (P), and Silicate (Si) in the ocean is a very important contributor to marine ecology (Tyrrell, 1999), as these elements are essential requirements for primary production (PP). Redfield (1934) found that the N to P ratio, which is approximately 16:1 in the ocean, decreased during phytoplankton growth. Similarly, Redfield et al., (1963) reported the classical C: N: P ratio of phytoplankton in the ocean, which is 106:16:1. This molar ratio is roughly constant in the deep ocean. However, in the coastal ocean, the concentrations of nutrients are not as consistent as Redfield theory suggests, varying with depth, distance from the shore, and seasonal conditions (Anderson and Sarmiento, 1994).

Nutrient data often predict physical properties such as mixing in the ocean. Previous studies mentioned that the nutrient/salinity ratio is a useful tool for identifying different water masses (Desmit et al., 2015; Duxbury and McGary, 1965; Hakanson and Eklund, 2010; Iwata et al., 2005; Ruddick and Lacroix, 2006). Theoretically, in the coastal ocean, nutrient concentrations should show an inverse relationship with salinity, as the main sources of nutrients are terrestrial. Duxbury and McGary (1965), for example used the nutrient/salinity ratio as a tracer to reflect the contributions of river runoff, deeper upwelled water, and their time-dependent variability near the Columbia River.

The Texas-Louisiana (LATEX) shelf in the northern Gulf of Mexico (GOM) has been

affected by coastal nutrient loading coming from two major terrestrial input sources (the Mississippi and Atchafalaya River System (MARS), which have different nutrient concentrations) leading to hypoxia. To investigate the relationship between nutrients and the marine ecosystem, and how this leads to hypoxia in the GOM, several projects have been conducted (e.g. Bianchi et al., 2010; Diaz and Rosenberg, 1995, 2008; DiMarco et al., 2010; Hetland and DiMarco, 2008; Laurent et al., 2012; Quigg et al., 2011; Rabalais et al., 1995, 2007; Rabalais and Turner 2001; Rowe and Chapman 2002).

Like the coastal GOM, the coastal sea off western Korea (CSK) is also a semi-enclosed basin and is affected by freshwater discharge from river plumes. Differences include having a strong tidal front and an increased nitrogen input source from atmospheric nitrogen deposition (AN-D) (Chen et al., 2011; Liu et al., 2003; Liu et al., 2016; Zhao et al., 2015) and groundwater (Kim et al., 2010). AN-D has increased in the CSK owing to industrial development in China during the last few decades, which has led to increased N-emission, and this contributes to ocean production (He et al., 2010; Kanakidou et al., 2016; Kim et al., 2011; Lawrence et al., 2000; Paerl et al., 2002). Several studies have also suggested that AN-D will become an important controlling factor in future in the GOM (e.g., Duce et al., 2008; Lawrence et al., 2000; Paerl et al., 2002).

1.2. Previous model studies related to hypoxia in the Gulf of Mexico (GOM)

The long-term average size of the hypoxic area, which occurs when dissolved oxygen (DO) concentrations are less than 2 mg/L (1.4mL/L; 62.5 μM) during mid-summer in the northern Gulf of Mexico (GOM), has increased since the mid-1980s (Rabalais et al., 2002; Bianchi et al., 2010). Every summer since 1985, apart from three years, the National Oceanic and Atmospheric Administration (NOAA) has monitored the hypoxia area (Figure 1). As can be seen from Figure

1 while there is considerable variability from year to year, the latest five-year mean is approximately double the long-term mean.

In the coastal GOM, with terrigenous nitrogen inputs mainly coming from fertilizer usage, sewage, and animal feed lots, the increasing primary production rate leads to increased carbon fluxes and respiration rates during decomposition. This causes hypoxia owing to the consumption of oxygen during respiration (Bauer et al., 2013; Justic et al., 2007; Zhang et al., 2013). NOAA has suggested that the use of fertilizers be cut drastically to reduce the hypoxia (Hypoxia Action Goal Plan Report, 2005, 2008). However, nutrient reduction in the watershed is still voluntary and hypoxia in the GOM is still occurring.

To examine the several biological and physical drivers of hypoxia in the GOM, several model studies have been conducted during last few decades. Various predictive models have shown that high primary production is caused by nutrient loading from the rivers, while biological and physical processes are also critical factors for hypoxia occurring in the coastal GOM region (Table. 1).

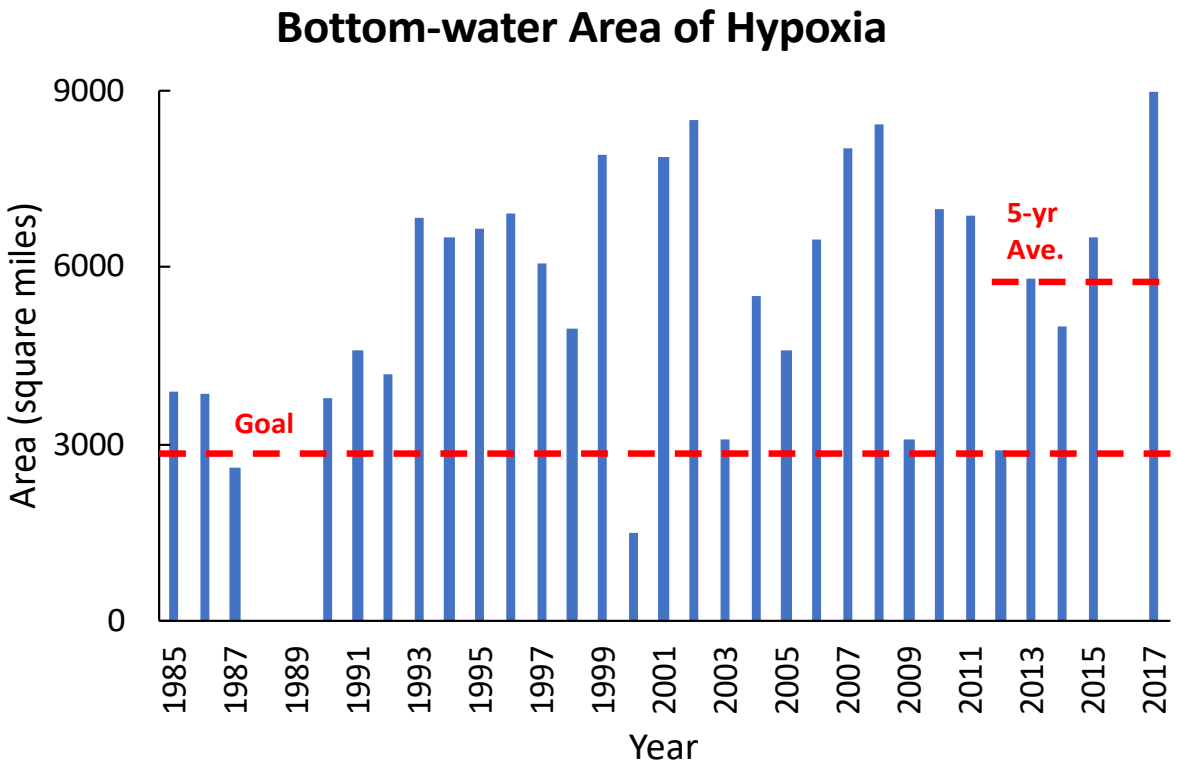

Figure 1. The chart shows the size of the hypoxia area, with less than 2 mg/L of oxygen, from 1985 to 2017 (Replotted from NOAA website data).

Table 1. Model comparison between this study and previous studies in the GOM.

Model / Class	Data collection	Key features	References
Biological Water Quality model	Only covers C6 station (Vertical data) (Justic et al., 2002)	• Vertical transport >> horizontal transport (Justic et al., 2002) • Westward advective flow (Scavia et al., 2004) • Estimated carbon flux and oxygen exchange between two regions (Bierman et al., 1994)	Bierman et al., 1994 Justic et al., 1996, 2002, 2003 Scavia et al., 2004
Physical Hydrodynamic (numerical) model	Based on observational oxygen data (respiration parameterizations)	• Examining simple parameterizations of respiration below the pycnocline • Excludes respiration rate from local primary production	Hetland & DiMarco 2008
Coupled (Physical + Biological) Simulation model	N cycling (Only used C6 station-vertical) + physical model (Hetland & DiMarco 2008)	• Revised version of the plankton model (Fasham et al., 1990) in ROMS and expanded to include oxygen as an additional component	Fennel et al., 2011, 2013
Coupled (Biological + Chemical) **N-mass balance model**	**Context of observational nutrient data**	• **Considers AN-D input source and calculates carbon fluxes using stoichiometry based on CNP ratio**	**This study**

Previous biological models focused on the mechanism of hypoxia in the GOM based on complex biological processes rather than the physical processes, and they only considered riverine N sources to predict hypoxia (Bierman et al., 1994; Justic et al., 1996, 2002, 2003; Scavia et al., 2004). Bierman et al. (1994) estimated carbon flux and DO concentration changes in the Louisiana inner-shelf regions, with wind stress as the only physical factor in their oxygen mass balance model. They did not consider other physical drivers such as tidal mixing, stratification or advection in their model because they assumed oxygen changes were mainly caused as a result of biological factors such as respiration and photosynthesis. Justic et al. (2002) developed a two-layer box model, which emphasized vertical transport rather than horizontal transport, to simulate oxygen and carbon budgets for understanding eutrophication processes. The model divided the box into two layers based on the pycnocline (above and below the pycnocline), and their results still showed that terrigenous nitrogen inputs from the Mississippi were the main cause of hypoxia in the GOM. However, it is difficult to explain the hypoxia in the whole GOM region with their model results because they only used one station (C6; LUMCON). Scavia et al. (2003) calculated the hypoxic area using a physical-biological model that considered the oxygen balance as being driven by the total terrigenous nitrogen load (May and June data) from the rivers. Their model only reflected one-dimensional horizontal dynamics along the shelf and the model would be regarded as a probabilistic hindcast model as it had to be tuned each year.

However, several studies have pointed out that other sources are likely to increase primary production in the coastal region, for example, benthic diffusion or coastal upwelling (Hetland and DiMarco, 2008; Rowe et al., 2002). Hetland and DiMarco (2008) produced a complex, more realistic hydrodynamic model coupled with several simple oxygen respiration models to separate the effects of stratification and circulation on the formation and maintenance of the hypoxic zone

on the Texas-Louisiana Shelf. Recent models from Fennel et al. (2011, 2013) used nitrogen components and oxygen biogeochemistry, and they considered the complex biological and physical processes involved in predicting and controlling hypoxia. As a result of the model studies in the GOM, we now know that large-scale hypoxia is caused by a complex interaction of biological processes, eutrophication, and physical processes including stratification, winds, and currents (Hetland and DiMarco, 2008; Bianchi et al., 2010; Forrest et al., 2011; Feng, 2012; Jorge et al., 2014). Feng (2012) considers wind as a factor to estimate the temporal and spatial variability of the hypoxic area. She used both statistical and numerical models to examine the influence of those factors on the hypoxic area in the northern GOM. Her model over predicted the size of the hypoxia area by 23% compared to observations, while the previous models from Scavia et al. (2003) and Turner et al. (2006) showed that their simulations of hypoxic area were 140 ~ 210% larger than the observed area.

1.3. Rowe and Chapman 2002 model

A paper by Rowe and Chapman (2002), here after called 'RC02', defined three theoretically different zones over the Texas-Louisiana shelf close to the Mississippi and Atchafalaya River mouths to predict the effects of nutrient loading on hypoxia along the river plume and over the shelf. They named these the brown, green, and blue zones (three zone hypothesis). Nearest the river mouths they set the 'brown' zone, where the nutrient concentrations are high, but the discharge of sediment from the river reduces light penetration and limits primary productivity within the plume. Further away from the river plume, they set a 'green' zone with available light and nutrients, and high productivity. In this region, the rapid depletion of nutrients is due to biological uptake processes that depend on the season and river flow (Bode and Dortch,

1996; Dortch and Whitledge, 1992; Lohrenz et al., 1999; Turner and Rabalais, 1994). Still further offshore, and also along the river plume to the west, there is the so-called 'blue' zone, which is dominated by intense seasonal stratification and a strong pycnocline, so that in the surface layer nutrients are limiting at this distance from the rivers and most primary production is fueled by recycled nutrients (Dortch and Whitledge, 1992). Their model suggests that the edges of the zones (geographical regimes) change over time depending on river flow, biological processes, and productivity (Figure 2). The important concept of the RC02 model is that they consider nutrient concentration is fully supported by river input and that passing from the brown zone to the green zone will reduce nutrient concentration as a result of dilution and biological uptake. There are low nutrient concentrations in the blue zone, likely leading to nitrate limitation. It is important to note that the three zones hypothesis of RC02 was theoretical and that the model only considered the layer above the pycnocline. A new paradigm incorporating the sub-pycnocline layer is shown in Figure 3.

While, RC02 is a theoretical model that describes how the coastal GOM region is affected by river plume, it has not been tested using real nutrient data to determine the truth of the three zone hypothesis. This suggests that more research is needed to examine the complicated biological processes in the coastal GOM most affected by the two rivers (the brown and green zones). Sylvan et al. (2006) suggested that the coastal GOM, especially near the Mississippi River delta mouth, is phosphorous-limited for phytoplankton growth at certain times, rather than being nitrogen-limited, which is the more normal condition in the ocean. Moreover, several studies elsewhere [the UK, Czech Republic, Tahiti, NE Atlantic, and Colorado front range (Baron et al., 2000; Cornell et al.,

1995; Doney et al., 2007)] show that increasing atmospheric nitrogen deposition (AN-D) has affected environmental phenomena in the ocean such as eutrophication, changing the limiting factor from N to P, and led to observed biological production changes. However, all previous model studies for the GOM have reflected only riverine N as the predominant input source, and no one considered AN-D as an input source to this region.

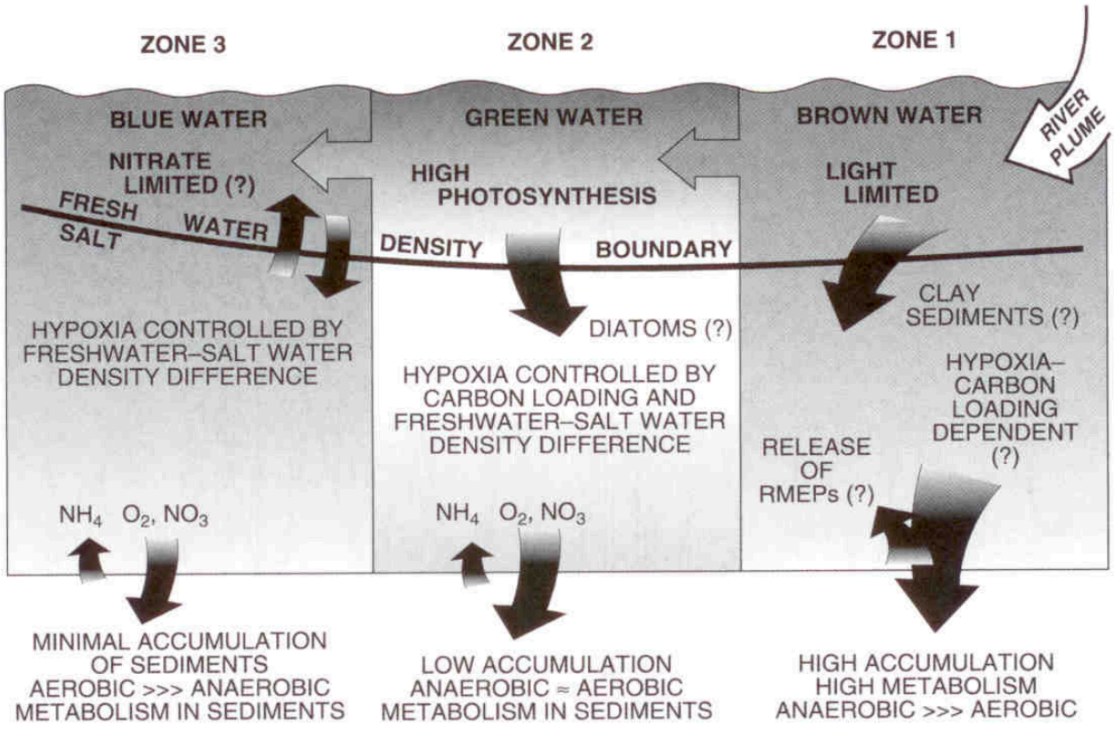

Figure 2. The Rowe and Chapman three zone hypothesis, which described the physical and biochemical processes that initiate and sustain hypoxia on the Texas-Louisiana Shelf, [Rowe and Chapman, 2002]. *Reprinted with permission of Gulf of Mexico Science.*

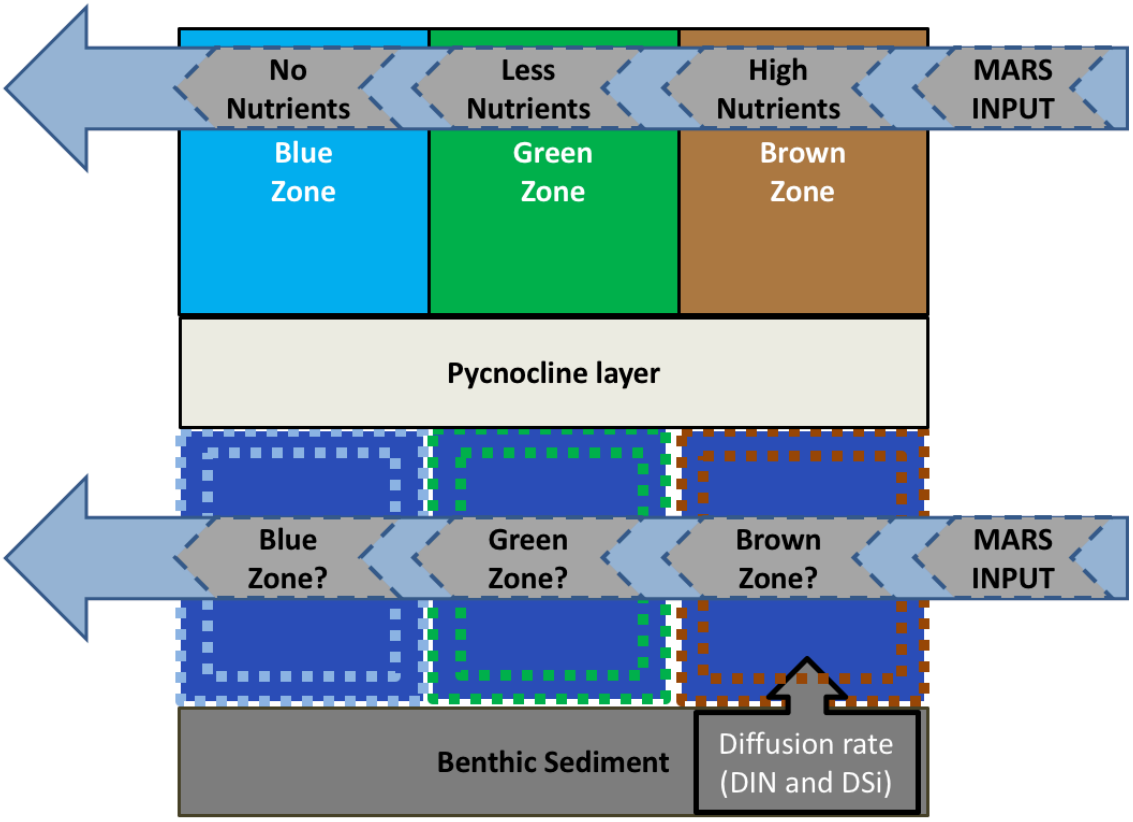

Figure 3. Concepts of RC02 three zone hypothesis in a two-layer model above and below the pycnocline layer. It is uncertain how changes in the edges of each zone are related above and below the pycnocline. Blue arrows show the water flow through the system.

1.4. Background studies in the Coastal Sea off Korea (CSK)

The Coastal Sea off western Korea (CSK) shows several similar characteristics with the GOM. The CSK is also a semi-enclosed basin and affected by a freshwater discharge from a river plume like the coastal GOM (Liu et al., 2003), although this is much smaller than the discharge from the MARS (the average discharge in the Keum river is 2,000 m^3/s, while that in the MARS is 20,000 m^3/s) In the past few decades, the CSK in the Yellow Sea has also been affected by eutrophication caused by coastal nutrient loading coming from local rivers, e.g., in the Keum estuary, but this is generally very localized (Figure 4). Also, there are small scale outbreaks of hypoxia during the summer in coastal areas such as Cheonsu bay, close to the Keum River mouth (Lee et al., 2018).

There are four different water masses such as Gyunggi Bay-influenced Water Mass (GBWM), Keum River-influenced Water Mass (KRWM), Yellow Sea Bottom Cold Water Mass (YSBCWM) and Cheonsu Bay Water Mass (CBWM) (Figures 4 and 42) (Lim et al., 2008). Several studies have been conducted to investigate the solution to eutrophication in this region (e.g. Bashkin et al., 2002; Lim et al., 2008). However, this region is much more complicated than the GOM because of the strong tidal regime, and the input of Asian dust, largely from China, and a different nitrogen input source, AN-D, which can cause biogeochemical changes in the ocean (Bashkin et al., 2002; Chen et al., 2011; Lim et al., 2008; Liu et al., 2003, 2017; Tan et al., 2017; Yeo and Kim, 2002; Zhao et al., 2015).

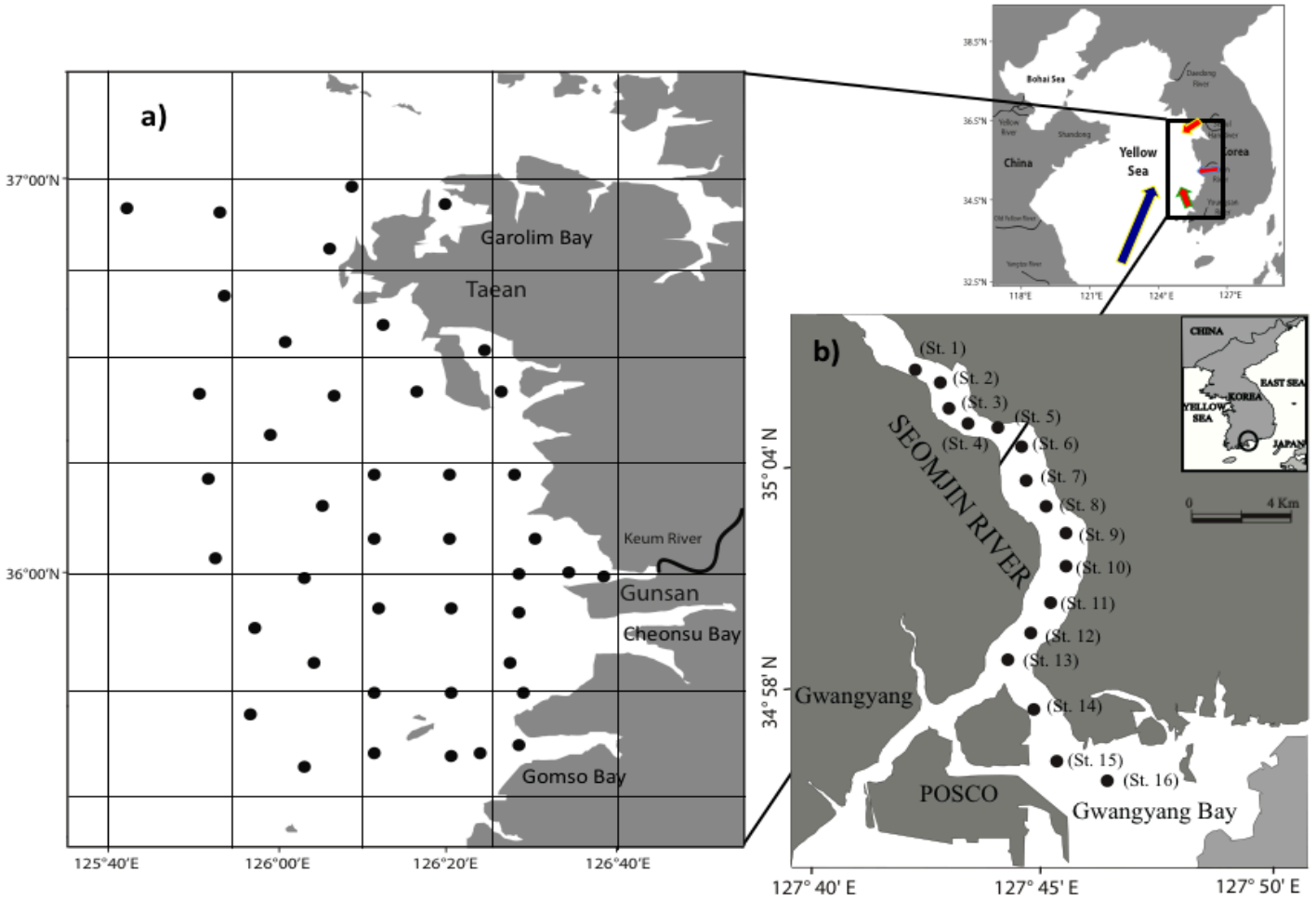

Figure 4. Study sites and sampling area off the Korean coast. Figure (a) shows all of the sampling areas within the Mid-western Coastal Sea off Korea (MCK), which is mostly affected by Keum River inputs and Figure (b) shows only the region likely affected by the Seomjin River Estuary (SRE).

1.5. Another nitrogen input source: Atmospheric Nitrogen Deposition (AN-D)

Increasing Atmospheric Nitrogen Deposition (AN-D) has affected environmental phenomena in the ocean such as eutrophication, changing the limiting factor (N-limited to P-limited), and biological production (Cornell et al., 1995; Doney et al., 2007). Global ammonia (NH_3) emissions have been increasing since 1970, and the anthropogenic NOx emissions from Asia have increased enormously, although such emissions in the US appear to be stable or even decreasing (Akimoto, 2003; Behera et al., 2013; IPCC Report, 2014) (Figure 5). Therefore, AN-D into the coastal ocean will likely increase, and this will be an additional N input source into the water column (Duce et al., 2008; He et al., 2010; Kanakidou et al., 2016; Kim et al., 2011; Lawrence et al., 2000; Paerl et al., 2002).

Although previous studies argued that AN-D would be negligible in the GOM because it only supplied less than 3% of total N input (Goolsby et al., 1999; Turner and Rabalais.1994), there are several studies of AN-D that show it makes a much greater contribution to the total N load to the ocean than previously thought, thus affecting production in the coastal zone (Alexander et al., 2000; Boynton et al., 1995; Fisher 1991; Jaworski et al., 1997). The question of whether AN-D is becoming a major factor for coastal production or remains a negligible one is still undetermined; this factor, however, cannot be ignored in the future because global AN-D has increased enormously, particularly from anthropogenic activities in Asia, and any reduction in riverine input of nitrogen will make the AN-D more important.

On the coast near Corpus Christi, TX, total AN-D (NH_4^+ and NO_3^-) has been increasing since 1997 from 9.95 kg N/ha-year to 11.50 kg N/ha-year (Wade and Sweet, 2008). However, measured AN-D amounts entering into the Chinese regional seas through 2008 to 2010 were 11.9 kg N/ha-month (equivalent to 142.8 kg N/ha-year) in the Yellow Sea and 5.6 kg N/ha-month

(equivalent to 67.2 kg N/ha-year) in the South China Sea (Luo et al., 2014; Zhao et al., 2015). The Yellow Sea and the South China Sea suffer from eutrophication, particularly along the Chinese coast, leading to hypoxia through AN-D input and riverine N input (Luo et al., 2014; Wang et al., 2016). This indicates that the new nitrogen input through AN-D can likely change the primary production rate and affect organic carbon fluxes leading to increases in both hypoxia area and severity in the future (Figure 6).

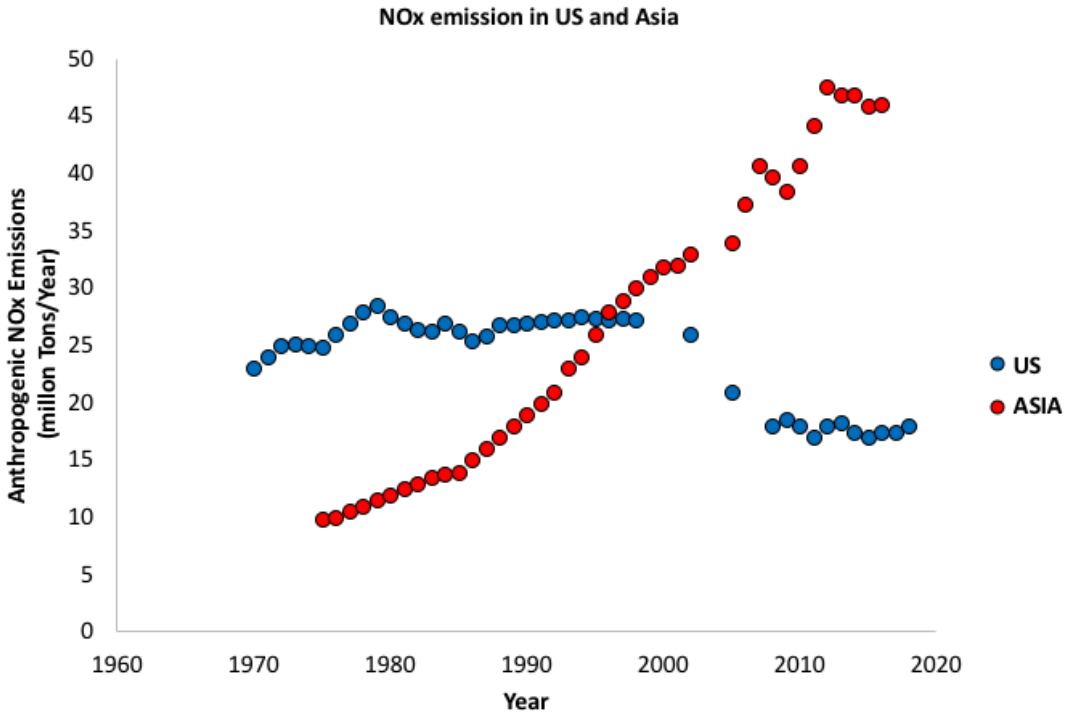

Figure 5. NOx emissions within the US and Asia. In Asia, NOx emission has increased rapidly since 1975 due to increases in industry and power plants. However, NOx emissions in the US have decreased since 2000 owing to economic and environmental policy controls. Data prior to 2000 are taken from Akimoto (2003); later data are from IPCC (2014) and EPA (https://www.epa.gov/air-emissions-inventories/air-emissions-sources)

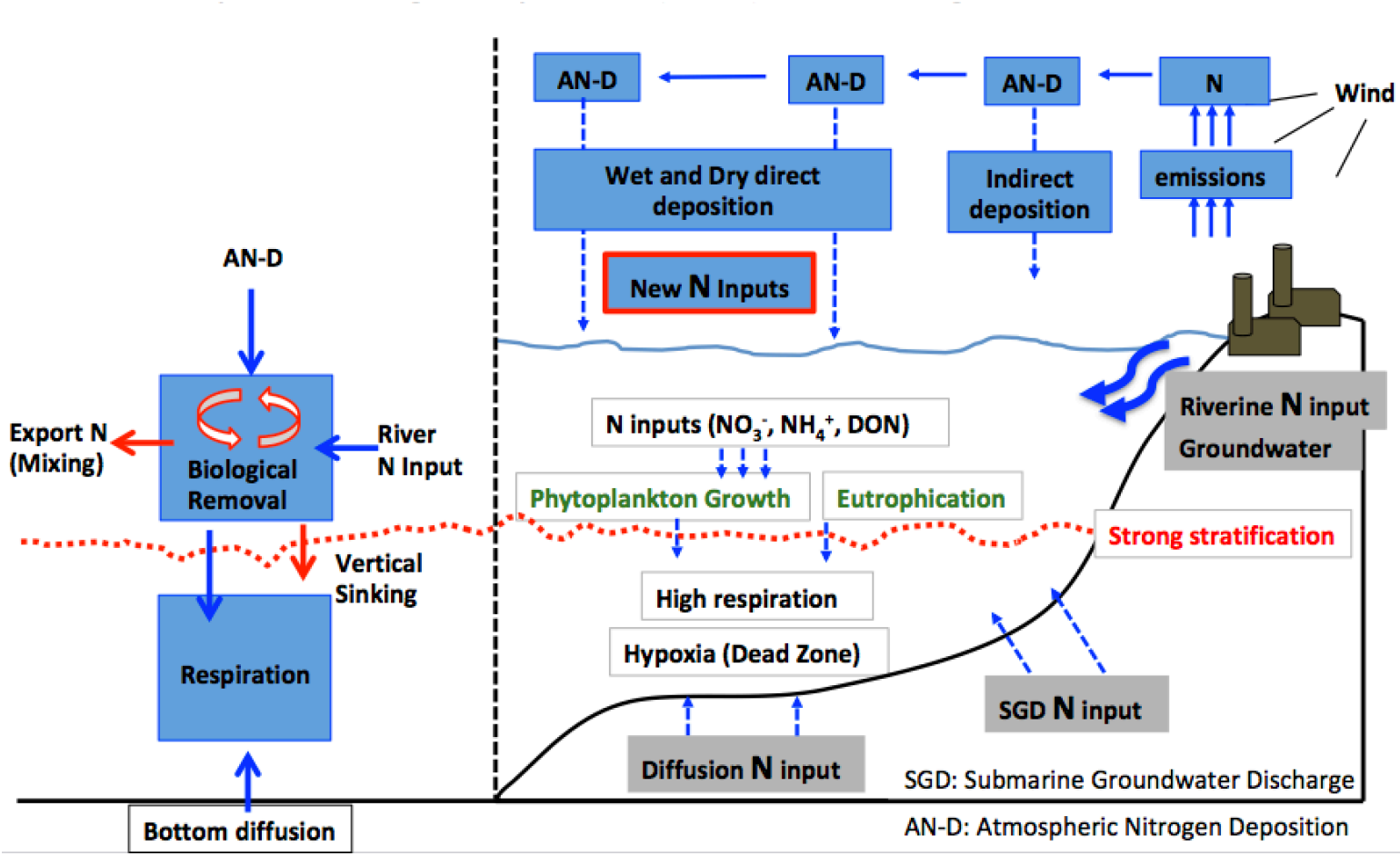

Figure 6. The concept of AN-D and mass balance budget with box model

1.6. Objectives and hypotheses

The objective of this study is to use changes in water chemistry to (a) investigate the relationship between nitrogen inputs and the biological processes in the coastal GOM, (b) produce a N-mass balance model of the region to determine the nutrient mass balance budget from two different water masses off the Texas-Louisiana Shelf, (c) calculate potential primary production rates, organic carbon fluxes, and oxygen demand rates by biological production through the N-mass balance model, and (d) compare biological production in the GOM and the CSK based on different nitrogen input sources such as AN-D. In addition, the main idea of this study is to use the data to check the RC02 three zone hypothesis, define how the boundaries between the three zones vary over time, and apply the methodology of the N-mass balance model to another region such as the CSK. To achieve the objectives, their related hypotheses are outlined below.

Hypothesis 1. (H1): The RC02 hypothesis is a good description of nutrient supply to coastal waters.

1-1) we can use nutrient concentrations to define the edges of zones in the GOM and CSK.

1-2) we can identify the variability between cruises

1-3) we can use Korean data to see if RC02 applies elsewhere

1-4) we can expand RC02 to include the layer below the pycnocline

Hypothesis 2. (H2): The Mississippi and Atchafalaya rivers have different nutrient concentrations that can be used to show which river supports production on different areas of the shelf.

2-1) we can use nutrient-salinity plots

2-2) we can estimate potential production, carbon fluxes, and oxygen demand from a box model and compare the model output with data (based on ^{14}C and O_2 estimates)

Hypothesis 3. (H3): **Changes in the ratios of the AN-D and riverine N flux will affect carbon cycling in coastal waters**

3-1) we can do comparative studies using the model with different inputs in the GOM and Korea.

1.7. Dissertation overview

This dissertation is organized into five chapters.

The background, research objectives, and hypothesis of this study are presented in Chapter I. The historical observation data used in this study are provided in Chapter II. In Chapter III, the methodology of using nutrient/salinity relationships as a means of identifying coastal regions is discussed. The research results demonstrate Hypothesis 1) related to Objective (a) based on using nutrient/salinity relationships. In Chapter IV, the N-mass balance model and how nitrogen fluxes affect productivity in the GOM and the CSK are presented. The research results address Hypotheses 2) and 3) related to Objectives (b) to (d) through a new N-mass balance model. Chapter V summarizes the main conclusions of this study and provides suggestions for future research.

This research is the first time that the RC02 hypothesis has been examined using nutrient/salinity relationships, while the N-mass balance budget will be used with a stoichiometry model (C: N: O ratio) to calculate potential biological production and organic carbon fluxes based on the nutrient data. This work looks at the variability of the organic carbon fluxes and oxygen

demand in the brown and green zones as described by the RC02 hypothesis. Moreover, our model results may be applied to nitrogen management strategies related to coastal production generally because we can predict the effects of multiple N input sources and fluxes more specifically (Hameedi et al., 2007; Rabalais et al., 2007), and the model has been extended to another coastal hypoxic region.

CHAPTER II

HISTORICAL OBSERVATION DATA

2.1 Gulf of Mexico data: MCH, LATEX, LUMCON and NEGOM

The Gulf of Mexico (GOM) is a semi-enclosed sea that connects in the east to the Atlantic Ocean through the Florida Straits, and in the south to the Caribbean Sea through the Yucatan Channel. Over the last few decades, many researchers have defined the Mississippi and Atchafalaya River Systems (MARS) as the major pathway of nutrient and freshwater discharge to the northern Gulf of Mexico (Alexander et al., 2008; Rabalais et al., 2002; Robertson and Saad, 2014) (Figure 7). The MARS drains 41% of the contiguous United States (Milliman and Meade, 1983). Overall, there are more than 20 major river systems around the Gulf of Mexico and the MARS discharges approximately 64% of the total to the northern side of GOM, which amounts to about 10.6×10^{11} m^3 per year (= 3.4×10^4 m^3 per second). The remaining 36% comes from other U.S. rivers or from Mexico and Cuba (Nipper et al., 2004).

At the Old River Control Structure on the lower Mississippi River approximately 25% of the Mississippi River's water is diverted into the Atchafalaya River and the remaining 75% stays in the Mississippi River. The 25% of the water from the Mississippi river combined with the Red river makes up the flow to the Atchafalaya River (Figures 7a and 8). It should be noted that, the Red River contains lower nutrient concentration than the Mississippi River.

Hydrographic data from four projects - LATEX (The Louisiana-Texas Shelf Physical Oceanography Program), MCH (Mechanisms Controlling Hypoxia), NEGOM (North Eastern Gulf of Mexico) and monthly data from LUMCON (Louisiana Universities Marine Consortium) were collected from the National Oceanographic Data Center (https://www.nodc.noaa.gov)

covering the period from 1991 through 2014 (Table 2) and quality controlled (QC) to remove inconsistencies and anomalies in the data (e.g. removing outliers, missing data interpolation). First of all, the data were separated into summer (May ~ July) and winter (November ~ March) periods to look at the seasonal variation. During summer, there is high precipitation, snowmelt, and river runoff to bring lots of nutrients to the GOM. Owing to these nutrients, high biological uptake occurs during phytoplankton growth, so, it is hard to see the pattern against salinity changes. Second, all of the nutrient data sets were plotted against salinity to see if there were any consistent relationships, this was also done year-by-year and cruise-by-cruise. The study sites and sampling areas are shown on the map (Figure 7). Stations shown in Figure 7a and b are from LATEX (Green dots, February 1993), LUMCON (Blue dots, 1998 - 2010), MCH (Red dots, March 2005), and NEGOM (Orange dots, November 1997 - 1999). LUMCON data were the only data set collected seasonally on a consistent basis (Figure 7a, b and Table 2), and there were few winter cruises in any program.

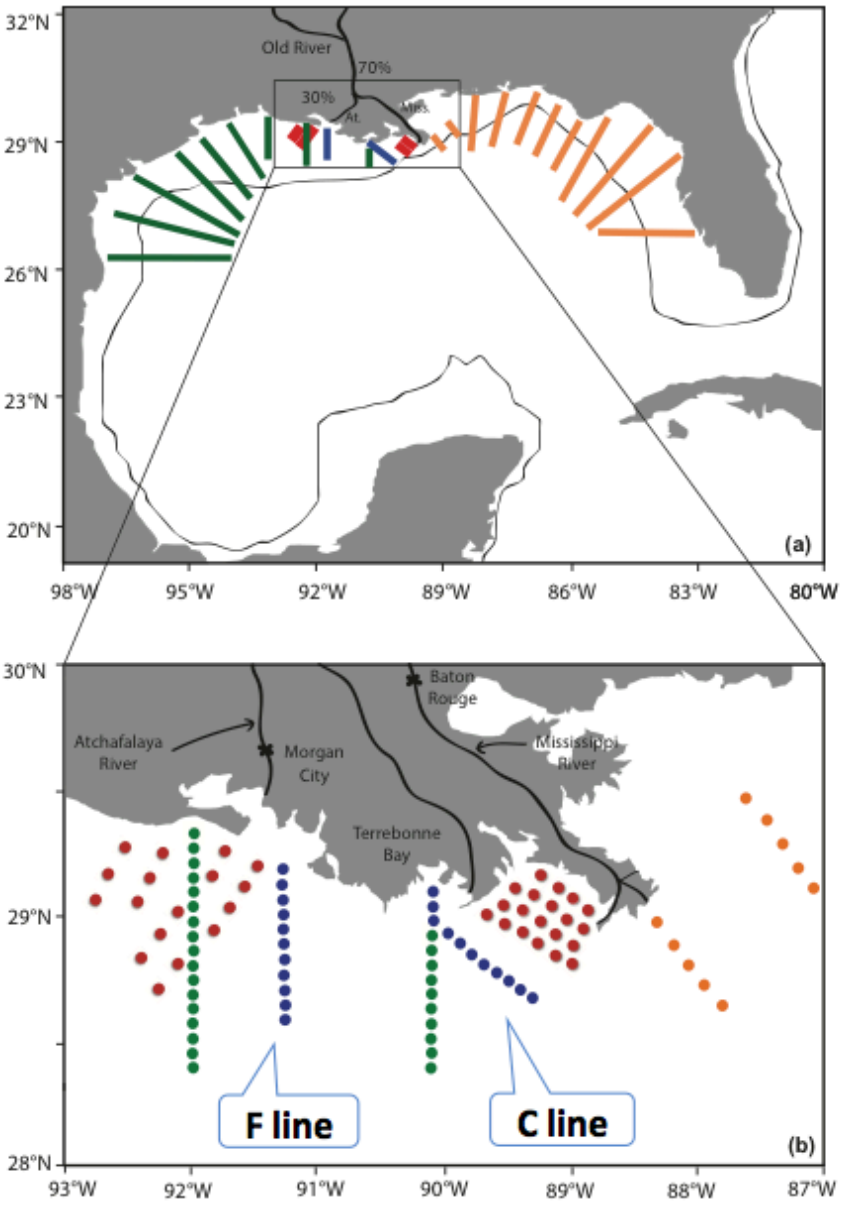

Figure 7. Study sites and sampling area. Figure (a) shows all of the sampling areas during winter within the northern GOM, which includes the LATEX and NEGOM non-point source sampling grid. Figure (b) shows only the region likely affected by MARS inputs. The, C lines are near the Mississippi River boundary (90°W to 89°W) and the F line is near the Atchafalaya River boundary (93°W to 91°W), respectively. MCH data are widely distributed across the region; these station positions are from March 2005. The symbols and color information are in Table 2. Additional stations off the Terrebonne Bay are not shown as they were not used in the initial analysis.

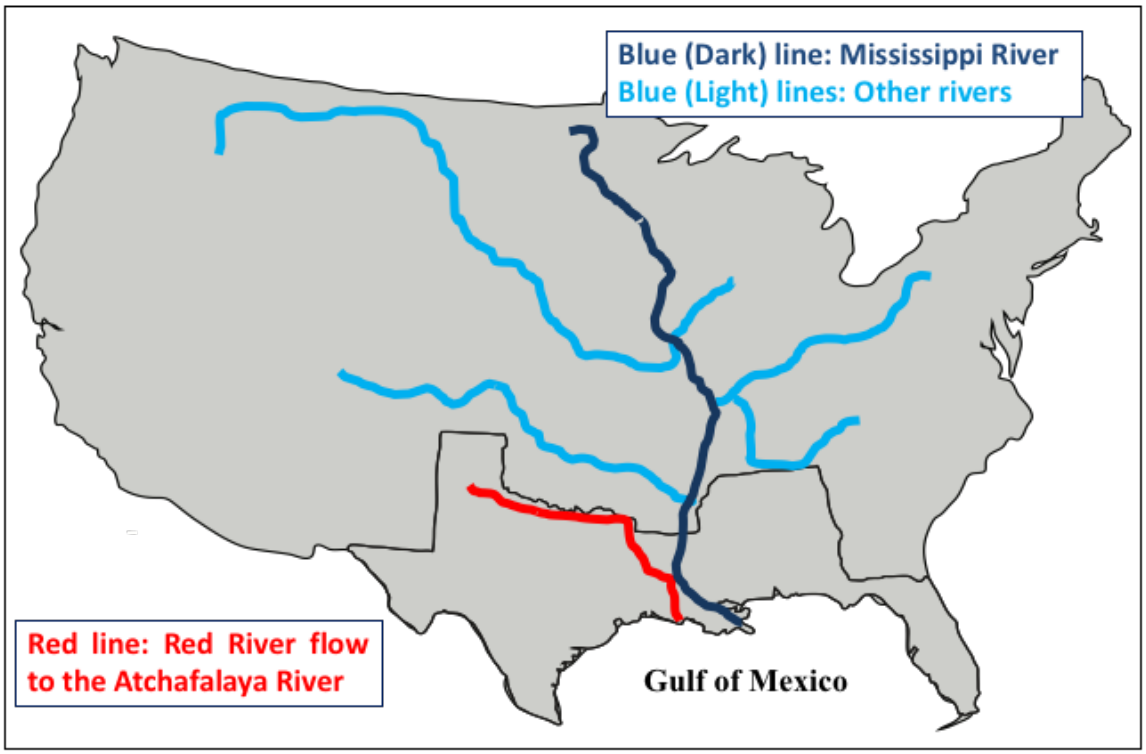

Figure 8. Mississippi and Atchafalaya rivers drainage basin map. Blue light lines indicate all other rivers in the US. Dark blue line indicates the Mississippi River flow and red line represent red river flow to the Atchafalaya River.

Table 2. Sampling dates, location, and projects list in the GOM. Summer data are excluded in each project period and only winter period data are given. Parameters examined were Temperature (T), Salinity (S), DIN, DIP, and DSi. All research cruises sampled near the Mississippi and Atchafalaya Rivers (Figure 7a, b). The C transect was occupied approximately monthly by LUMCON while sampling along the F transect was less frequent. LUMCON data were the only data set collected seasonally on a consistent basis, and there was only one winter cruise for both LATEX and MCH programs. In addition, NEGOM winter data were collected over a three-year period.

Project Name	**LATEX**	**LUMCON**	**MCH**	**NEGOM**
Project Period	1991 - 1994	1998 - 2010	2003 - 2014	1998 - 2000
Filtering winter period	Feb-93	1998-2010	Mar-05	Nov-97, 98, 99
Symbol of the maps	Green dot	Blue dot	Red dot	Orange dot
Sampling Location	From 89°W to 94°W, 28°N to 30°N			From 82°W to 90°W, 28°N to 30°N

2.2 24-hour continuous observation data from LATEX shelf

24-hour continuous data were collected from the anchored Conductivity-Temperature-Depth (CTD) stations from the MCH cruises within the LATEX hypoxia region. Dissolved oxygen data were sampled every 30 ~ 60 minute from dusk to dawn, and these can provide estimates of net and gross primary production and respiration. The data were from MCH projects only and the anchor stations are located near the Atchafalaya River, at (29°N, 92°W) which is close to the F line and the Mississippi River, at (29°N, 89.5°W) which is close to the C line, respectively (Figure 7).

2.3 Data from the Coastal Sea off Korea (CSK)

The study area in the coastal sea off Korea (CSK) covers Mid-western Coastal Sea off Korea (MCK) and Southern Coastal of Korea (SCK). Our specific study area was limited to two regions; 1) the MCK from the Taean Peninsula to Gomso Bay and 2) the Seomjin River Estuary (SRE) near the SCK (Figure 4). The MCK is located along the eastern side of the Yellow Sea, which lies between China and Korea (Figure 4a). The Yellow Sea covers about 380,000 km^2 area with a 44m average water depth, and numerous islands are located on its eastern side (Liu et al., 2003).

The SRE flows into the SCK via Gyeongsangnam-do and Jeollanam-do (Kim et al., 2010) (Figure 4b). The length of SRE is nearly 303 km, and the drainage basin is about 4900 km^2 (Park et al., 2012). The annual mean flow rate within the SRE and precipitation within the catchment were about 86.16 $m^3 s^{-1}$ and 1,711 mm in 2006 (Park et al., 2012). The SCK is mainly affected by the SRE and freshwater discharge of the river plume, containing pollutants and nutrients from the

nearby industries. Owing to the SRE plume, huge amounts of nutrients have discharged into the ocean annually.

The MCK shows various environmental characteristics. There is a strong tidal front in the coastal area near the Taean Peninsula due to sea floor topography and the coastal configuration (Park, 2017; Park et al., 2017). Additionally, the MCK is affected by several bays (Garolim Bay and Cheonsu Bay), a big artificial lake (Saemangeum lake), the Keum river estuary, and a freshwater discharge from the Keum river plume that contains high concentrations of nutrients (Lim et al., 2008). The annual mean flow rate within the Keum River and precipitation within the catchment were about 70 m^3 s^{-1} (normal period), 170 m^3 s^{-1} (flood period) and 1,208.1 mm per year during 2003 to 2005 (Yang and Ahn 2008). The CSK hydrographic data (nutrient, salinity, oxygen) were collected during several research projects in the MCK and the SRE (Table 3 and Figure 4), and the data put through QA/QC routines to remove inconsistencies and anomalies in the data based on e.g. removing outliers or missing data interpolation.

Table 3. Sampling dates, location, and projects list in the CSK. Parameters examined were Temperature (T), Salinity (S), Dissolved Oxygen (DO), DIN, DIP, and DSi.

Project location	Coastal Sea off Korea (CSK)	
	Mid-western Coastal Sea off Korea (MCK)	**Southern Coastal of Korea (SCK)**
Study area	Keum River	Seomjin River Estuary (SRE)
Sampling period	2003-2005	2006-2009
Project reference	Lim et al., 2008	Kim et al., 2010

2.4 End-member concentrations

Cattaldo et al. (2006) used multiple end-member values to examine a mixing model in the Southern Ocean and explained how the end-members produced conservative or non-conservative mixing behavior. To determine nutrient concentrations in the GOM freshwater end-members, data were obtained from the USGS for stations at Baton Rouge on the Mississippi River and Morgan City on the Atchafalaya River. We estimated the variability of the freshwater end-member from nutrient concentrations in the river water. The concentration of nitrate + nitrite (NO_{2+3}) at Baton Rouge from 1992 through October 2016 varied between 50 ~ 200 μM, being generally lower in winter than in spring due to the timing of ice melt from the US continent. We set the spring period as March to May, summer as May to August, fall as September to October, and winter as November to February based on previous projects' definition (Lim et al., 2008). In Figure 9, we show the flow and inorganic N data from February 18th 2015 through October 22nd 2016 to compare end-member data from the two rivers for the only period when the data overlap. The two rivers generally showed similar changes, although the concentrations were very different in each year. Most of the measured freshwater nitrate + nitrite data were between 10 ~ 200 μM, with highest values around 175 ~ 200 μM and lowest values around 10 ~ 20 μM. Lowest values are from the Atchafalaya River, while the Mississippi River values are higher than Atchafalaya River because the Mississippi River has higher nutrient concentrations than the Red River.

MCK end-member data were from literature papers (Lee and Yang, 1997; Lim et 2008; Yang and Ahn, 2008). The range of measured freshwater nitrate + nitrite concentrations were very similar to the GOM, with highest values again around 170 ~ 200 μM and lowest values again around 10 ~ 20 μM. In the coastal waters near the Keum River mouth the concentrations change based on seasons and precipitation, varying typically between 10 ~ 70 μM, and decreasing

offshore. Generally, nutrient concentrations are inversely related to the salinity, and increase with increasing freshwater discharge during the rainy season, as shown from 500 days of continuous observation data (Lee and Yang, 1997). These patterns are similar to GOM end-member data and show more clear peaks in concentration during the rainy season (July to September) due to the high precipitation in the MCK.

We make the initial assumption that changes in nutrient concentration between the freshwater end-member and coastal seawater are conservative and that concentrations will decrease consistently as salinity increases. We have used only NO_2+NO_3+NH_4 (DIN) and Si (DSi) data in our calculations. The estimated average annual values of the freshwater end-members are 70 μM ~ 100 μM (DIN) and 80 μM ~ 120 μM (DSi), respectively. More details about DIN end-member range, standard deviation, median, and average are given in Table 4.

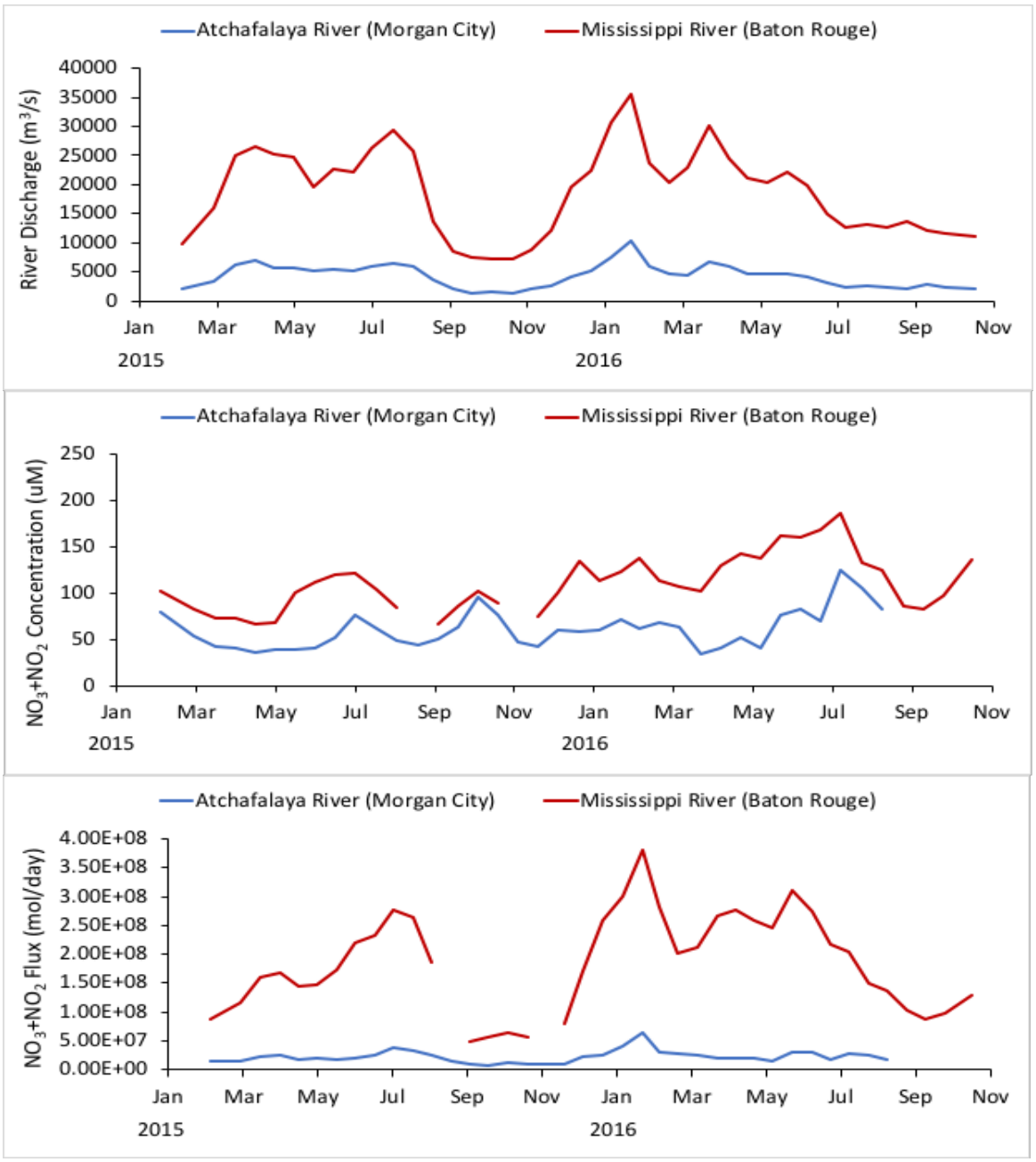

Figure 9. DIN fluxes from the Atchafalaya River at Morgan City and the Mississippi River at Baton Rouge (data are from USGS). We cut off from the data (February 18th, 2015 through October 22th, 2016) to compare the two periods with consistent data sampling. The upper Figure (a) indicates river discharges (m^3 s^{-1}), the middle Figure (b) indicates concentration of NO_{3+2}, and the bottom Figure (c) indicates nitrate + nitrite flux (mol day^{-1}). Baton Rouge has fewer data than Morgan City. In all graphs blue shows Atchafalaya River dates, red Mississippi River data.

Table 4. Overall range, Freshwater end-member range, Median, Standard deviation, and Average from DIN concentration at Morgan City, Baton Rouge and for the Keum River, respectively.

DIN	Morgan City	Baton Rouge	Keum River
Overall range	0 ~ 150 μM	0 ~ 200 μM	0 ~ 200 μM
Freshwater range (Annual)	70 ~ 100 μM	70 ~ 100 μM	70 ~ 100 μM
Average	74.05 μM	112.6 μM	118.7 μM
Median	69.97 μM	106.38 μM	105.38 μM
STDEV	22.51 μM	35.01 μM	34.01 μM

2.5 Atmospheric Nitrogen Deposition (AN-D) data

AN-D data from around the US are sparse. The only data in the GOM region were collected near Corpus Christi (Wade and Sweet, 2008). Most US data have been collected along the east coast of the US (Table 5). There are more data from the coastal China region for the Yellow Sea (Luo et al., 2014; Wang et al., 2016; Zhao et al., 2015) (Table 5). However, all these data were limited due to the broad sampling coverage, and the values of AN-D showed a big difference between the regions (Table 5). While AN-D data in the Asian region were above 67 kg/ha/year, most of the AN-D data collected from the eastern side of the US were under 10 Kg/ha/year, suggesting there is not a large contribution to total N loads to the GOM or North Atlantic Ocean. There may be local, small-scale contributions from individual rivers or estuaries but these are unlikely to affect the whole of the coastal GOM. In addition, the concentrations were dependent on sampling methods and it is hard to distinguish between riverine N sources and AN-D sources.

However, the AN-D concentrations show approximately an order of magnitude difference between the GOM and the CSK due to the continuing industrial development in East Asia and the resulting N emissions (Wang et al., 2016; Zhao et al., 2015). All AN-D concentrations were converted to Kg/ha/year for use as a new N input source in the N-mass balance model in Chapter IV.

Table 5. Atmospheric Nitrogen Deposition (AN-D) in USA and Asia regions.

Watersheds	AN-D (Kg/ha/year)	References
Casco Bay, ME	1.45	Castro and Driscoll. 2002
Merrimack River, MA	1.2 ~ 4.0	Alexander et al. 2000
Long Island Sound, CT	1.84	Castro and Driscoll. 2002
Delaware Bay, DE	2.2 ~ 4.4	Castro and Driscoll. 2002 Goolsby. 2000
Chesapeake Bay	1.4 ~ 17.4	Alexander et al. 2000 Castro, M. S et al. 2000 Castro and Driscoll. 2002 Goolsby. 2000
Gulf of Mexico	9.95 ~ 11.50	Wade and Sweet. 2008
Coastal Sea off Korea & Yellow Sea	67.2 ~142.5	Luo et al. 2014 Zhao et al. 2015 Wang et al. 2016

CHAPTER III

NUTRIENT/SALINITY RELATIONSHIPS AS A MEANS OF IDENTIFYING COASTAL REGIONS

3.1 Introduction

As is well known, temperature and salinity are useful conservative tracers for identifying different water mass in the ocean (Mamayev, 1975). In the deeper part of the ocean, water masses mix along isopycnals, however, in the coastal ocean the water masses are mixed by winds and currents etc. (Emery and Meincke, 1986; Emery, 2003). However, using temperature/salinity relationships can only explain the physical processes and cannot help to explain biological processes in the ocean (Boyle et al., 1974). Several recent studies have evaluated the effects of physical-chemical coupling on biological processes not only in the coastal ocean but also in brackish water regions and estuaries (Harrison et al., 2008; Tang et al., 2015; Wu et al., 2016; Ye et al., 2015).

Generally, nutrient concentrations in estuarine regions can vary in two different ways, either conservatively or non-conservatively (Loder and Reichard, 1981). Within a river plume, the distance from the land is also related to the concentration of a terrestrial material such as a nutrient, if there is conservative mixing between freshwater and coastal seawater (Pujo-Pay et al., 2006; Wu et al., 2016). Conservative mixing leads to a linear correlation between nutrient (e.g. DIN) concentration and salinity changes. As state earlier, for most components, when going from land to the ocean, there is an inverse relationship with salinity (Johnson et al., 2008; Knee et al., 2010), and this is particularly the case for nutrients (Wang et al., 2016). On the other hand, owing to seasonal changes, nutrients can be non-conservative, with a non-linear correlation with salinity,

caused by the combination of biological activity and mixing between freshwater and salt water. If a system shows non-conservative mixing, this may tell us that there are additional internal sources or sinks in the mixing region.

Several papers have used linear regression to analyze water masses and predict nutrient and chlorophyll-a concentrations from the salinity (e.g. Iwata et al., 2005; Desmit et al., 2015). Hakanson and Eklund (2010) also used linear regression to predict chlorophyll concentration from a nutrient and salinity model. Foster (1973), who did not show a linear trend, used UV absorbance to look at mixing off Fiji, while Liss (1976) used the Si/salinity ratio to look at riverine influences in the UK.

In addition, Kim et al. (2011) used nutrient/salinity relationships to define where the excess nutrients are entering the oligotrophic ocean around the volcanic island of Jeju in Korea. They concluded that all the excess nutrients came from Submarine Groundwater Discharge (SGD), which is new pathway contributing to coastal production. Most of studies for using nutrient/salinity relationships were conducted in the coastal ocean or an estuary and were attempts to determine extra sources of nutrients and differentiate between organic matter decomposition and uptake by phytoplankton and bacteria (Wu et al., 2016).

In this study, the relationship between nutrients and salinity was used to identify the source of water in the coastal regions of the GOM. We modified the RC02 model to quantify where the edges of each zone occur and compared our results with those from Lahiry (2007), who only used salinity components. We also applied our method to two separate regions of the CSK. The Mid-western Coastal Sea off Korea (MCK) has only one freshwater input source from the Keum River, but there are three different water masses offshore with different nutrient concentration (Lim et al.,

2008). The other region is the Seomjin River Estuary (SRE), which has also one freshwater input source from the Seomjin River with strong tidal exchange.

3.2 Methodology: Correlations between nutrient and salinity relationships

In this study, we used nutrient and salinity relationships to identify coastal regions of the GOM and CSK. Firstly, in the GOM, we filtered out summer data so as to determine different river water sources using nutrient and salinity relationships. During summer, it is hard to see the linear mixing pattern offshore due to high biological nutrient consumption over the shelf during phytoplankton growth, which results in a non-linear mixing pattern. However, we believe that RC02 still holds, but that the brown zone is found much close inshore where we were unable to sample. Thus, we used only winter nutrient and salinity data in our initial analyses since winter nutrient concentrations are more conservative than in summer. We then applied these relationships to the summer data.

In conservative mixing, the nutrient concentration along the salinity can be linearly changed and we produced the equation followed by Boyle et al. (1974).

$$\boldsymbol{N_C = m * S + N_0} \text{ – Eq. 1}$$

where $\boldsymbol{N_c}$ is the concentration of nutrients including DIN and DSi, m is a slope, $\boldsymbol{S}$ is salinity, and $\boldsymbol{N_0}$ represents N-intercept of nutrients, respectively. We calculate the range of each intercept using our end-member data and Eq. 1 applied to a modified RC02 theoretical model.

The important concepts of the RC02 model are that they consider nutrient concentrations are fully supported by river input because the surface seawater concentration in the offshore GOM

is low, that passing from the brown zone to the green zone will reduce nutrient concentration, and that nutrient concentrations in the blue zone are always low. In RC02 model, they mentioned that there is no physical boundary between the zones because the water is continuously moving and the edges of the three zones are changed from time to time.

While keeping the basic RC02 hypothesis, we modified their theoretical model, using historical nutrient data from the GOM region. In the low salinity region, we set a 'brown' zone, where the nutrient concentration decreases linearly as salinity increases, and where we can assume (a) that there is conservative mixing, and (b) that the biological processes are less important than the physical mixing process. Thus, we set the boundary of the brown zone as the point at which the slope of the linear portion of the nutrient/salinity plot changes. This will vary from cruise to cruise based on river flow, nutrient concentration, and phytoplankton activity. In the mid-salinity region, where the biological processes are more important than physical processes, we set a 'green' zone. Lastly, the offshore high salinity region is suggested as a 'blue' zone with minimal nutrients and there are only limited biological processes. Due to the low nutrient concentration in the blue zone, we set the green-blue boundary based on DIN concentration less than 1 μM from the GOM data (Figure 10).

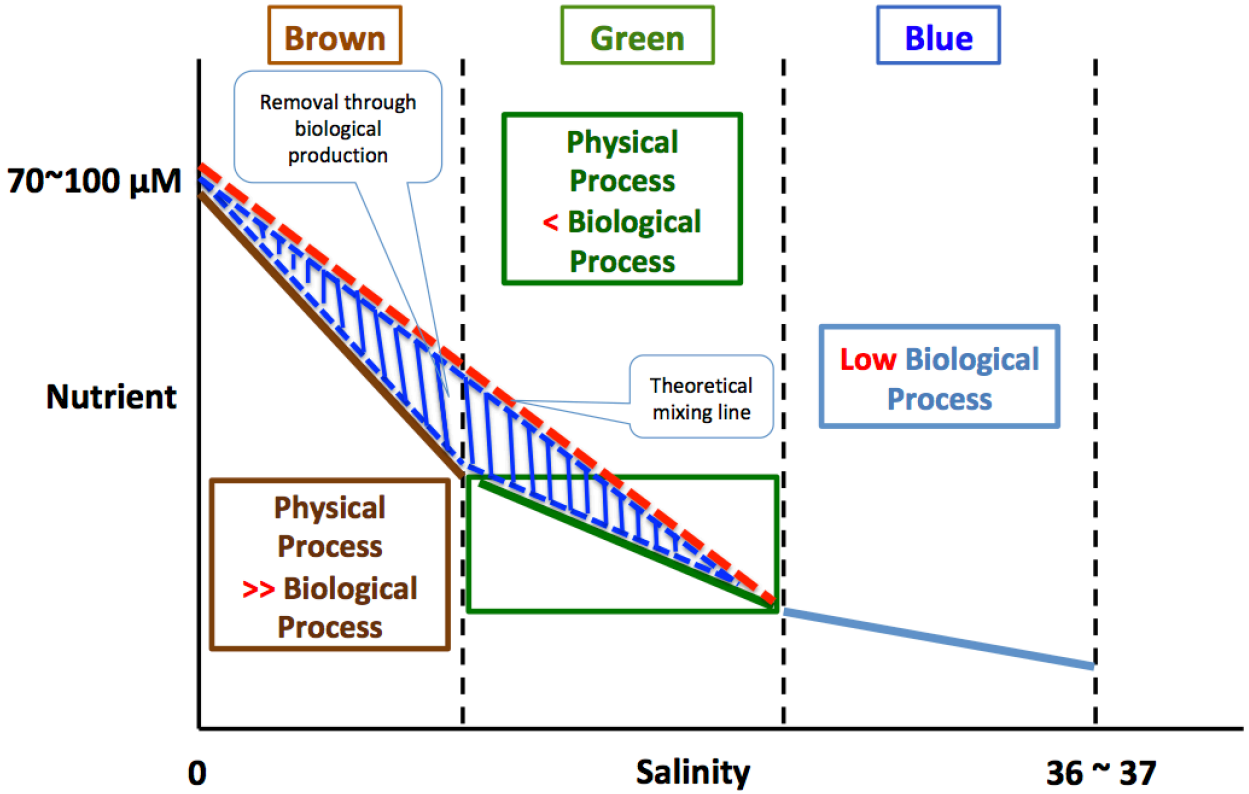

Figure 10. Graph concept for defining the edges of the three zones using nutrient/salinity changes, modified from the three zone hypothesis of RC02. While production is still occurring in the blue zone, the biological process is very low because of the low nutrients. The red dotted line indicates the theoretical mixing line and the blue shaded triangle indicates theoretical removal through the biological production in the brown and green zones. The area between this and the measured nutrient concentration indicates the amount of nutrients taken up by phytoplankton.

3.3 Results: Nutrients and salinity relationships as tracers for water masses

3.3.1 MCH data (M4 cruise; March 2005)

Almost all of the MCH cruises took place during the spring and summer period because they were investigating the development of hypoxia on the Louisiana shelf. Plotting summer data from these cruises (not shown) showed no obvious differences between the Mississippi and Atchafalaya regions of the shelf, mainly because the nutrient concentrations were too low.

Data from the only winter cruise in March 2005, however, showed that there is a distinct difference between the two different water sources (Figure 11). Red dots indicate sampling data from near the Mississippi River delta and blue dots are from near the Atchafalaya River mouth. There was a strong linear relationship at salinity < 22 near the Atchafalaya for both DIN and DSi and below a salinity of 28 in the region near the Mississippi. We estimated the concentration of the freshwater end-member from USGS data and determined the range of the annual freshwater end-members for DIN in both rivers as 70 μM ~ 100 μM and as 80 μM ~ 120 μM for DSi. Based on the observational data slopes for the MCH M4 cruise, the DIN end-members (i.e., estimated N-intercept of nutrients) were 64.88 μM for the Atchafalaya River and 73.65 μM for the Mississippi River, respectively. DSi end-member concentrations were estimated similarly as 86.96 μM for the Atchafalaya River and 104.61 μM for the Mississippi River, respectively. Thus, the intercepts produced from nutrient/salinity relationship plots from this cruise fall within the envelope estimated from the USGS data. In Figure 11, we assume the straight line between salinity 0 to 28 is the theoretical mixing line in the Mississippi and salinity 0 to 22 for the Atchafalaya rivers from their end-member data. These intercepts refer only to this cruise and this could change during other cruises depending on how much water is coming from each river, as well as mixing from coastal currents and winds. We can then use the actual data to estimate the theoretical maximum

biological production rate (removal rate through biological production) in regions such as the brown zone where the biological processes are assumed to be less important than physical processes.

The salinity-nutrient (DIN and DSi) relationships for the different water sources have different gradients during this cruise. For DIN, both slopes are similar and significant ($P < 0.0001$) with $R^2 = 0.8078$ for the Mississippi river region (C) and 0.7798 for the Atchafalaya river region (F), respectively. At salinities > 33, there is no difference because both regions are mainly offshore water. However, the DSi/salinity slope near the Mississippi differs from that near the Atchafalaya, with R^2 is 0.5512 for the Mississippi region and 0.9721 for the Atchafalaya region. P is < 0.0001 again in both regions. Off the Atchafalaya, the DIN (NO_{3+2}) and DSi concentrations are approximately constant at higher salinity (around 25) until the salinity reaches 33. Based on the data from this one cruise, we can apparently use winter nutrient and salinity relationships as tracers for mixing from the two major different water masses in this region.

We tested Figure 10, on the MCH M4 data. We have divided the regions off both rivers into three zones based on winter MCH M4 nutrient (DIN and DSi) data with their associated salinity changes. Figure 12 shows how DIN/salinity and DSi/salinity changes are different near both rivers. The blue dots indicate data from off the Atchafalaya and the DIN (NO_{3+2}) and DSi concentrations are virtually constant at higher salinity (from around 25 to 33). The red dots indicate data from near the Mississippi and only DSi concentration is constant at higher salinity (around 25) until salinity reaches 33. Note that this is the first time the three zones of the RC02 hypothesis have been determined using real observational nutrient data.

According to RC02, in the low salinity area, (the 'brown' zone), located near the river mouth, nutrient concentrations are high with light limitation due to suspended silt and clay. In the

mid salinity area, (the 'green' zone) the concentrations of nutrients are approximately constant until the salinity reaches 33, where the high-salinity offshore water becomes a major component of the surface layer. In the high salinity area, where salinity is over 33, (the 'blue' zone) the nutrient concentrations seem to increase again due to regeneration from the bottom sediment, but this is only important below the pycnocline. From our MCH M4 data, it is hard to distinguish between the green and blue zones, as in the real world the nutrients concentration decreases continuously until we reach concentration below 1 μM. It is important to note that the three zones hypothesis of RC02 was theoretical and only considered the layer above the pycnocline. We also identified the edges of three zones below the pycnocline layer, which they did not mention, in chapter IV using our N-mass balance model.

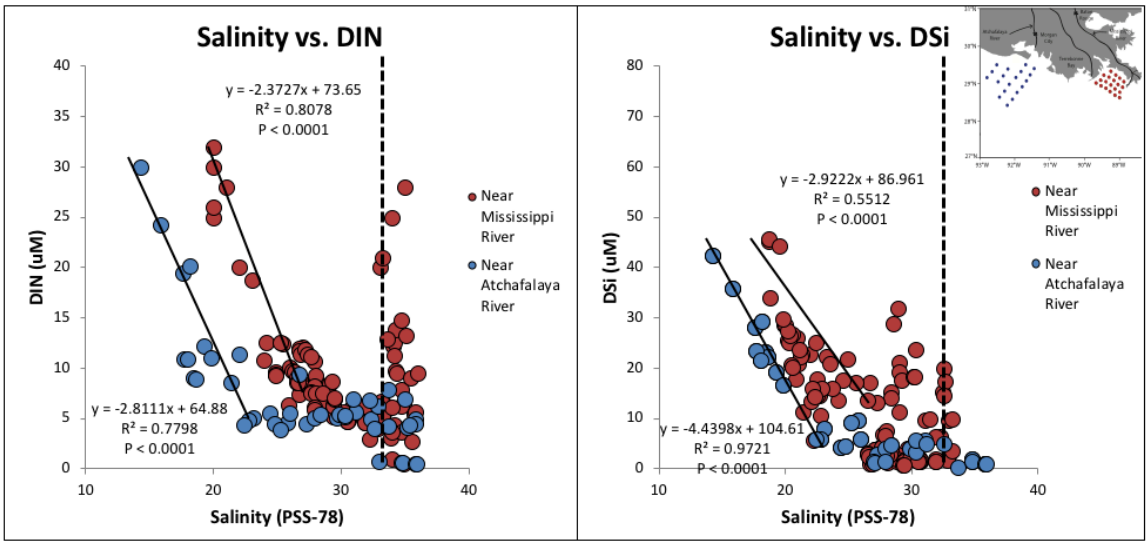

Figure 11. MCH (March 2005) data from the only winter cruise. All nutrients (DIN, DSi) data above and below the pycnocline layer were plotted against salinity. High nutrient data over salinity 33 near the Mississippi and Atchafalaya Rivers were from below pycnocline layer, which were divided by vertical dotted line. Red dots are from the Mississippi River data and blue dots are from the Atchafalaya River.

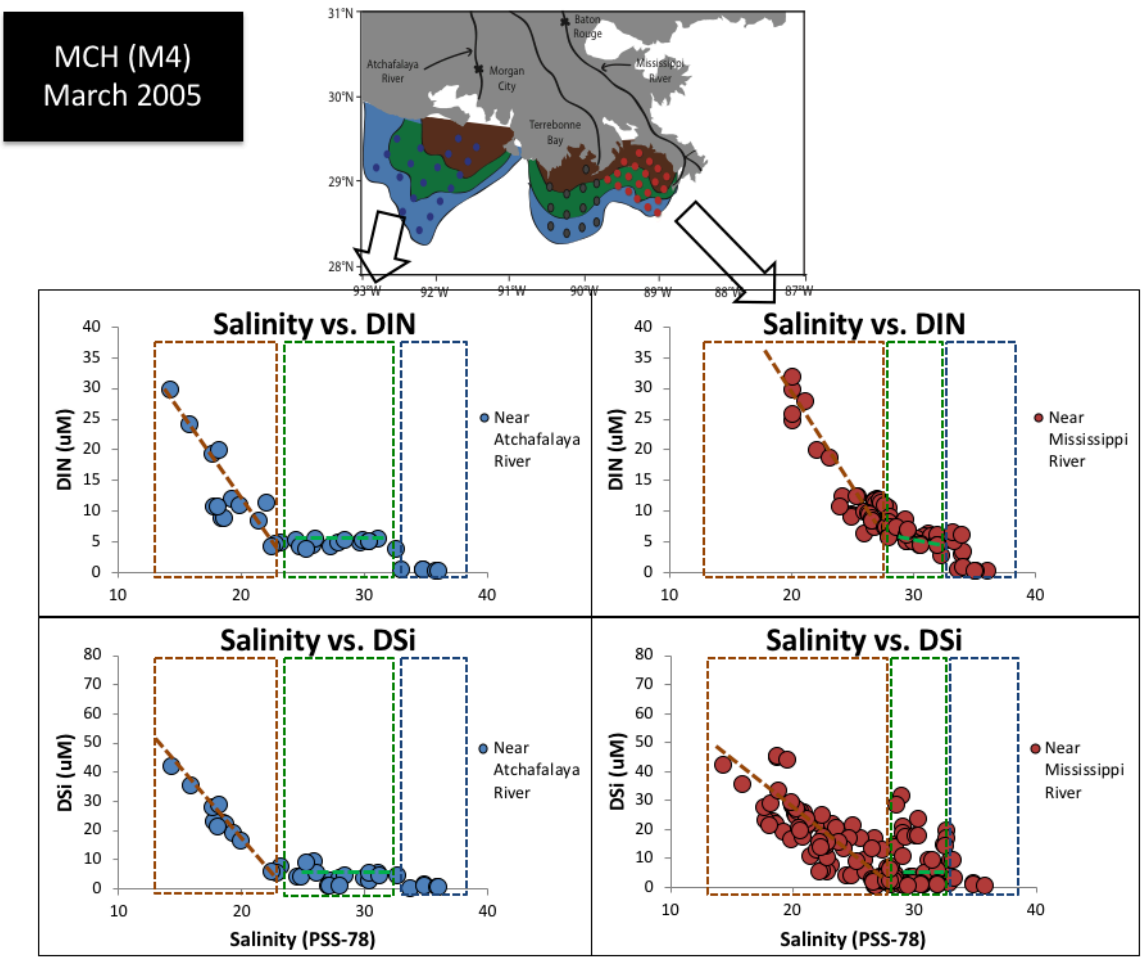

Figure 12. MCH M4 (March 2005) DIN and DSi data were used to define three boxes following Rowe and Chapman (2002). Brown, Green, and Blue dotted boxes were separated by DIN and DSi concentration against salinity changes. Note that all the data from below pycnocline layer were excluded.

3.3.2 LATEX data (H04 cruise; February 1993)

There are very few other cruises from the region in winter. The LATEX H04 cruise (February 1993) provides the only winter data from the LATEX project and typically the DIN graph in Figure 13 shows a similar pattern to the MCH M4 graph in Figure 11. Early 1993 was very wet relative to the long-term mean (RC02), so this may have overwhelmed the contribution from the Red River, which provides much of the flow in the Atchafalaya River.

In Figures 13 and 14 from the LATEX data (February 1993), the blue dots indicate the F-transect, where the data were sampled off the Atchafalaya and the DIN (NO_{3+2}) and DSi concentrations decreased between salinities of 20 to around 33 and then increased again below the pycnocline the same reason as in the MCH data. The red dots indicate the C-transect, where the data were sampled west of the Mississippi. During the LATEX H04 cruise period, the end member data was not measured from the USGS. Thus, we initially used the annual range of the end-member from the USGS, which is the same for the MCH data for DIN was 70 μM ~ 100 μM and for DSi was 80 μM ~ 120 μM. Note that these ranges could change depending on actual USGS measurements. For the LATEX H04 cruise, the slope (m) was calculated from equation 1 as about -1 both near the Mississippi and Atchafalaya River regions. Based on these observational data slopes, the DIN end-member (i.e., estimated N-intercept of nutrients) from the Atchafalaya River is 35.95 μM and 47.93 μM for the Mississippi River, and DSi end-members are 82.86 μM for the Atchafalaya River and 82.33 μM from the Mississippi River, respectively.

The DIN and DSi relationships for the different water sources have different slope gradients during this LATEX H04 cruise. For DIN, both slopes are similar and highly significant ($P < 0.0001$) with $R^2 = 0.8553$ for the Mississippi river region (C) and 0.8624 for the Atchafalaya river region (F), respectively. As for the MCH M4 data, there is no difference at salinity over 33

since both regions are mainly offshore water. Also, the DSi/salinity slopes near both regions are highly significant ($P < 0.0001$) and similar, with R^2 are 0.9620 for the Mississippi region and 0.8892 for the Atchafalaya region.

We also applied our modified RC02 three zone hypothesis (Figure 10) to the LATEX H04 data (Figure 14). On both lines of Figure 14, the DSi concentration in the green dotted box (green zone) is between 32 ~ 34 off the Atchafalaya and 31 ~ 34 of the Mississippi. This indicates that during the LATEX H04 cruise period, there was a high DSi input from the river or mixing compared with MCH M4 cruise period.

It should be noted that the sampling locations from the MCH and LATEX cruises are different. In addition, the LATEX data do not show the constant pattern in the mid salinity area found during the MCH cruise. Thus, LATEX data results suggested that maybe we cannot see any green zone at this time because the data were only sampled along one transect, while MCH data were sampled over a larger region.

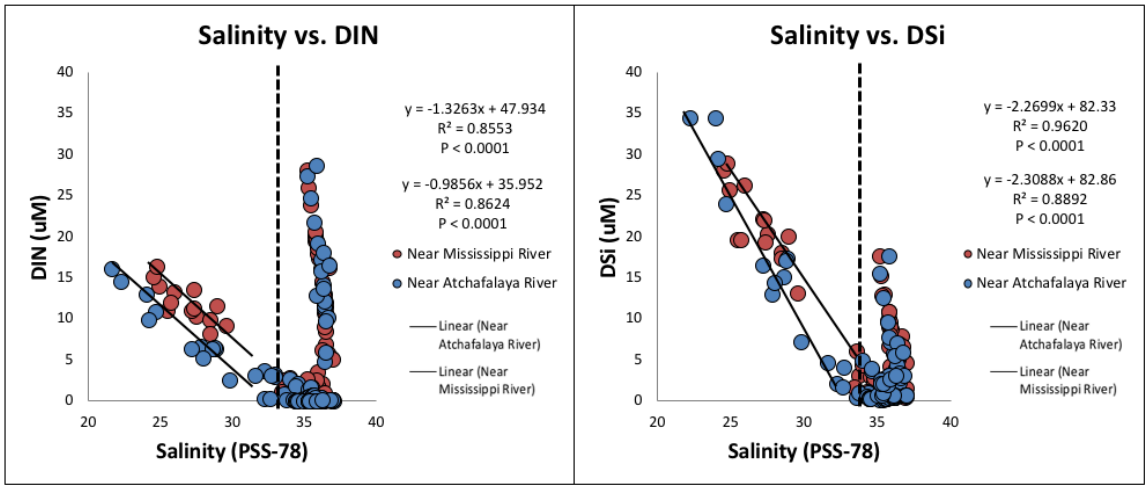

Figure 13. LATEX (February 1993) data from the only winter cruise. All nutrients (DIN, DSi) data above and below the pycnocline layer were plotted against salinity. High nutrient data over salinity 33 near the Mississippi and Atchafalaya Rivers were from below pycnocline layer, which were divided by vertical dotted line. For the Si/salinity graph, lower transect line indicates F transect (near the AR), and upper line is for the C transect (near the MR).

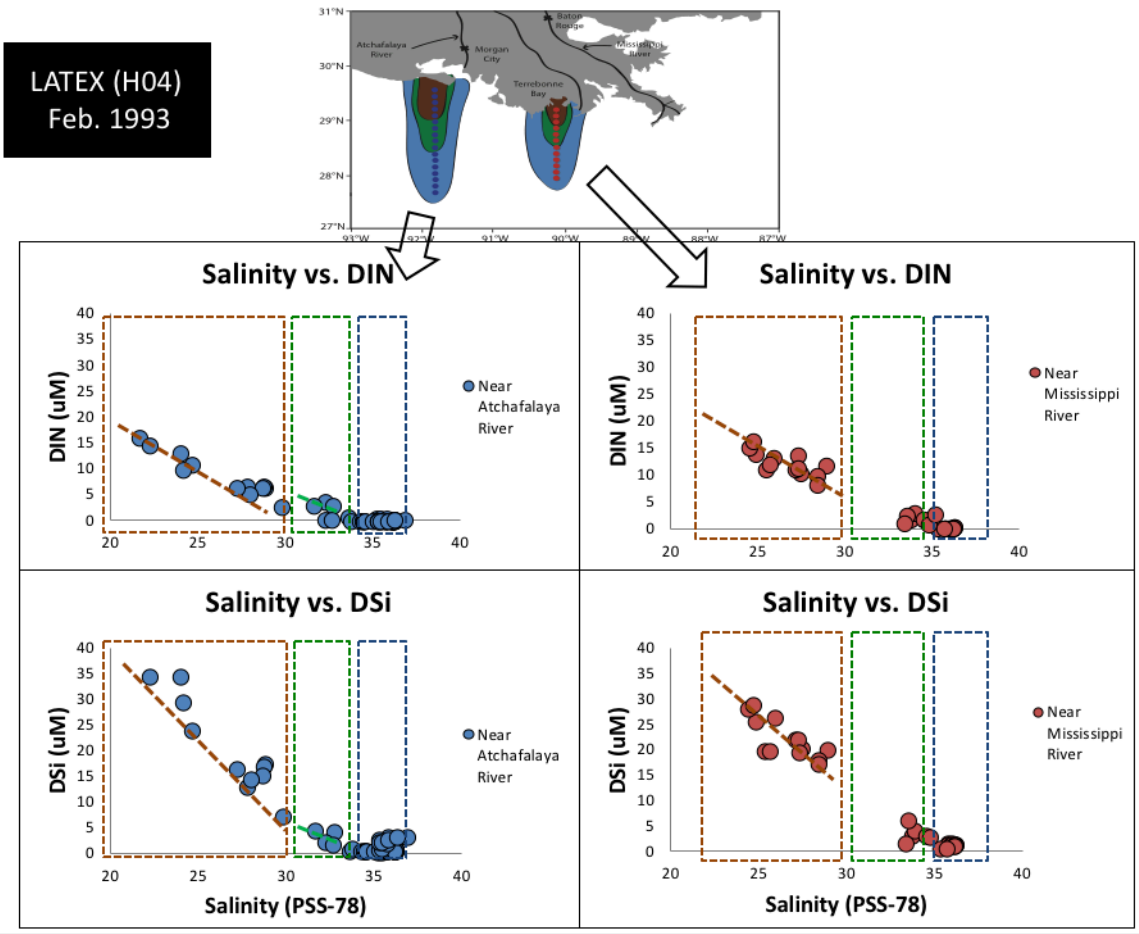

Figure 14. The only winter data in LATEX H04 (February 1993) show similar DIN and DSi concentration patterns along both transects and divide the area into three zones as discussed previously. Both transects' brown zones appear to show a conservative mixing with DIN/salinity changes. Also, the green zones on each transect have different slopes from the brown zones from both DIN/salinity and DSi/salinity.

3.3.3 LUMCON data (C & F transects above/below pycnocline layers)

Similar to LATEX data, the sampling stations for LUMCON data were along only one transect near each river, and so do not cover a large region as do the MCH M4 data. We compared the water masses from the two rivers and how the patterns were changed between samples from above and below the pycnocline layer. The data from LUMCON cruises took samples each month during the year because they were investigating the development of hypoxia on the Louisiana shelf. The work started in 1985 and was continuous until 2010. In this study, we used the winter data only from 1998 through 2010. The monthly LUMCON data showed differences above and below the pycnocline layer, and the C and F regions have different pycnocline layer depths. The approximately depths of the pycnocline layer for the C and F regions were 10m and 15m, respectively.

These differences between the regions were mainly caused by different nutrient concentrations coming from each river and sampling areas. We assumed that C line data were from the Mississippi and F line data were from the Atchafalaya River, respectively. Red dots indicate sampling data from near the Mississippi River region and blue dots are from near the Atchafalaya River region (Figure 15). In addition, near data from F line have stronger nutrient/salinity relationships than C line data. This may be because the sampling stations in C line are not as close to the Mississippi River mouth as the F transect is to the Atchafalaya.

Along both transects, nutrient concentrations are more conservative above the pycnocline layer than below it. Also, data above the pycnocline layer have a more variable salinity distribution due to the influence of the river plumes. The range of possible concentrations occurs from the mixing of open ocean water and coastal freshwater. However, below the pycnocline layer, most of the high nutrient concentrations were plotted in high salinity. It seems that the bottom sediment

diffusion affects the data (Rowe 2001; Nunnually et al., 2014), however, this is only apparent in winter when production is lower than in summer (Figure 16). In summer, these nutrient/salinity relationships deteriorate because of uptake by phytoplankton. The bold green lines show estimated nutrient/salinity relationships based on river water (S=0) concentrations at Morgan City and Baton Rouge. The vertical dotted line at S=33 is taken as the control for open ocean water.

In winter, the DIN/salinity or DSi/salinity relationships vary systematically with distance from the two sites of river input to the coastal GOM, as found for the MCH and LATEX winter data. This pattern, however, is not clearly shown in the summer data due to lack of data sampling near the low salinity region. The bold green lines show the range of each river's end member data and the black line indicates the relationship for the data set.

There were both DIN/salinity and DSi/salinity relationships for data above and below the pycnocline layer from both the Atchafalaya and Mississippi rivers between salinity 10 to 32. However, the relationships above the pycnocline layer, showed better correlations for DIN and DSi along the salinity gradient (based on R^2 values). Winter R^2 values were 0.6011 (DIN/salinity) and 0.7851 (DSi/salinity) in the Atchafalaya River and 0.1471 (DIN/salinity) and 0.3658 (DSi/salinity) in the Mississippi river, respectively (Figure 15). P is < 0.0001 in both regions. However, R^2 values, during summer were less than 0.075, (not shown in this dissertation) and considerably less robust than for the winter data due to the strong biological activity.

The Atchafalaya river winter data show a clear mixing line across the whole salinity range because production is at a minimum and physical mixing is more important than biology. We also tested the modified RC02 three zone hypothesis (Figure 10) on the LUMCON cruise data and there is no real sign of a green zone because the sampling stations cover only one transect near each river, which leads to different results from MCH and LATEX data.

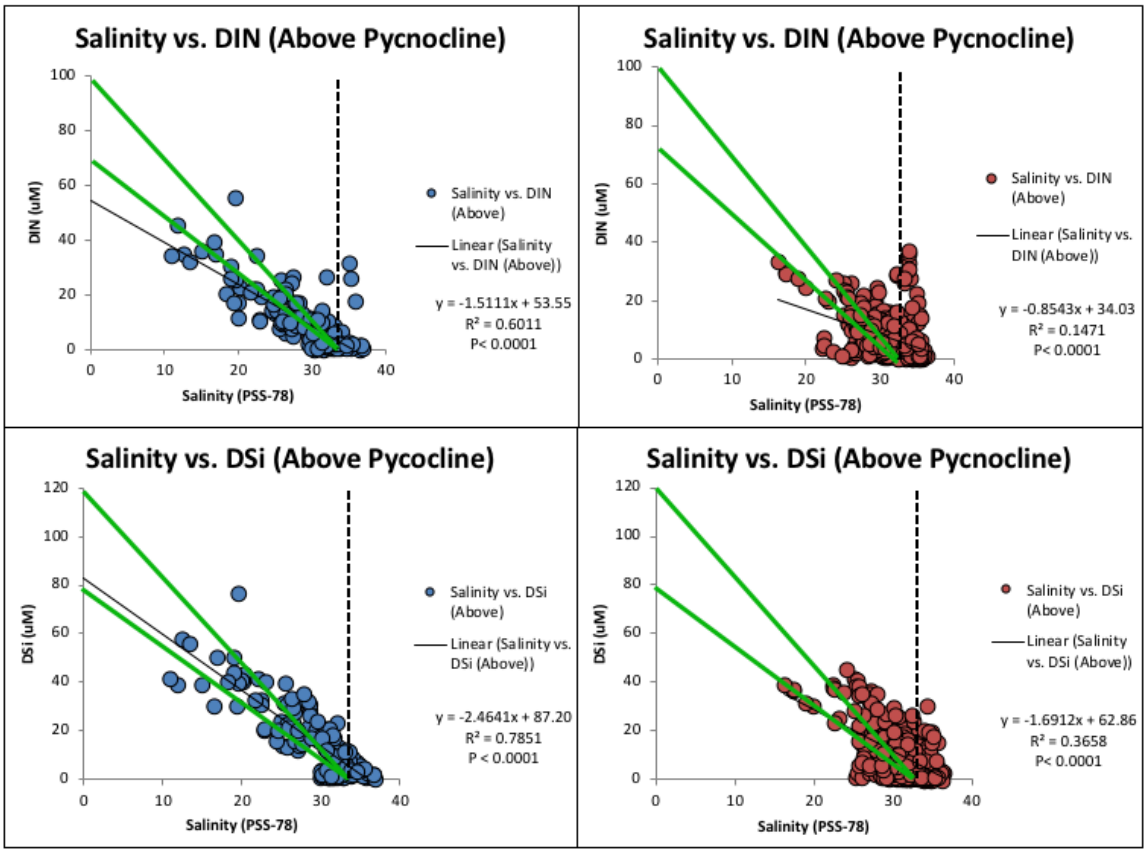

Figure 15. LUMCON (1998~2010) data from the winter cruises. The upper Figure includes DIN concentration against salinity above pycnocline layer data and the lower Figure includes DSi against salinity above pycnocline layer data. Red dots are from the C line data and blue dots are from the F line data. The bold green line indicates estimated Nutrient/salinity relationship based on river water and dotted vertical line at S=33 is taken as the control for open water.

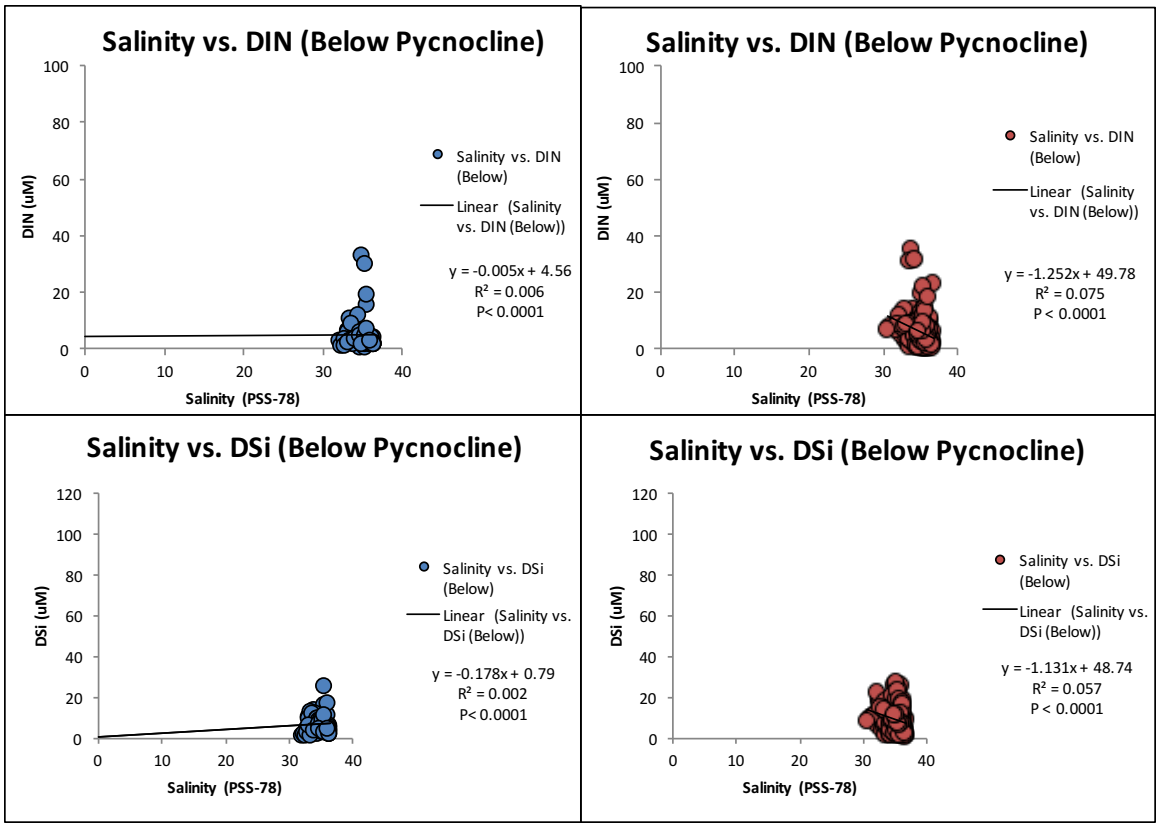

Figure 16. LUMCON (1998~2010) data from the winter cruises. The upper Figure includes DIN concentration against salinity below the pycnocline layer and the lower Figure includes DSi against salinity below the pycnocline layer. Red dots are from the C line data and blue dots are from the F line.

3.3.4 NEGOM winter data

Most of our historical data from the GOM were sampled across the LATEX shelf. On the other hand, the NEGOM projects were conducted in the Eastern GOM and these projects were conducted from 1998 to 2000 during three different periods (November, May, and August). Figure 17 shows the DIN concentration plotted against the salinity changes for all nine cruises (N1 ~ N9). In Figure 17, data from blue dots indicate the data from above the pycnocline and the red dots indicate those from below the pycnocline. First, we took data from lines 1 to 4, where the sampling locations are close to the Mississippi River mouth. Those four transects are plotted on Figure 7a in orange. We plotted all depth data because low data were collected above the pycnocline layer.

Comparing the LATEX shelf of the GOM with the eastern GOM, the NEGOM region is generally oligotrophic and has different nutrient supply sources such as the Mississippi River, mixing, currents and upwelling from the DeSoto Canyon (Belabbassi et al., 2005). Most of the water supply from the NEGOM area comes through South Pass of the Mississippi delta, which discharges into the deep water. In this region, however, high nutrient, concentrations do not affect the coastal zone directly due to the Coriolis effect and the region is resupplied from the open ocean region through upwelling (Belabbassi et al., 2005). Due to these localized environmental characteristics, there is lack of low salinity and high nutrient water in the NEGOM region (Figure 17).

Most NEGOM data, below the pycnocline layer, indicate high salinity with high nutrient concentrations in all seasons. Usually, close to the Mississippi river, the nutrient concentration (nitrate) is higher in all seasons except late summer and early fall (Cooper et al., 1996). However, above the pycnocline layer data show that the DIN concentration is reversed relative to the salinity gradient during summer when the river water forms a plume along the shelf edge. Cruises N2 and

N4 have a number of low salinity samples with high DIN concentrations from salinity 20 to 25 and DIN 20 to 30 μM where the data were sampled near the Mississippi delta (Green dotted circle in Figure 17).

This low salinity water is along the edge of the shelf, and it might be the localized characteristic in this region. Even close to the Mississippi river mouth, there is almost no nutrient supply in the eastern GOM and few high nutrient concentrations points. NEGOM data did not show a relationship between DIN and salinity, as in the Western GOM, owing to the different water masses involved. Thus, we cannot use the NEGOM data to test the RC02 three zone hypothesis.

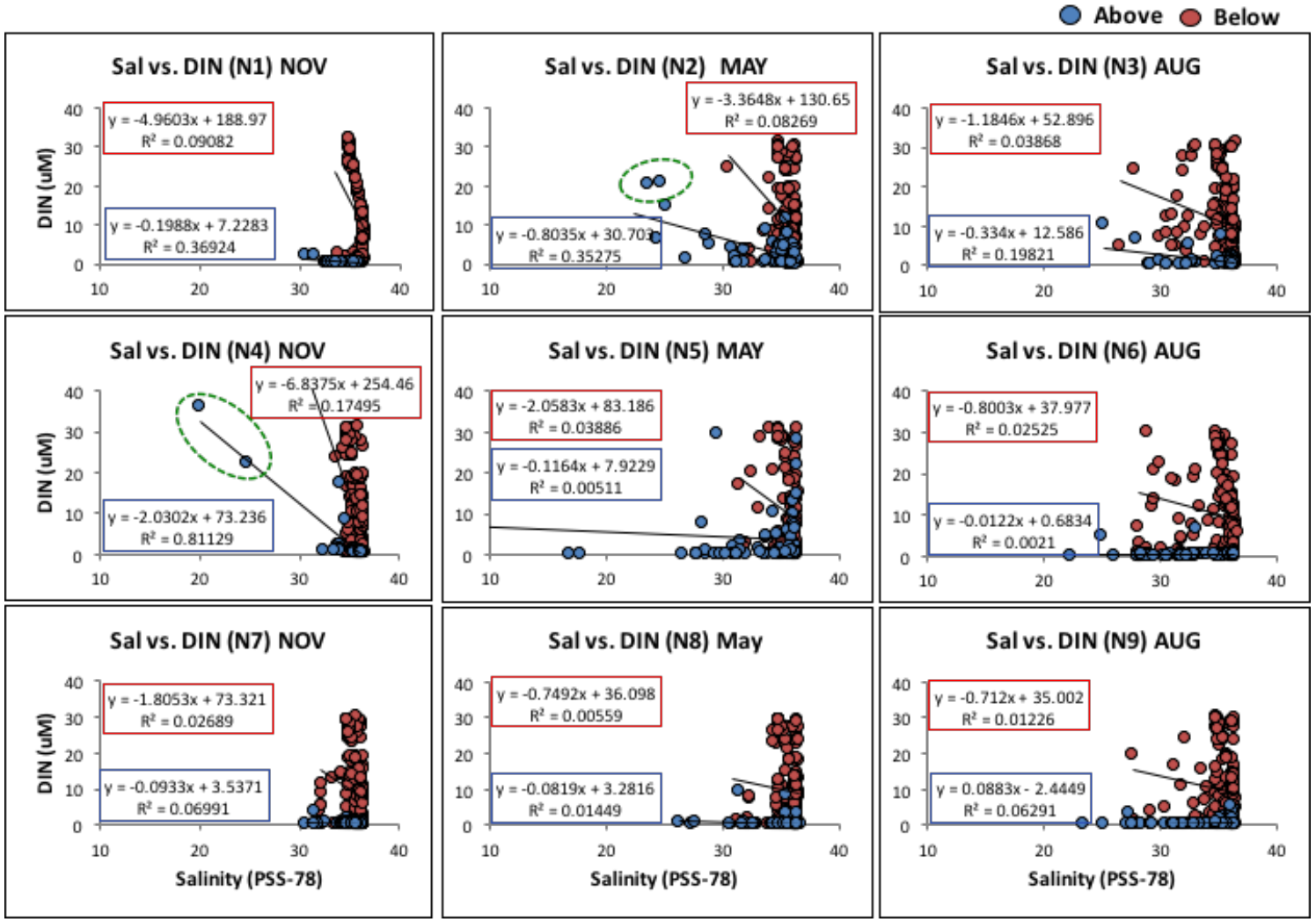

Figure 17. Different seasons of DIN concentrations against salinity changes of three years for all NEGOM cruises in 4 transects near the Mississippi river mouth. The data of cruises name were in each graph with N1 ~ N9. Blue dot indicated above the pycnocline layer and red dot indicated below the pycnocline layer. Green dotted circle data were sampled near the Mississippi river mouth.

3.3.5 Quantification of RC02 model from historical data

We tested the RC02 model (Figure 10) based on all the data from the GOM and CSK. While it is difficult to recognize the physical boundaries of each zone because ocean water is moving continuously, we can at least estimate the portions of the edges of each zone from our results. Figure 18, which we modified from Figure 10, shows that each zone's salinity and slope range can be quantified by the previous data. While production is occurring in the blue zone, the biological activity is very low due to the low nutrient concentrations, and this region is normally well offshore where the salinity is higher than 31 ~ 33. In the green zone, where the salinity is typically between 20 ~ 25 and 31 ~ 33, biological processes are more important than physical processes and the nutrient concentration is related to productivity. In contrast, physical processes are more important than biological processes in the brown zone where the salinity is under 20 ~ 25.

When freshwater with high nutrients and seawater with low nutrients are mixed together, they will produce a linear mixing relationship (red dotted line in Figure 18), if we assume physics is more important than biology because each salinity region has different biological and physical properties. The red dotted line indicates the theoretical mixing line between salinity 0 to 33, which includes the brown and green zones, and the blue shaded triangle indicates theoretical removal through the biological production in these two zones (Figure 18). Also, we assume that the area within the triangle indicates the amount of nutrients taken up by phytoplankton.

Based on this concept, we can initially set the nutrient and salinity concentrations at the zonal boundaries based on data from previous projects in the GOM (Table 6), which have not

been quantified before. Based on the MCH data, the salinity and nutrient ranges of each zone in GOM are like this: brown zone for salinity between 15 ~ 25, for DIN 5 ~ 75 μM, green zone for salinity between 25 ~ 32, for DIN 1 ~ 5 μM, and blue zone for salinity between 32 ~ 35, for DIN 0 ~ 1 μM, respectively. Similarly, each boundary was divided and identified by salinity from LATEX and LUMCON, however, it was hard to divide the nutrient range between the green and blue zones.

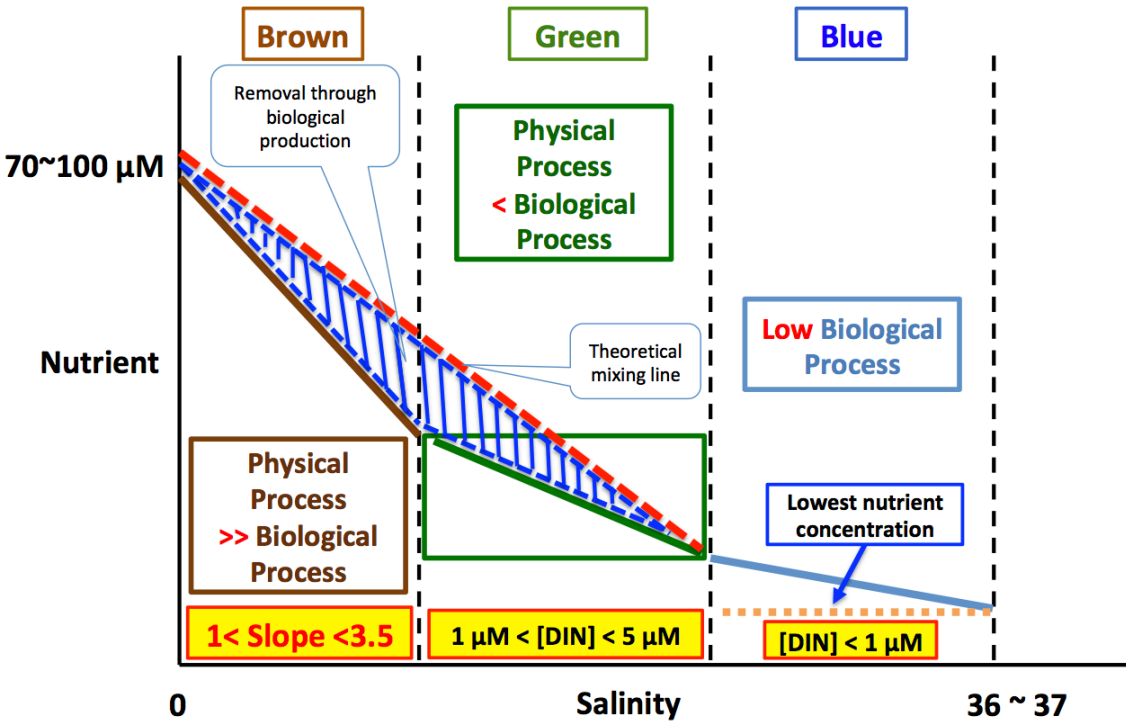

Figure 18. Nutrient and salinity ranges of each zone based on our previous data results. The Figure was modified from Figure 10 using our data to quantify the nutrient and salinity ranges of each zone.

Table 6. Salinity and nutrient (DIN) ranges change during winter during different cruises in the GOM.

Study area	Projects name	Brown Zone	Green Zone	Blue Zone
		Salinity (PSS-78)		
Gulf of Mexico (GOM)	MCH	15 ~ 25	25 ~ 32	> 36
	LATEX	21 ~ 31	31 ~ 33	> 36
	LUMCON	15 ~ 33		> 36
		DIN (μM)		
	MCH	5 ~ 75	1 ~ 5	0 ~ 1
	LATEX	1 ~ 18	0.3 ~ 1	0 ~ 0.3
	LUMCON	5 ~ 50	0~5	

3.3.6 Mid-western Coastal Sea off Korea (MCK) and Seomjin River Estuary (SRE) data

Based on the GOM results (Figures 11, 12, 13 and 14), we determined the edges of the three zones, which vary from cruise to cruise. The RC02 hypothesis specifically allows for changes in the area of each zone as nutrient concentrations and river runoff vary during the year. Lahiry (2007) concluded in her thesis that the three zones hypothesis may be more significantly applicable to smaller spatial scales (within 10 Km). Thus, it might apply better to the coastal sea off South Korea, as the spatial scale of the Texas-Louisiana shelf is about 15 to 20 Km both alongshore and offshore according to Li et al. (1996). We have therefore applied the RC02 three zone hypothesis to the MCK and the SRE.

The MCK data were collected during four different seasons from 2003 to 2005, while SRE data were collected in 3 different seasons from 2006 through 2008 (Table 3). The data from the MCK showed similar patterns in either summer or winter due to high nutrient concentrations coming from the Keum River, which is the only terrestrial nutrient source. Typically, the MCK has four different water masses that combine (Upper right Figure 4), and there is a substantial tidal effect on coastal regions, which is different from the LATEX region. Given the small numbers of data points in each cruise where the DIN concentration is greater than 5 μM, Figure 19 also contains a plot of all the cruise data, which shown a consistent relationship throughout the year. Close to the Keum river mouth, the edge of the brown zone can be clearly identified from conservative mixing of nutrient concentrations along the salinity gradient (Figure 19). For these reasons, we defined the edge of the brown zone using slope's change in nutrient and salinity relationship. However, the boundary between the green and blue zones is hard to distinguish because water masses are mixed quickly with tidal energy (Lim et al., 2008). Thus, we defined

each boundary based on nutrient concentration (DIN only) for the green zone less than 5 μM and the blue zone less than 1 μM or more, respectively (Table 7).

The data suggest that the salinity and DIN ranges of the brown zone in the MCK are 16 ~ 31 and 5 ~ 75 μM respectively. This range is not physically fixed and can vary as the river end-member concentrations change in the low salinity regions. However, this range was more consistent than in the GOM during the three years of our observation cruises in both summer and winter owing to high nutrient concentrations coming from the Keum River. The ranges of salinity in the green zone were between 31 ~ 32 and for the blue zone 32 ~ 34.5, however it was hard to distinguish changes in nutrient (DIN) concentration through the green to blue zone because of substantial tidal exchange and water mass mixing with ocean water (Table 7).

In Figure 19, in the MCK, all four seasons' DIN/salinity slopes are different. The brown zone shows a clear relationship with salinity, but the data from the blue and green zones all cluster near zero. However, the SRE has a clearer pattern of salinity change as because it is a simple river system, while the MCK has a complicated mixture of water masses from offshore such as Yellow Sea Bottom Cold Water Mass (YSBCWM). In Figure 19, the pattern of the slopes is similar to that in the GOM, with negative slopes in all three zones, but the edges of each zone vary depending on the season.

Because the SRE is an estuary system, it has more conservative mixing conditions between river water and seawater. However, we can see clear patterns of nutrient sinks and sources through non-conservative mixing. We plotted the ammonium (NH4) concentration with our nutrient/salinity graphs and found that NH4 was high in the brown zone only during winter periods (March and December) and decreased downstream based on salinity changes. This seemed to be caused by high production during autumn and regeneration from the sediment within the brown

zone, a shallow area with high sediment turbidity coming from the freshwater discharge. Thus, we set the brown zone here in the SRE, especially, this region where the salinity ranges between 10 and 20 has high productivity (Yang et al., 2005) (Table 7).

The map in Figure 20 indicates three zones in the SRE based on salinity concentrations, but these differ from boundaries based on nutrient/salinity relationships (other Figures in Figure 20). For instance, based only on salinity, there is a blue zone near Gwangyang Bay, however, there is no blue zone when we use nutrient/salinity relationships. The results show that there are no clear boundaries between the green and blue zones and it is hard to isolate these two regions. It seems that the open ocean water is not fully mixed into Gwangyang Bay within the tidal period in this region and that our sampling stations are not fully within the blue zone. This can be determined by more sampling in the open ocean area in the near future.

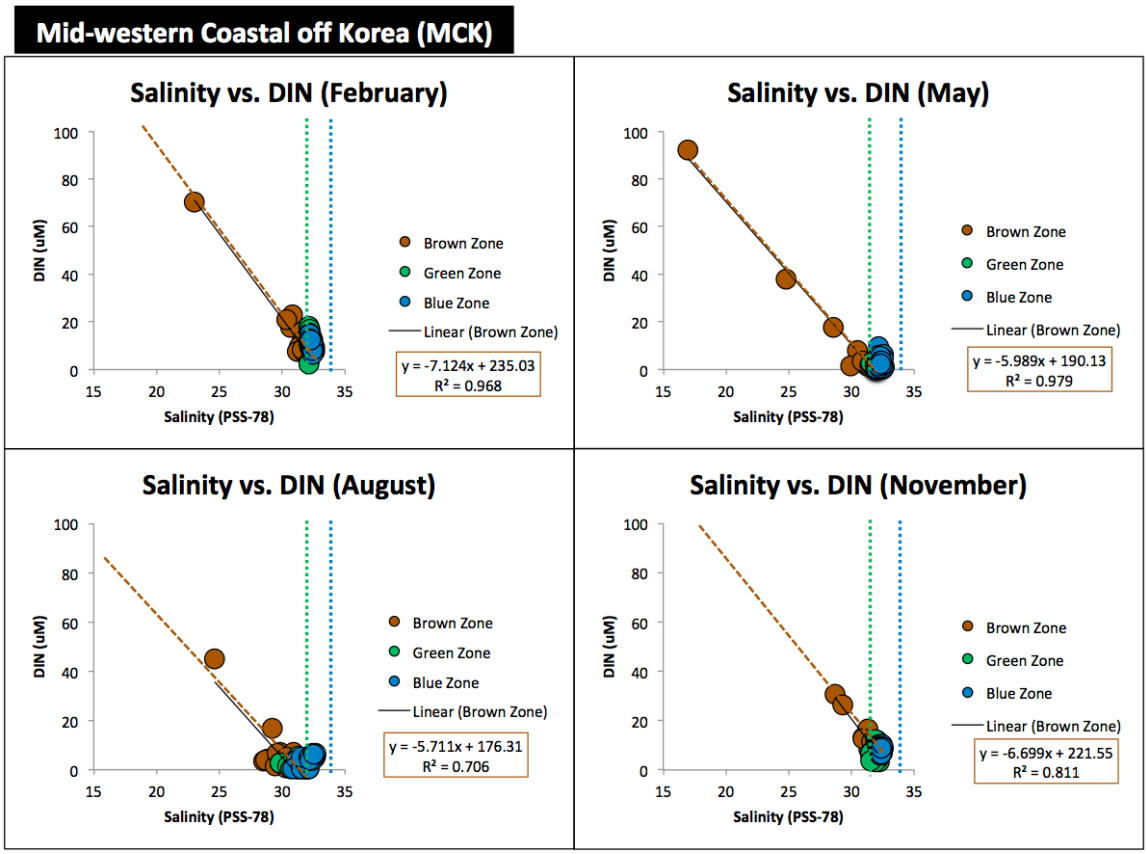

Figure 19. DIN concentrations plotted against salinity in the MCK during four different seasons. The dotted vertical lines with three different colors indicated the edges of each zone. The edge of the brown zone is clearly isolated using nutrient/salinity relationships, however, the edges of the green and blue zone are hard to isolate.

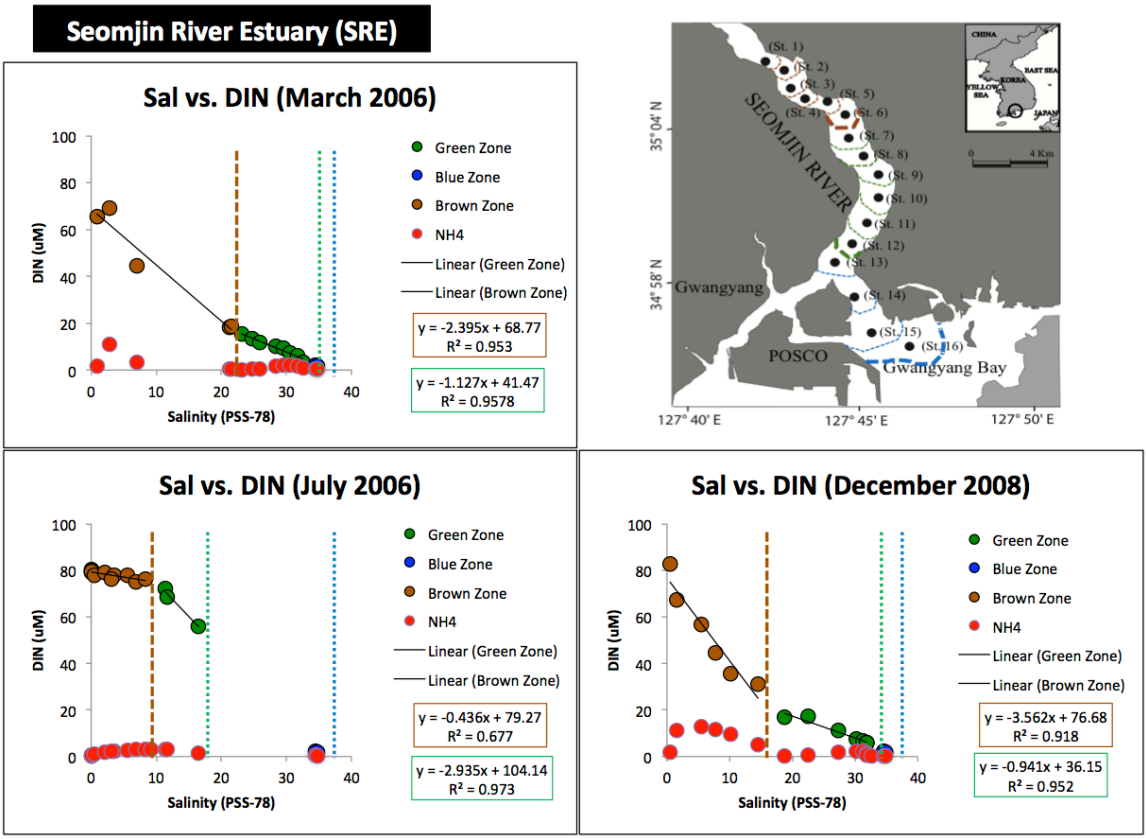

Figure 20. DIN concentrations plotted against salinity in the SRE during three different seasons. The map shows the edges of the three zones based on salinity concentration data, which suggests the blue zone is only in Gwangyang Bay. However, it is hard from these data to determine the boundary between the green and blue zones.

Table 7. Nutrient (DIN) and Salinity ranges change in different cruise data of the MCK and SRE in each zone

Study area		Brown Zone	Green Zone	Blue Zone
		Salinity (PSS-78)		
Coastal Sea off Korea (CSK)	MCK	16 ~ 31	31 ~ 32	32 ~ 34.5
	SRE	0 ~ 22	22 ~ 33	> 36
		DIN (µM)		
	MCK	5 ~ 75	0 ~ 5	
	SRE	20 ~ 85	1 ~ 20	0 ~ 1

3.3.7 Identifying the edges of RC02 three zones using nutrient/salinity relationships

We applied observational nutrient data to the RC02 model, which has not been done before, to identify the edges of each zone. It should be remembered that the RC02 hypothesis specifically allows for changes in the area of each zone as nutrient concentrations and river runoff vary during the year. RC02 mentioned that there are no physical boundaries to the water flow and so the boundaries of each zone vary depending on the extent of the plumes and local biological production. Based on previous results, which were applied to individual cruises (Table 6), we defined each zone using nutrient/salinity relationships over the LATEX shelf. First, we used MCH M1 ~ M8 (April, 2004 ~ March, 2007) data to define each zone, except MCH M6 and M7 because there are missing data points due to environmental issues (hurricanes) during both cruises.

Figures 21 and 22 shows the boundaries of the three zones using nutrient/salinity relationships and applying the RC02 model to the data. The nutrient/salinity relationship is higher near the Mississippi and Atchafalaya River mouths than offshore owing to the high nutrient concentrations and low salinity water that are discharged. Based on observational data and Equation 1, we set the slope of the nutrient/salinity relationship line in the brown zone as being 3. As we mentioned in section 3.2.1, the green and blue zones were set by DIN concentration of 1 ~ 5 μM for the green zone and less than 1 μM for the blue zone because nutrient concentrations were too low in both zones. Especially, data from both M3 and M5 cruises showed no brown zone in sub-region C near the Atchafalaya River (Figures 21 and 22). It seems that the river water was rapidly mixed during discharge within Atchafalaya Bay. In addition, from these results we can initially see where the water masses flow and mix. For instance, in MCH M4 cruise data, the boundary of the green zone in sub-region A, located near the Mississippi River, continuous to in sub-region B between the Mississippi and Atchafalaya rivers.

Note that these ranges vary by a factor of two or more in other regions such as the coastal sea off Korea because the input functions (i.e., the nutrient concentrations in the rivers) and advection, coupled with strong tidal effects, will be different. In addition, there may be high nutrient input sources from the SGD or AN-D that will also cause changes in the relationship in other regions.

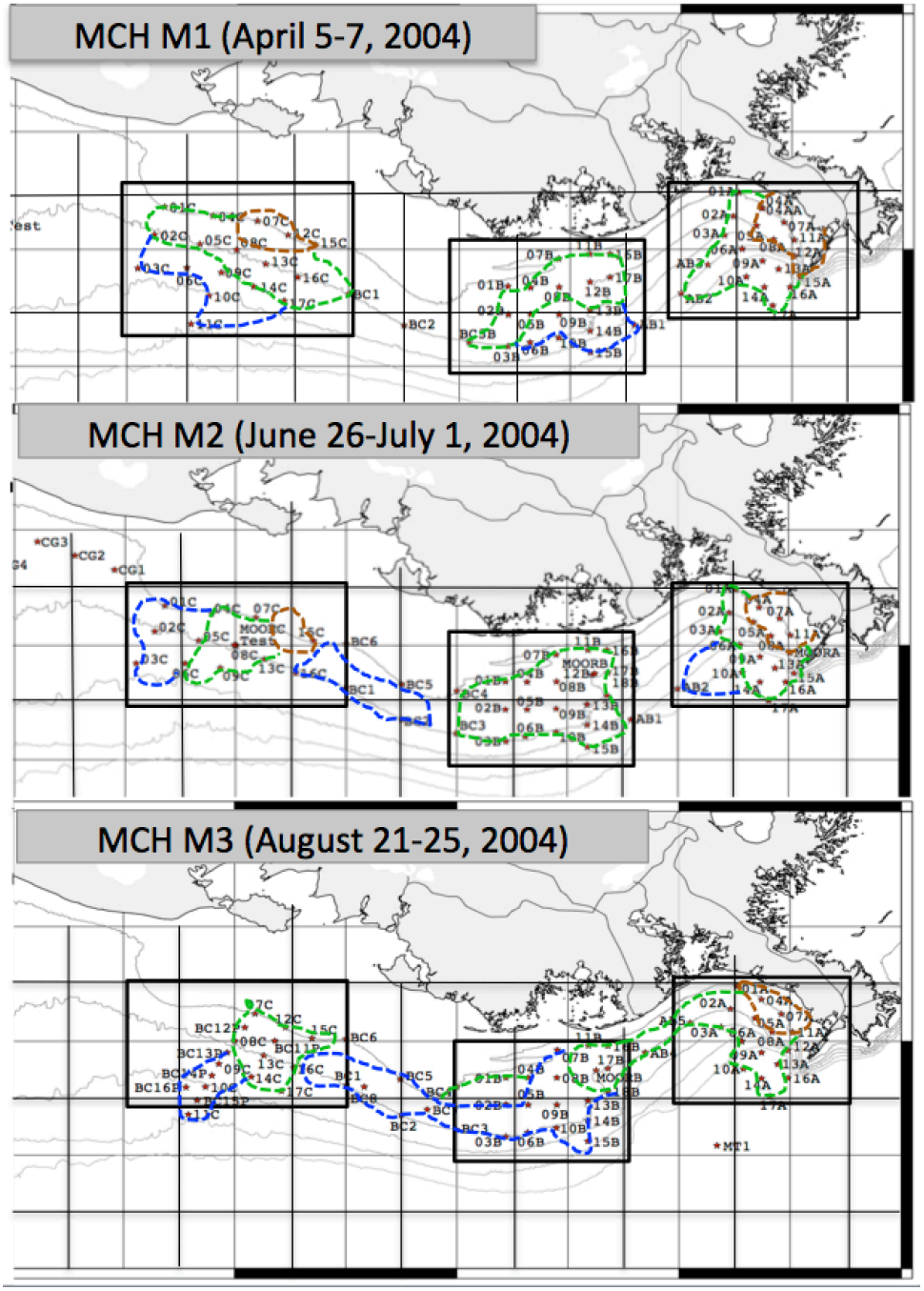

Figure 21. Identifying the edge of three zone using the nutrient/salinity relationships during MCH M1 to M3. The cruise data conducted from April 2004 to March 2007. The slope of nutrient/salinity relationship line in the brown zone as being 3, in the green and blue zone were set by DIN concentration 1 ~ 5 μM for the green zone and less than 1 μM for the blue zone.

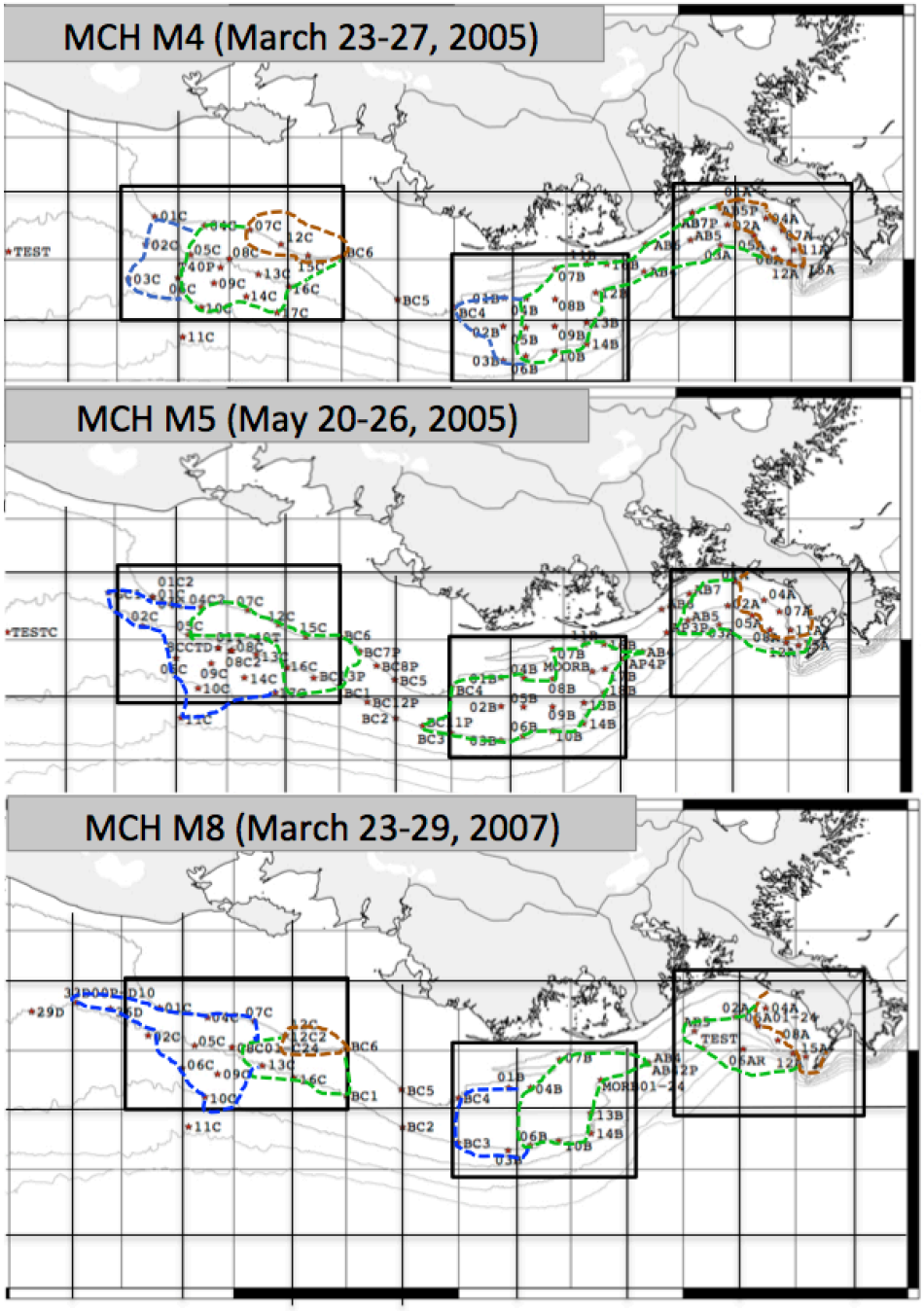

Figure 22. Identifying the edge of three zone using the nutrient/salinity relationships during MCH M4 to M8 except M6 and M7. The cruise data conducted from April 2004 to March 2007. The slope of nutrient/salinity relationship line in the brown zone as being 3, in the green and blue zone were set by DIN concentration 1 ~ 5 µM for the green zone and less than 1 µM for the blue zone.

3.4 Discussion

Salinity and temperature are well known as water mass conservative tracers in the ocean (Boyle et al., 1974; Mamayev, 1975). Nutrient concentration also shows a linear correlation with salinity because of conservative mixing between freshwater and coastal seawater in the coastal ocean (Loder and Reichard, 1981; Pujo-Pay et al., 2006; Wu et al., 2016). Due to the limitation of temperature/salinity relationship, which only can explain the physical processes in the ocean (Boyle et al., 1974), several studies used a nutrient/salinity relationship to analyze water masses and predict biological processes in the ocean (Desmit et al., 2015; Liss, 1976; Kim et al., 2011). Our study also used nutrient/salinity relationship to identify the water sources in the coastal GOM. Also, this study quantified the edges of the RC02 three zones in the GOM and the CSK and compared our results with those from Lahiry (2007).

Lahiry (2007) applied DO and salinity components to the RC02 hypothesis to define the edges of the zones in the coastal GOM. The limited simulation results from Lahiry (2007) indicated similar patterns to our results that used nutrient/salinity relationships such as in MCH M1 (April 5 ~ 7, 2004) and M3 (August 21 ~ 25, 2004) data near the Mississippi River mouth (Figures 21, 22, and 23). This region showed more conservative mixing than further west because the low salinity water with high nutrients was less diluted with offshore water (Figure 23). Thus, either using DO and salinity relationships or nutrient and salinity relationship shows similar boundaries in this region.

However, her results mainly resulted in different boundaries of the three zones compared with our results near the Atchafalaya River and between the Mississippi and the Atchafalaya river region (Figure 22). In particular, the results near the Atchafalaya River were very different (Figures 21, 22, and 23). It seems that the data were sampled further away from the Atchafalaya

River and there was mixing in the Atchafalaya Bay. However, our results showed the green zone further away from the Atchafalaya River. This seems that using nutrient and salinity relationships can cover more complex biological processes occurring with two different water masses mixing, which the Lahiry (2007) method cannot cover. Therefore, we believe that using nutrient and salinity relationships to differentiate three different zones is a more sensible way to look at biological processes in the GOM than the previous study from Lahiry (2007).

In addition, when we applied our method on small scales to the MCK and SRE (section 3.3.6), where there is also high nutrient input from river discharges to the coastal ocean, the results showed a clear pattern and we could see more clearly how biological activities led to sinks or excess sources. In particular, owing to the high nutrient concentration from the Keum River that is supplied to the MCK region (Lee and Yang, 1997; Lim et al., 2008), the data showed a clear pattern in brown zone. However, for the green and blue zones it was still hard to determine where the boundary between them (Figure 19). This was a similar problem with the GOM data during some cruises.

In the SRE, however, which is an estuary system where the water mixes conservatively (Kim et al., 2010), the boundaries of the three zones were clearly identified. This may result from factors such as the different size of each region in the GOM, MCK, and SRE, or from different forcing factors, different water masses, and strong tidal exchange, which leads to rapid water mass mixing. Also, SRE data showed that there was non-conservative mixing during summer due to biological uptake, while during the winter there was conservative mixing. For these reasons, in the green zone, the nutrients ranges were different between the GOM and the SRE. Moreover, the SRE system is a much simpler than that of the GOM and the MCK, so mixing processes are far less important.

Still, it is hard to define the physical edges of each zone because water is always moving (not at steady state). In any future study to quantify the RC02 three zone hypothesis, we need to collect enough data to cover large spatial scales such as the GOM or choose a small-scale region or estuary, since we found a clearer pattern in the SRE than in the coastal ocean regions of the GOM or the MCK. We believe the RC02 model contributes future study in a small-scale size of estuary system. Also, we need to do more comparison with other methods such as the N-mass balance model described in Chapter IV to define more realistic physical boundaries. Therefore, these results led us to produce a N-mass balance model to determine not only where the edge of each zone is, but also how the areas of the zones, together with their associated primary production and organic carbon fluxes, vary with different nitrogen input factors.

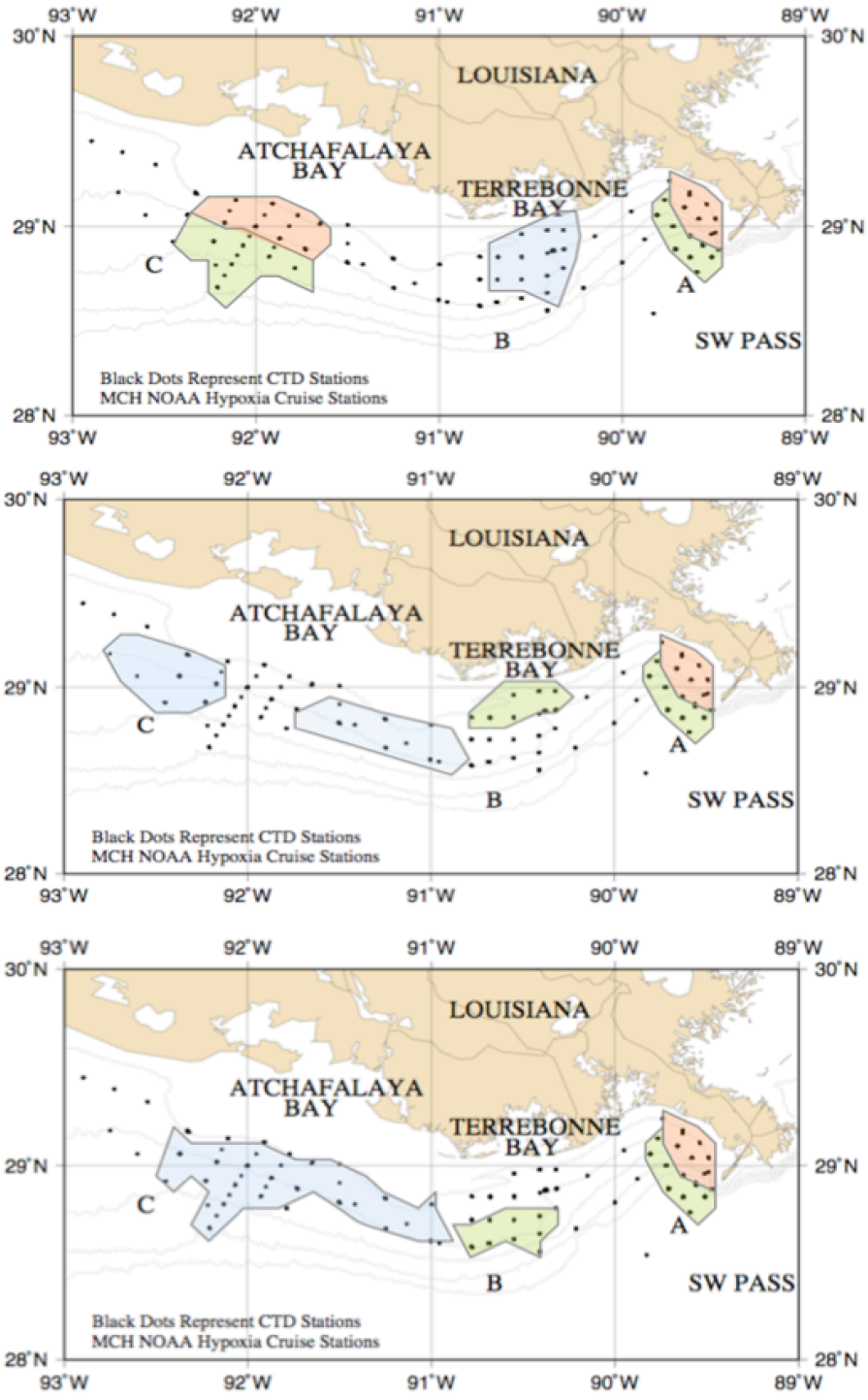

Figure 23. The results from Lahiry (2007) for the April (MCH M1), June (MCH M2), and August 2004 (MCH M3) cruises were based solely on salinity data. Areas shaded in brown, green and blue represent the Brown, Green and Blue zones respectively.

CHAPTER IV

HOW NITROGEN FLUXES AFFECT PRODUCTIVITY IN THE GOM AND KOREAN COASTAL WATERS

4.1 Introduction

The mass balance model is a useful tool to calculate nutrient or carbon fluxes and to estimate production in the coastal ocean (Kim et al., 2011). This model can provide us a better understanding of biological mechanisms that lie behind data observations. However, in the GOM, except for Bierman et al. (1994), who used a mass balance model to estimate carbon flux and oxygen exchange, most productivity has been measured by the ^{14}C method (Lohrenz et al., 1999; Quigg et al., 2011). Also, most model studies in the GOM have been based on numerical or simulation models to predict the size of the hypoxic zone.

In previous model studies (Fennel et al., 2006, 2011, 2013; Green et al., 2008; Hetland and DiMarco 2008; Justic et al., 2002; Scavia et al., 2004; Rowe et al., 2002), the authors used only limited data sets even though they called them physical, biological, or biogeochemical models. For instance, Scavia et al., (2004) used oxygen data to determine the parameters of their model. However, this model had no forecasting ability and could only be used in hindcast mode and even then, each year had to be treated separately. The benthic respiration biological model from Rowe et al. (2002) was also driven by local temperature and oxygen concentrations. Fennel et al., (2006) used nitrogen components to describe their biological model and extend the dissolved oxygen data into their new biochemical model (Fennel et al., 2013).

In our study, however, we used our N-mass balance model with more than 20 years of nutrient data, especially DIN (Dissolved Inorganic Nitrogen) and DSi (Dissolved Silica) data, to

calculate potential primary production rate, which is related to overall oxygen demand. We focused on nutrient data and produced a simple nutrient mass balance model with two depth layers and on/off shore sections to not only test the RC02 three zone hypothesis but also identify the edges of the three zones and how they vary over time.

It is hard to isolate the RC02's three zone boundaries, or even the presence of two different water masses, using nutrient/salinity relationships with summer data due to high biological uptake during summer. Thus, in this chapter, we use a N-mass balance model to identify the edges of the three different zones in the GOM and compare them to previous results from Lahiry (2007), who used salinity and DO initially. Also, the N-mass balance model was applied to the CSK to investigate whether the three zones can be identified there and compare how different input sources control primary production.

The big difference between previous model studies and this study is that we consider increasing AN-D and estimate future potential biological production and carbon fluxes with our model based on historical nutrient data. Also, we calculate potential oxygen demand using stoichiometry ratios. Thus, our model can be used to evaluate which factor among N loading from the river, AN-D, or benthic inputs can change carbon cycling in each box. Finally, we compare the results from Chapter III, in which we used nutrient/salinity relationships, with our N-mass balance model as a way to identify the three different zones.

4.2 Methodology: N-mass balance model

Our model consists of three sub-regions based on sampling location (Figure 24), and each sub-region contains a series of small boxes each one-quarter degree square (Figure 25), as followed by Belabbassi (2006). The quarter degree boxes in this study were separated into an upper box and a lower box, based on pycnocline depth, to estimate potential production, which we counted as an estimate of carbon flux. Theoretically, above the pycnocline, the primary production (PP) is higher than below the pycnocline layer (Anderson 1969; Sigman and Hain, 2012), which means that the two layers have different biological processes. The difference of PP between upper and lower boxes also depends on freshwater discharge rate and seasonal variation.

The N-mass balance box model is modified from previous models to calculate the net removal of DIN inside each box, which represents a potential primary production (PPP) (De Boer A.M. et al., 2010; Kim et al., 2011) (Equation 2).

$$\boldsymbol{F_{Atmo}^{DIN}} + \left(\boldsymbol{C_{Box}^{DIN}} \times \boldsymbol{A_{Bott}} \times \boldsymbol{F_{River}}\right) + \boldsymbol{F_{Bott}^{DIN}} - \left(\boldsymbol{C_{EX}^{DIN}} \times \boldsymbol{V_S} \times \boldsymbol{\lambda_{Mix}}\right) = \boldsymbol{F_{Removal}^{DIN}} \text{ – Eq. 2}$$

where $\boldsymbol{F_{Removal}^{DIN}}$ is removal by biological production, $\boldsymbol{F_{Atmo}^{DIN}}$ is the flux from atmospheric nitrogen deposition, which we consider the input term of the AN-D. $\boldsymbol{C_{Box}^{DIN}}$ is the DIN concentration in each box, $\boldsymbol{A_{Bott}}$ is the bottom area of each box, which we divided by quarter degree square size, and $\boldsymbol{F_{River}}$ is river discharge rate; these three factors are calculated for riverine N input. Also, $\boldsymbol{F_{Bott}^{DIN}}$ is the benthic diffusion, another input term. The output terms for water mixing are calculated from these factors; $\boldsymbol{C_{EX}^{DIN}}$ is the difference in DIN concentration between adjacent boxes, $\boldsymbol{V_S}$ is the water volume of each box, and $\boldsymbol{\lambda_{Mix}}$ is the mixing rate of each box to box. The details of the model definitions are given below in Table 8 and Figure 25. For instance, each arrow indicates input

(blue) and output (red) terms (Figures 24 and 25). Note that input/output terms were changed based on whether the boxes were above/below the pycnocline layer.

In the box above the pycnocline layer, there are two input terms; 1) Riverine N, and 2) atmospheric nitrogen deposition (AN-D) while the output terms are; 1) The exchange rate between each box (obtained by calculating different N concentrations between the east/west boxes and the on/offshore boxes), and 2) Removal by biological production (assuming that any other removal factors are neglected). We tested the RC02 three zone hypothesis in the upper box layer, in which we can also examine the horizontal influence (horizontal extent) of the river plume based on production rates. In order to calculate the net removal of DIN in a box above the pycnocline layer, we used our N-mass balance model in Equation 3.

$$\boldsymbol{F_{Atmo}^{DIN}} + \left(\boldsymbol{C_{Box}^{DIN}} \times \boldsymbol{A_{Bott}} \times \boldsymbol{F_{River}}\right) - \left(\boldsymbol{C_{EX}^{DIN}} \times \boldsymbol{V_S} \times \boldsymbol{\lambda_{Mix}}\right) = \boldsymbol{F_{Removal}^{DIN}} \text{ – Eq. 3}$$

$$\boldsymbol{F_{Bott}^{DIN}} + \boldsymbol{F_{Sink}^{DIN}} - \left(\boldsymbol{C_{EX}^{DIN}} \times \boldsymbol{V_S} \times \boldsymbol{\lambda_{Mix}}\right) = \boldsymbol{F_{Removal}^{DIN}} \text{ – Eq. 4}$$

However, below the pycnocline layer box, there are three input terms; 1) The benthic diffusion rate and 2) Vertical sinking from the box above the pycnocline layer, for which we used data from Qureshi (1995) while the output terms are; 1) The exchange rate between each box, and 2) Removal by biological production. We set the benthic diffusion factors as diffusion from the groundwater and nutrient regeneration by bacteria in the sediment and bottom water. However, there was no data on groundwater in the GOM. Thus, in equation 4, the benthic diffusion rate is synthesized from existing literature results (Rowe et al., 2002; Nunnally et al., 2014), and multiplied by the area of each box and the decomposition rate. To calculate the net removal of

DIN in boxes below the pycnocline layer, we used our N-mass balance model in Equation 4. Note that the benthic diffusion input term may be replaced by the SGD input term depending on region.

We calculated advective flow with riverine N input flux (where the water transport is generally from the east i.e., from near the Mississippi River, Sub-region A, to the west, near the Atchafalaya River, Sub-region C) during non-summer periods. During summer, the winds change direction from easterly to westerly, blocking the water flow to the west (Cho et al., 1998). We calculated advection flow from the LATEX current meter data (from April 1992 to December 1994) with U (west to east flow) and V (south to north flow) components (cm s^{-1}). Figure 26 indicates the mean values of coastal ocean current velocities. The range of the currents is 0 to 10 cm s^{-1}. Noted that these current velocities are not constant and change depending on time and day. However, we used the mean value of the current velocity for calculating the advective flow factor. In addition, we also calculated onshore/offshore movement flow as well.

As with a classic box model, we assumed four factors; 1) When we collected data, the study area is in a steady state condition, with equal input and output sources, 2) AN-D is evenly distributed across each area, 3) DIN is fully utilized by phytoplankton growth so we can neglect other removal factors, and 4) We consider biomass, which is measured by chlorophyll data in this region, as an actual primary production (APP). In this situation, we are ignoring denitrification, which leads to a loss of nitrogen from the system, and so our production numbers will likely be overestimated.

Because we assumed that this removed DIN is fully consumed by primary production, we can calculate potential carbon fluxes and oxygen consumption using the Redfield ratio ([C]: N: O: P = 106: 16: 138: 1). The PPP can be compared with real ^{14}C measurement data (Redalje et al., 1994; Lohrenz et al., 1998, 1999; Quigg et al., 2011) and dissolved oxygen data from MCH

mooring C (4/3/2005 ~ 7/10/2005) (Bianchi et al., 2010). Moreover, the PPP can be compared with the actual primary production (APP) measured as chlorophyll concentration (e.g. using chlorophyll to carbon ratio of 50: 1) (Riemann et al., 1989). Figure 24 shows the three sub-regions created by MCH (M1 ~ M8) sampling locations. Each small box is separated into an upper box and a lower box based on pycnocline depth defined by using a minimum Δ[DO] of 0.5 ml/L (Figure 25a).

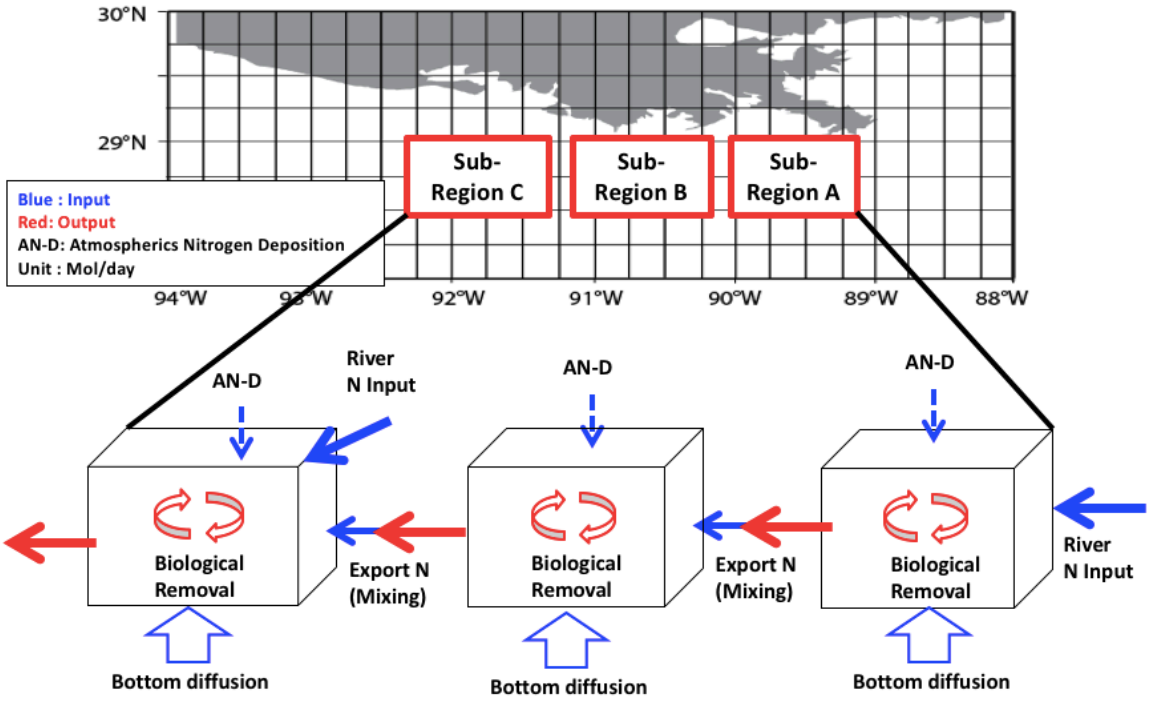

Figure 24. Each sub-region contains small boxes with quarter degree square size in a horizontal plane. Blue arrows indicate input terms and red arrows indicate output terms. The boxes are explained in more detail in Figure 25 a, which contains boxes above and below the pycnocline. Typically, for boxes above the pycnocline layer we considered input terms to be AN-D and Riverine N input, while, below the pycnocline we considered input terms to be bottom diffusion, which includes groundwater diffusion and in nutrient regeneration in the sediment (the benthic diffusion input term), vertical sinking, and riverine N input.

Table 8. The definition and values used in N-mass balance model to calculate DIN removal by biological production. (a) Each small box; (b) Wade and Sweet 2008; (c) Qureshi 1995.

Unit	Definitions	Value
A_{Bott} (m^2)	Area of box	6.2 X 10^8 m^2 (a)
C_{Box}^{DIN} (μM)	DIN concentration in each area (box)	
V_S (m^3)	Water volume of box	A_{Bott} X Pycnocline depth
C_{EX}^{DIN} (mmol m^{-3})	Different concentration between each box **C_{EX}= (C_{On} - C_{Off}) or (C_{East} – C_{West}) for DIN**	
λ_{Mix} (day^{-1})	Mixing rate of each box to box (**A reciprocal of the water residence time**)	
F_{Atmo}^{DIN} (mol day^{-1})	Diffusive flux from Atmospheric deposition (Bulk N deposition rate x A_{Bott} ($A_{surface\ of\ ocean}$) for DIN	1.4 X 10^5 mol day^{-1} (b)
F_{Sink}^{DIN} (mol day^{-1})	Vertical sinking of DIN flux from sediment trap data	0.1 ~ 1 gN m^{-2} day^{-1} (c)
F_{River} (day^{-1})	River discharge	
F_{Bott}^{DIN} (mol day^{-1})	Benthic diffusion from the bottom sediments	
$F_{Removal}^{DIN}$ (day^{-1})	Removal by biological production (**Assuming that the other removal factors are negligible**)	

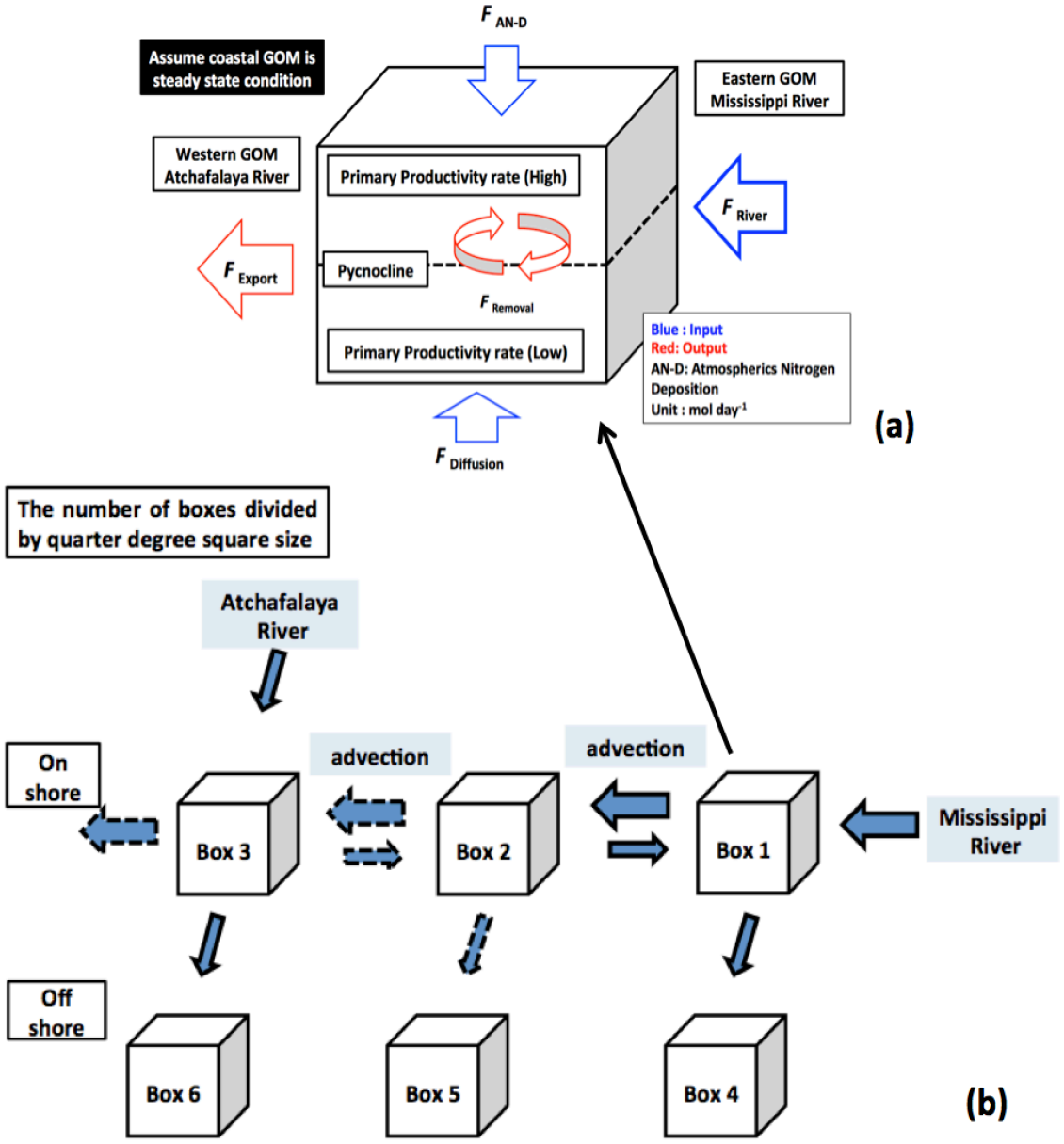

Figure 25. Figure (a) shows the input and output sources, which support the inventories of the new N-mass balance box model in the water column of the GOM (note that in this study, we only consider boxes above the pycnocline layer) and Figure (b) shows the concept of the number of boxes of quarter degree square size in a horizontal plane.

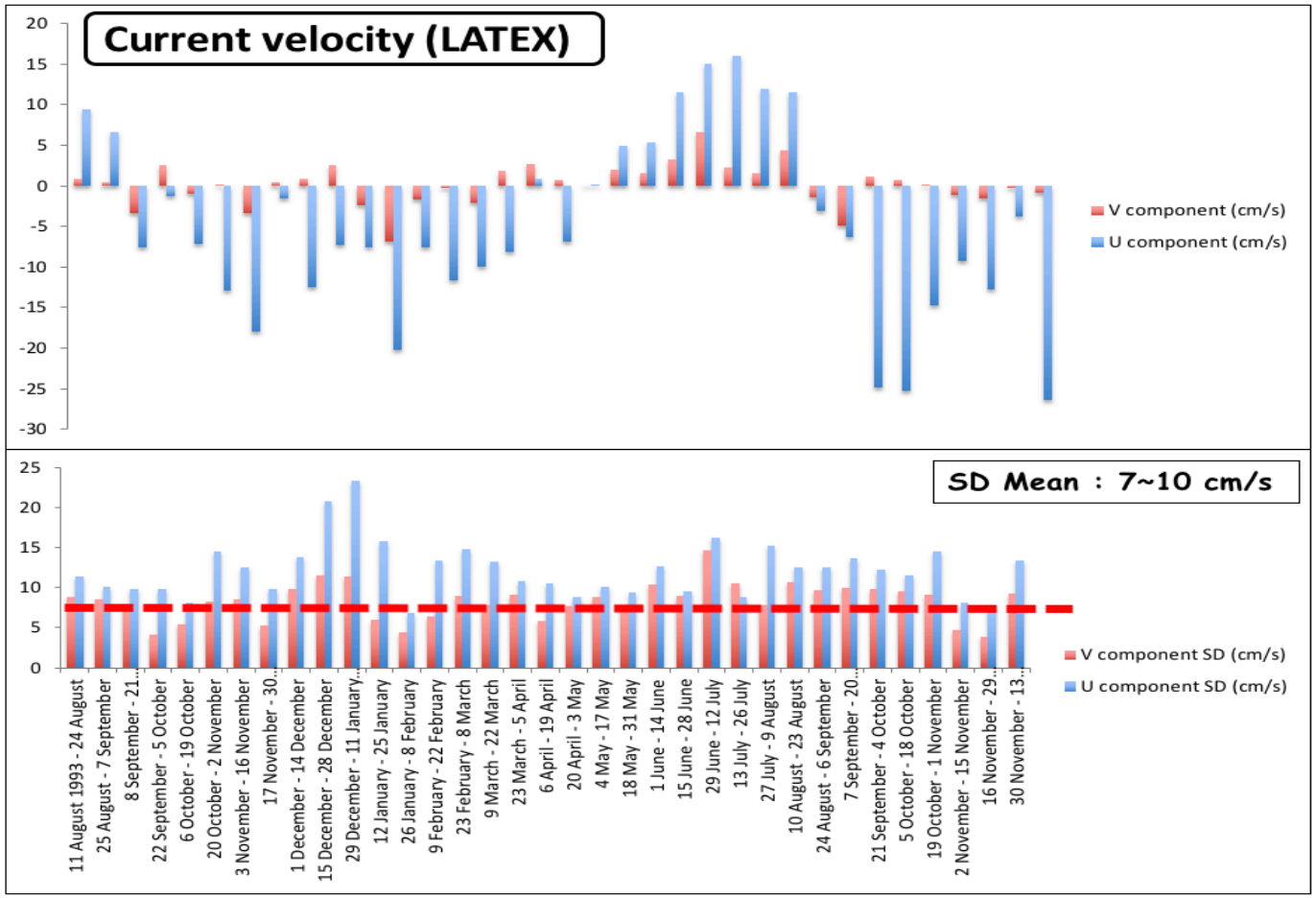

Figure 26. Mean ocean current velocity based on data from LATEX project.

4.3 Results: N-mass balance model to estimate coastal productivity

4.3.1 An N-mass balance model in the Texas-Louisiana Shelf

The existence of the three zones suggested by RC02 has been verified from winter data using nutrient/salinity relationships. Figure 27 shows the contour graph based on the mean concentration of DIN at each station during MCH M4 and LATEX H04 cruises. We calculated the mean [DIN] in each box, and then used the DIN/salinity relationship to define the edges of the three zones. Even where data were collected during different periods, near the coast salinity was consistently low, with high turbidity from the river water discharge. This was labelled the brown (river) zone.

We also estimated the PPP in the coastal GOM, using the N-mass balance model to estimate the carbon fluxes with different N input sources. The PPP rates near the river mouth were highest and we set the boundaries of production for each zone based on our N-mass balance model results. The PPP rate of the brown zone was over 2 gC m^{-2} day^{-1} because of the high input of N from river, AN-D, and benthic diffusion. We set the PPP rate in the green zone between 0.1 to 2 gC m^{-2} day^{-1} and that in the blue zone as less than 0.1 gC m^{-2} day^{-1}. These boundaries for each zone were based on mean [DIN] data. We also assumed that the AN-D input source was distributed equally to each area.

We identified the edges of the three zones above and below the pycnocline layer based on our N-mass balance model results (Figures 28 and 29). The boundaries above and below the pycnocline layer show different patterns for the edges of the zones, which RC02 did not determine. We considered the vertical sinking flux based on sediment trap data from Qureshi (1995) below the pycnocline layer to estimate PPP. High nutrient concentrations are supplied from the river close to the river mouth, and the upper and lower parts of the brown zones are roughly the same

in only MCH M1 (April 2004) sub-region A. Except for the M1 data, the boundaries of the brown zone are different in each layer. In the green zones where the nutrient source is not fully supported directly by the river, additional sources of N from vertical sinking, AN-D, and benthic diffusion caused changes in the edges of the zones. Typically, in the blue zone where biological production is low, it assumes that vertical sinking is the major factor to change the lower layer boundary. However, most of the blue zones in MCH M1 ~ M8 were roughly the same above and below the pycnocline. So, it seems that vertical sinking terms are minor controlling factors on the production below the pycnocline layer or our sampling time is faster than the vertical sinking time as an additional nitrogen source for bottom layer production (Figure 29). Thus, we initially identified the horizontal influence of the river plume in the layer below the pycnocline and the variation in the boundaries of the three zones, which RC02 did not calculate, based on the observational nutrient data from a bottom layer and our N-mass balance model.

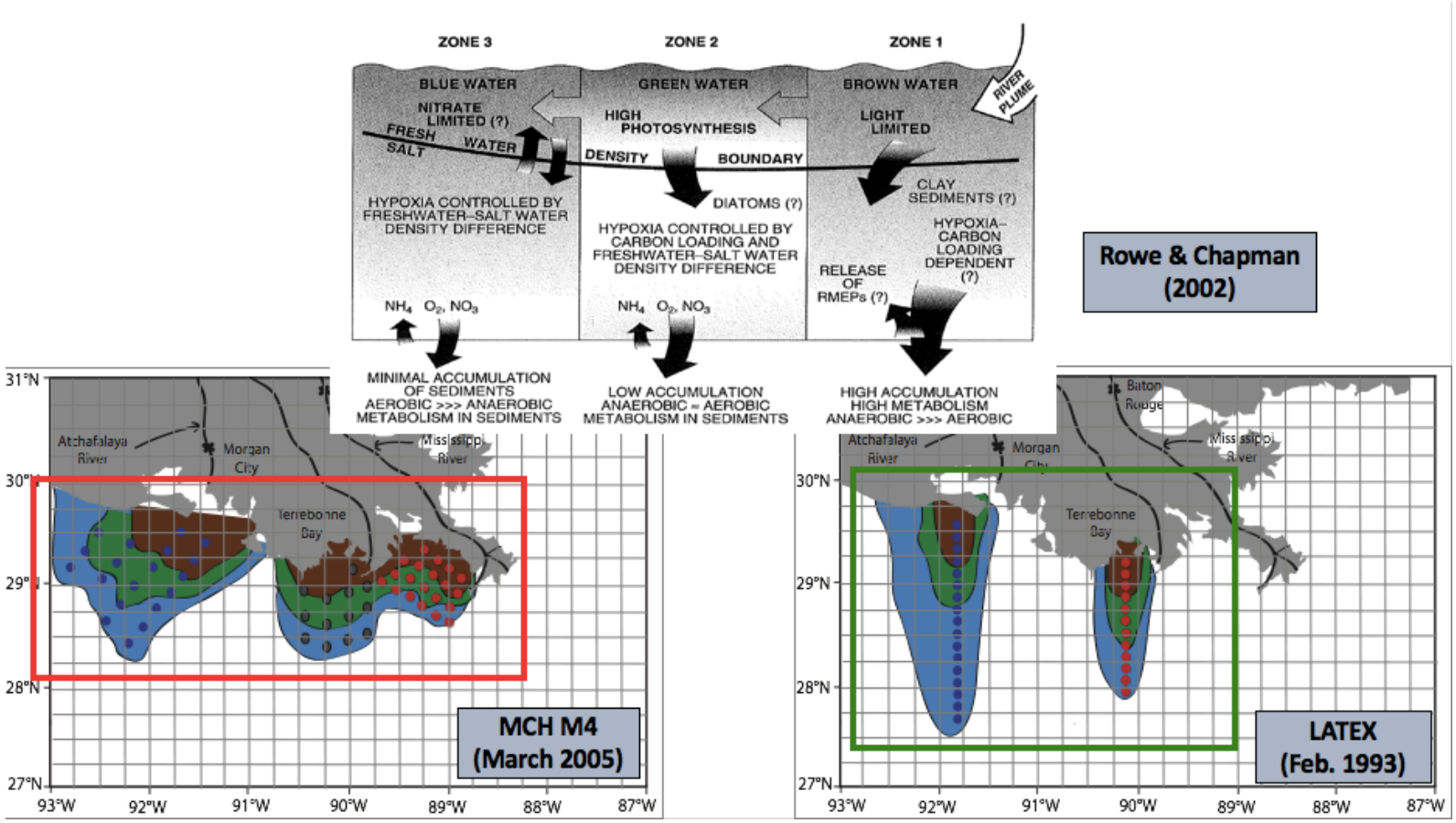

Figure 27. Extent of the three zones based on the mean concentration of nutrient (DIN) at each station during the MCH M4 and LATEX H04 cruises.

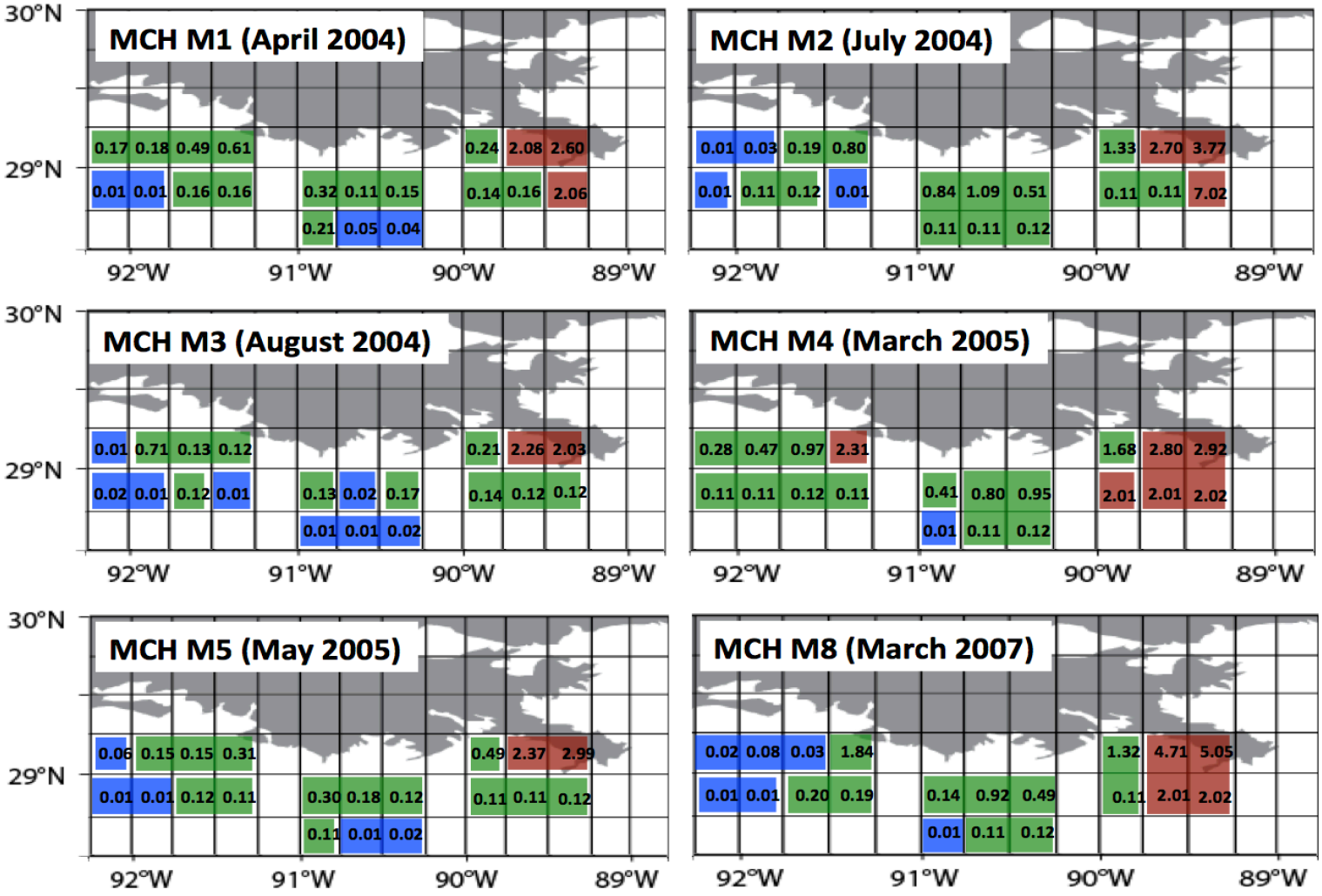

Figure 28. Areal distributions of the three zones using data from above the pycnocline, based on N-mass balance model results. Colors represent boxes found in each of the three zones. (Unit: gC m^{-2} day^{-1})

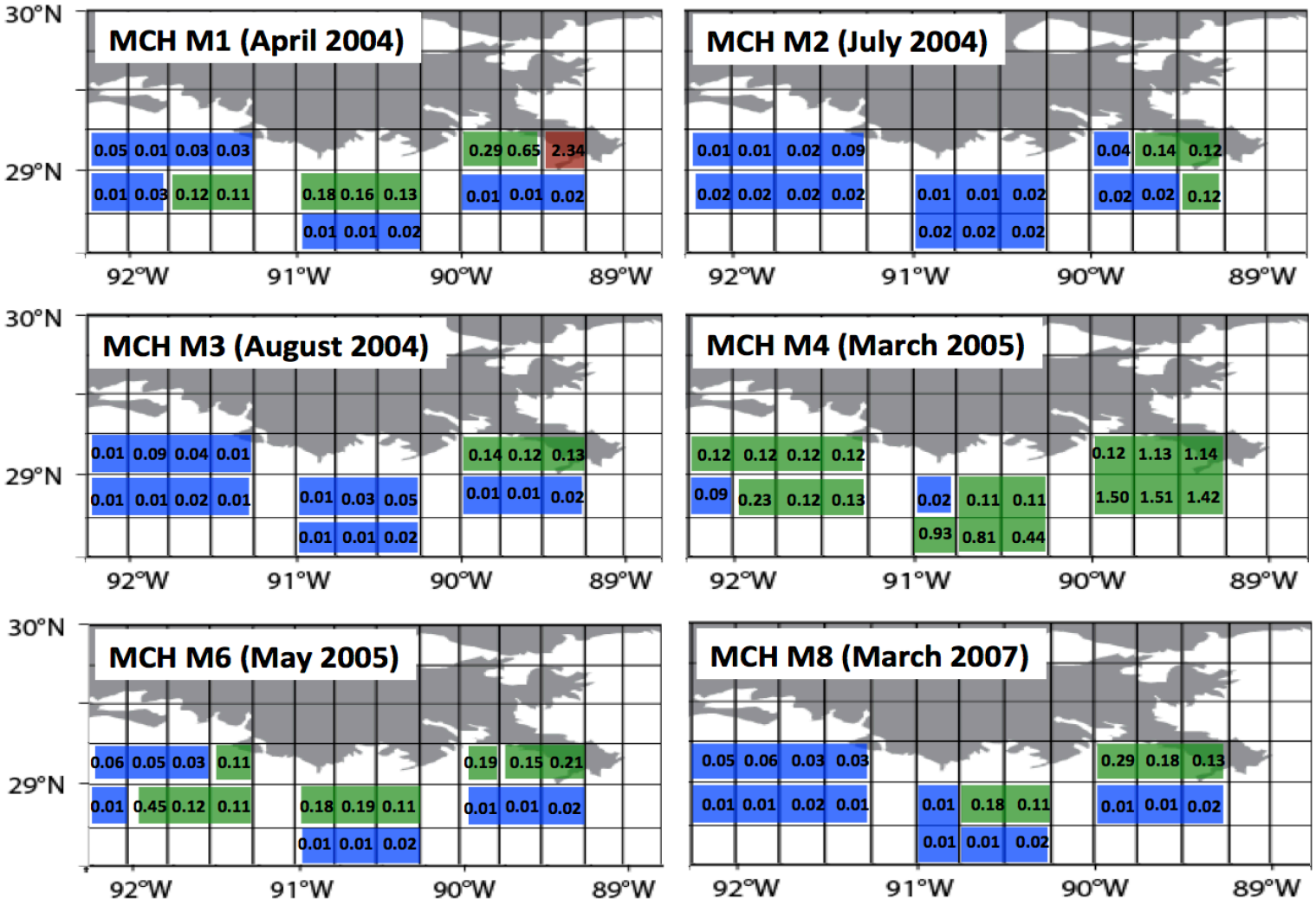

Figure 29. Areal distributions of the three zones using data from below the pycnocline, based on N-mass balance model results. Colors represent boxes found in each of the three zones. (Unit: gC m^{-2} day^{-1})

4.3.2 N-mass balance model calibration

The model calibration was done with previous literature data to check our model results would be sensible. We calculated the APP using a carbon to chlorophyll ratio of 50: 1 (Riemann et al., 1989) to compare with results from previous researchers. Literature data give PP rates in the coastal GOM of between 0.4 gC m^{-2} day^{-1} (winter) ~ 8 gC m^{-2} day^{-1} (summer) (Dagg et al., 2007; Redalje et al., 1994; Lohrenz et al., 1998, 1999). Also, Quigg et al. (2011) reported that the lowest integrated PP rates in 2004 on the outer part of the LATEX shelf were 0.07 gC m^{-2} day^{-1} (in March), 0.04 ~ 0.15 gC m^{-2} day^{-1} (in May), and 0.33 ~ 0.91 gC m^{-2} day^{-1} (in July).

The APP from cruises MCH M1 ~ M8 calculated using our model is reasonable based on comparison with previous research PP values (Table 9). Data from the MCH M2 cruise (June 26 ~ July 1, 2004) showed the highest APP in sub-region C, close to the Atchafalaya River input sources, while sub-region B showed the lowest APP. The APP ranges were similar to previous ^{14}C measurement PP values of between 0.04 ~ 0.91 gC m^{-2} day^{-1}. Our calculated APP were 0.28 ~ 0.48 gC m^{-2} day^{-1} in sub-region C, 0.11 ~ 0.25 gC m^{-2} day^{-1} in sub-region B, and 0.14 ~ 0.28 gC m^{-2} day^{-1} in sub-region A, respectively. Note that these ranges were calculated using only data from above the pycnocline and can vary depending on the carbon to chlorophyll ratio. Based on our model calculation, the PPP showed maxima in sub-region A (near the Mississippi river) and minima in sub-region B (between the Mississippi and Atchafalaya River) (Table 9). This is partly due to westward water flow as a result of the Coriolis effect and to wind direction reversals in summer that block the water flow to the west. Also, production decreased as a result of declining nutrient concentrations because nutrients are taken up by biological production while the water flows to sub-region B.

In sub-region C, MCH M4 (March 2004) had the highest PPP among the all MCH cruises. This probably depended on high nutrient concentrations being present during the winter period, when the region was affected by Atchafalaya River nutrient input. The difference between the APP and PPP is that APP was calculated from measured chlorophyll data, while PPP was calculated with our box model that assumes all nutrients were utilized by biological production (Table 9). In addition, we initially calculated the oxygen demand only for the MCH M1 data based on the Redfield carbon to oxygen stoichiometry ratio (106:138), and this shows us the overall oxygen balance near the coastal GOM (Table 11).

Table 9. The actual primary production (APP), which represent biomass and potential primary production (PPP) calculated from the upper layer box data. Note that in this study we assumed that all the chlorophyll concentration could be converted directly to production rates, which we considered as APP. APP is calculated with a carbon to chlorophyll ratio of (50: 1) to compare with previously published results (Dagg et al., 2007; Quigg et al., 2011) and PPP is calculated with the N-mass balance model.

Cruise	Sub-Region C		Sub-Region B		Sub-Region A	
	APP	**PPP**	**APP**	**PPP**	**APP**	**PPP**
MCH M1 (April 5-7, 2004)	0.28	0.22	0.23	0.15	0.23	1.21
MCH M2 (June 26-July 1, 2004)	0.48	0.19	0.11	0.46	0.14	2.50
MCH M3 (August 21-25, 2004)	0.33	0.17	0.15	0.06	0.16	0.81
MCH M4 (March 23-27, 2005)	0.33	0.71	0.15	0.40	0.28	2.24
MCH M5 (May 20-26, 2005)	0.30	0.12	0.25	0.12	0.18	1.03
MCH M8 (March 23-29, 2007)	0.36	0.33	0.17	0.30	0.18	2.54

4.3.3 Model scenarios in the Gulf of Mexico (GOM)

We tested the sensitivity of the model to changes of input/output parameters such as increasing AN-D and decreasing riverine N input. Assuming the model is robust, we investigated three model scenarios based on our model calibration (Table 10). In the first scenario, we cut riverine N input 60% based on the action plan goal of 5,000 Km^2 for the hypoxic area and increased the AN-D input by a factor of two based on increasing N emission predictions (Duce et al., 2008; Kanakidou et al., 2016; Lawrence et al., 2000; Paerl et al., 2002; He et al., 2010; Kim et al., 2011); this allowed us to determine the contribution of AN-D to the entire region instead of having only limited N input from the river. All the other N input terms except AN-D were decreased. Also, the AN-D input term is going to be affected by wind and this can ultimately affect carbon cycling. In the second scenario, we doubled the amount of AN-D as in scenario 1 and decreased riverine N input by 30% based on the hypoxia management plan goal (Hypoxia Action Goal Plan Report, 2005, 2008; Rabalais et al. 2009). In the third scenario, we increased riverine N input by 20% assuming the failure of the hypoxia management plan goal (Failed reference policy) while we set the AN-D amount equal with the first and second scenarios.

Figures 30 ~ 35 show representative model scenario results based on MCH M1 ~ M8 cruises. Each box number indicates the rate of PPP (gC m^{-2} day^{-1}) calculated by our N-mass balance model. Note that AN-D and benthic diffusion rates are fixed in our model scenarios due to data limitation. Based on our N-mass balance model calculation and model scenarios, we can initially estimate carbon fluxes from our PPP rate.

As can be seen in the scenario results for MCH M1 data (Table 11), the riverine N input source is still the major controlling factor in the coastal GOM region even when it is greatly reduced and the AN-D source is doubled. For instance, if we fail to reduce riverine N input in

future (increase riverine N input up to 20%), the potential carbon fluxes will increase by 17% of current conditions based on our scenario 3 results. In contrast, the AN-D input source only increased to 5% of total input terms and this indicates that AN-D input is still a minor factor in the GOM (Table 11). All the data from MCH M1 ~ M8 showed the same sort of variability as Figure 30 and details of how in each term varies are listed in Table 11. Note that in this model study, we used AN-D data only from Wade and Sweet (2008) as there are not enough AN-D data in the GOM. Furthermore, we calculated the overall oxygen demand based on the Redfield stoichiometry ratio, which has a carbon to oxygen ratio of 106:138 (Table 11). If the production is increased, overall oxygen demand will also be increased. The MCH M1 scenario result indicated that the overall oxygen demand would increase approximately 21% if we fail to reduce riverine N input.

Our model cannot predict the area of the hypoxic zones. Instead of the prediction, our model can investigate the effects of potential flux changes of each factor, such as AN-D, riverine input, or benthic diffusion, and calculate the overall oxygen balance for the region. These results still suggest that reducing nutrient inputs from the river is critical for the hypoxia management policy in the GOM (Hypoxia Action Goal Plan Report, 2005, 2008; Rabalais et al. 2009).

Our model can be applied to another region, the Coastal Sea off Korea (CSK), where the riverine N-input is the primary source of hypoxia in the coastal ocean but AN-D is considerably more important. In the CSK, several studies have indicated that the AN-D concentration in approximately 10 times higher than in the GOM and that AN-D will be a major controlling factor in the future (Duce et al., 2008; He et al., 2010; Kim et al., 2011; Lawrence et al., 2000; Paerl et al., 2002). Thus, we applied our model to the CSK and compared the coastal production mechanism with that in the GOM.

Table 10. Investigated model scenarios and simulated changes imply deviations from the reference values used in the nominal model simulation.

Nominal Value	MCH M1-M8 cruise data and reference values in Table. 8
Scenario 1	Doubled increase in AN-D input and cut riverine N input 60% based on Action plan goal to 5,000 Km^2
Scenario 2	Doubled increase in AN-D input and 30% decrease in riverine N input based on Action Goal plan (Gulf of Hypoxia Task Force)
Scenario 3	Doubled increase in AN-D input and 20% increase in riverine N input based on failed reduce riverine N source from the fertilizer (Failed reference policy)

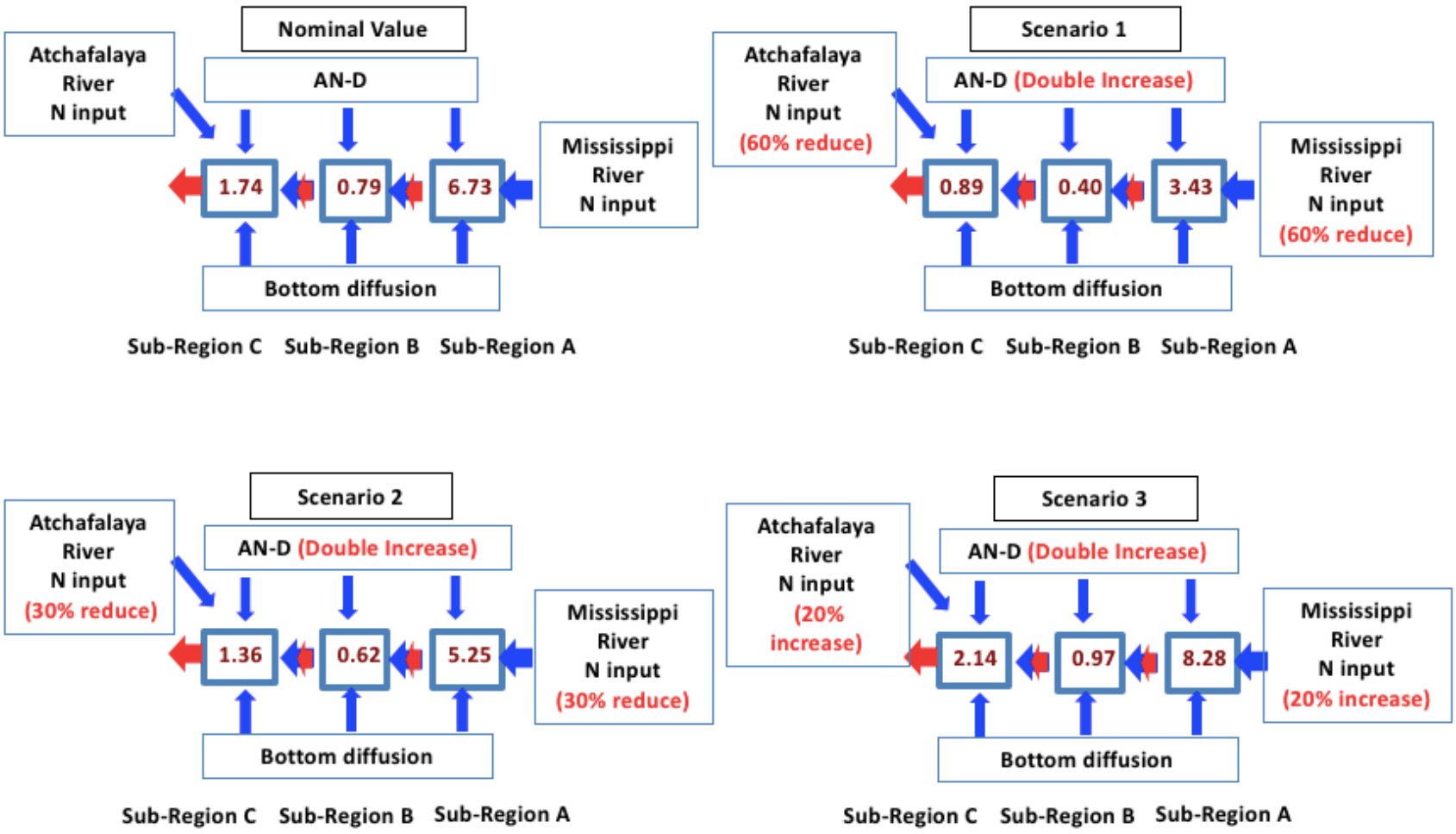

Figure 30. Representative Model scenario results based on MCH M1 (April 5 ~ 7, 2004) cruise. Each box number indicate rate of potential primary production (gC m^{-2} day^{-1}).

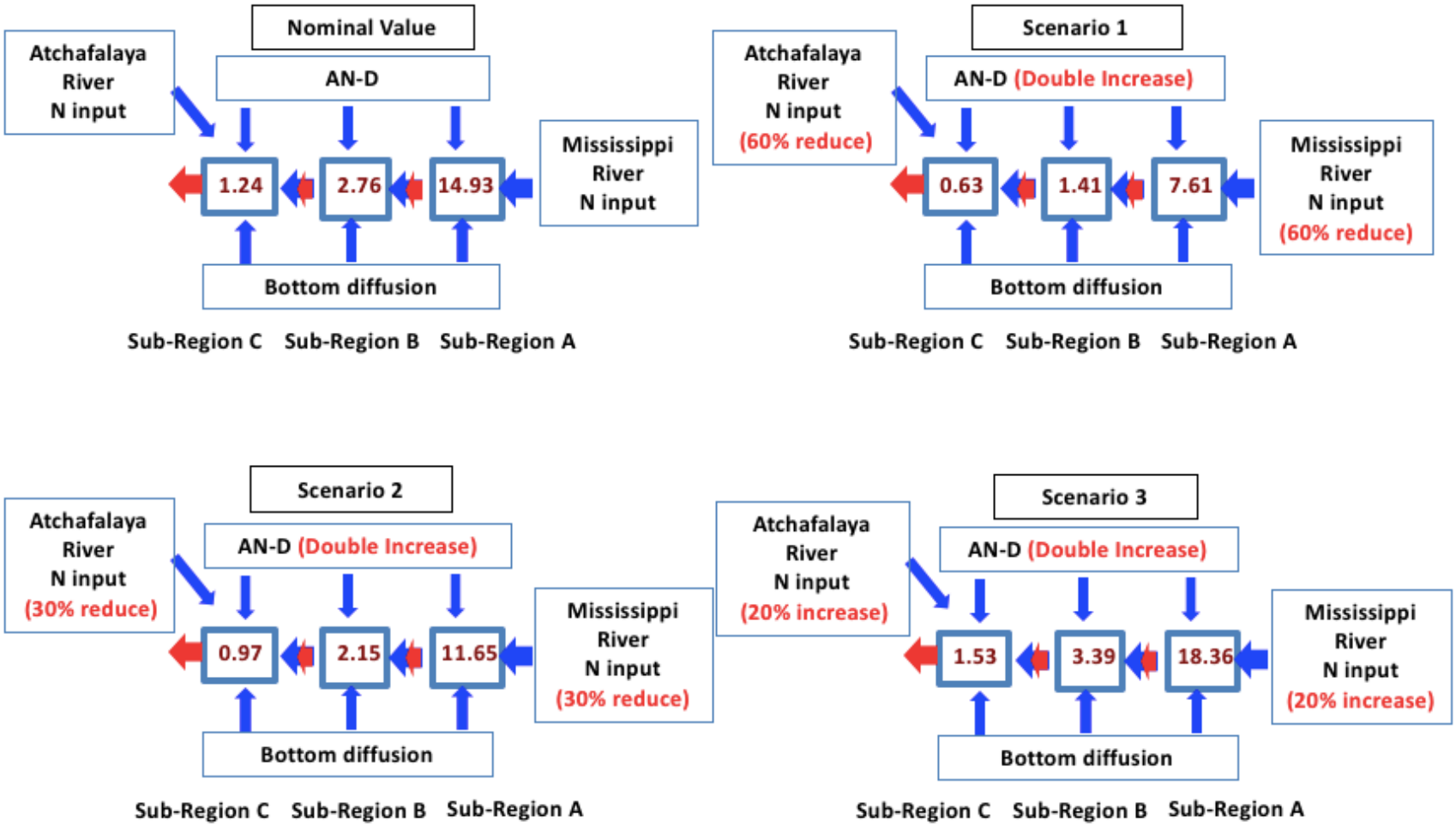

Figure 31. Representative Model scenario results based on MCH M2 (June 26 ~ July 1, 2004) cruise. Each box number indicate rate of potential primary production (gC m^{-2} day^{-1}).

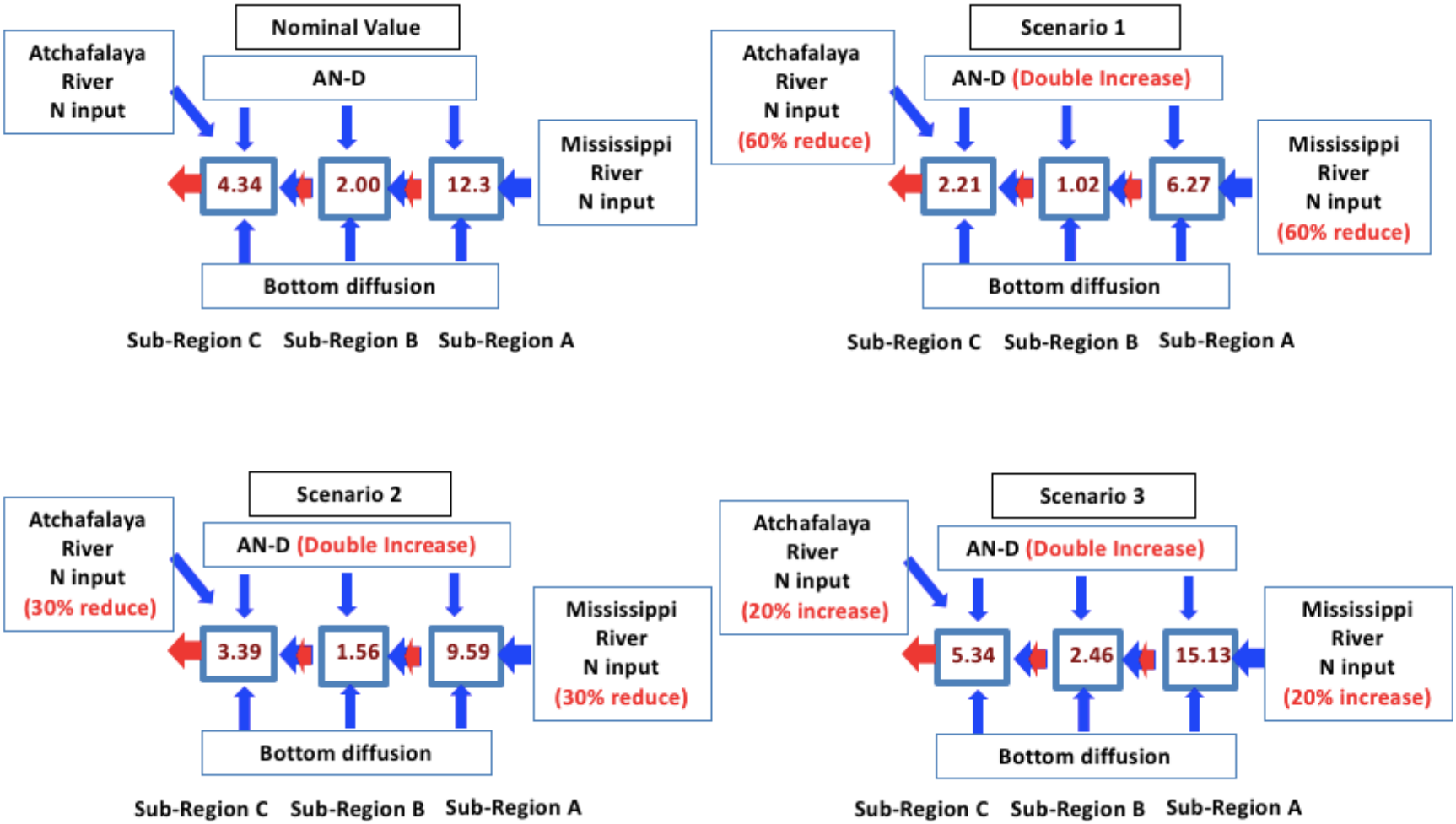

Figure 32. Representative Model scenario results based on MCH M3 (August 21 ~ 25, 2004) cruise. Each box number indicate rate of potential primary production (gC m^{-2} day^{-1}).

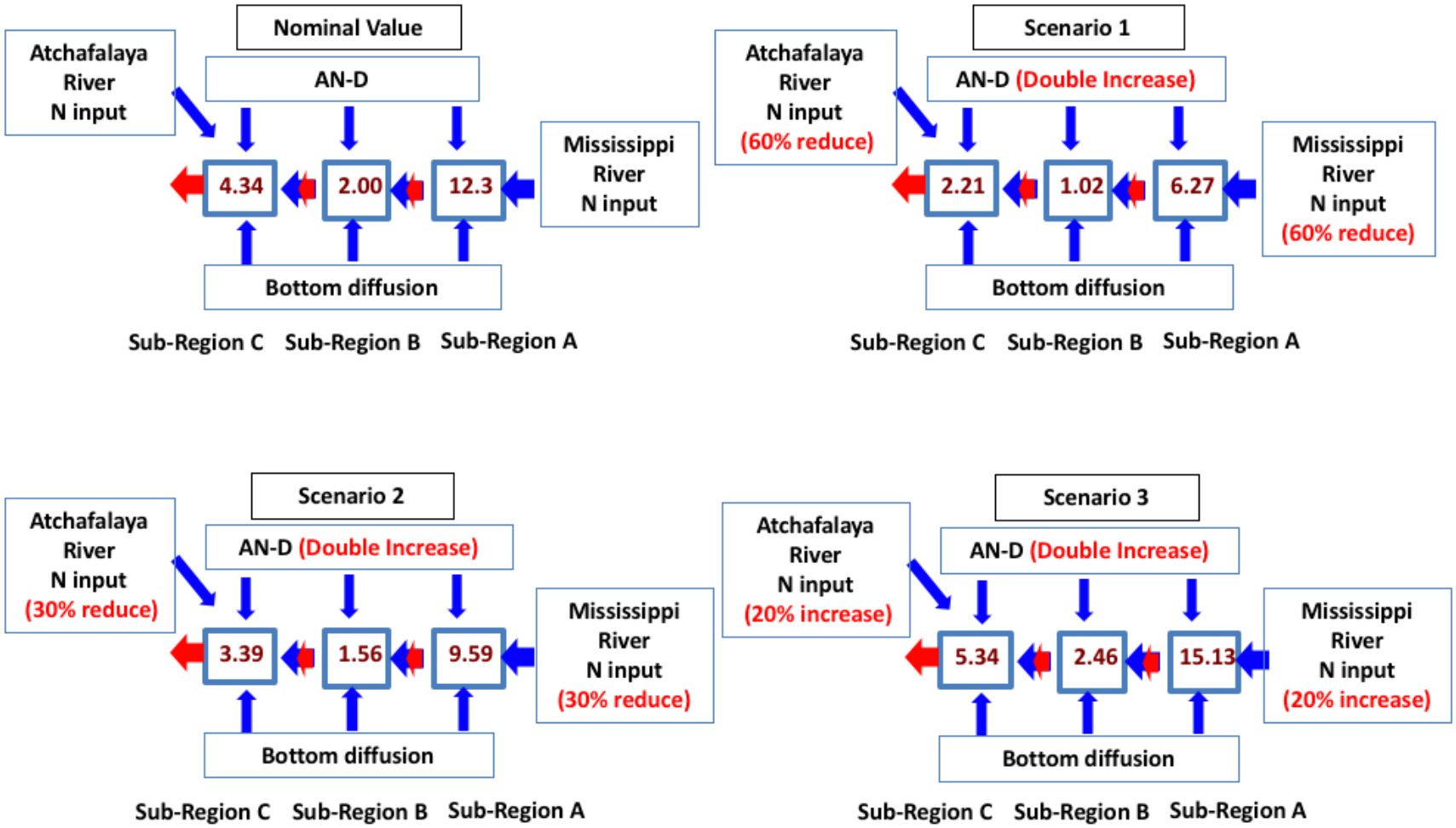

Figure 33. Representative Model scenario results based on MCH M4 (March 23 ~ 27, 2005) cruise. Each box number indicate rate of potential primary production (gC m^{-2} day^{-1}).

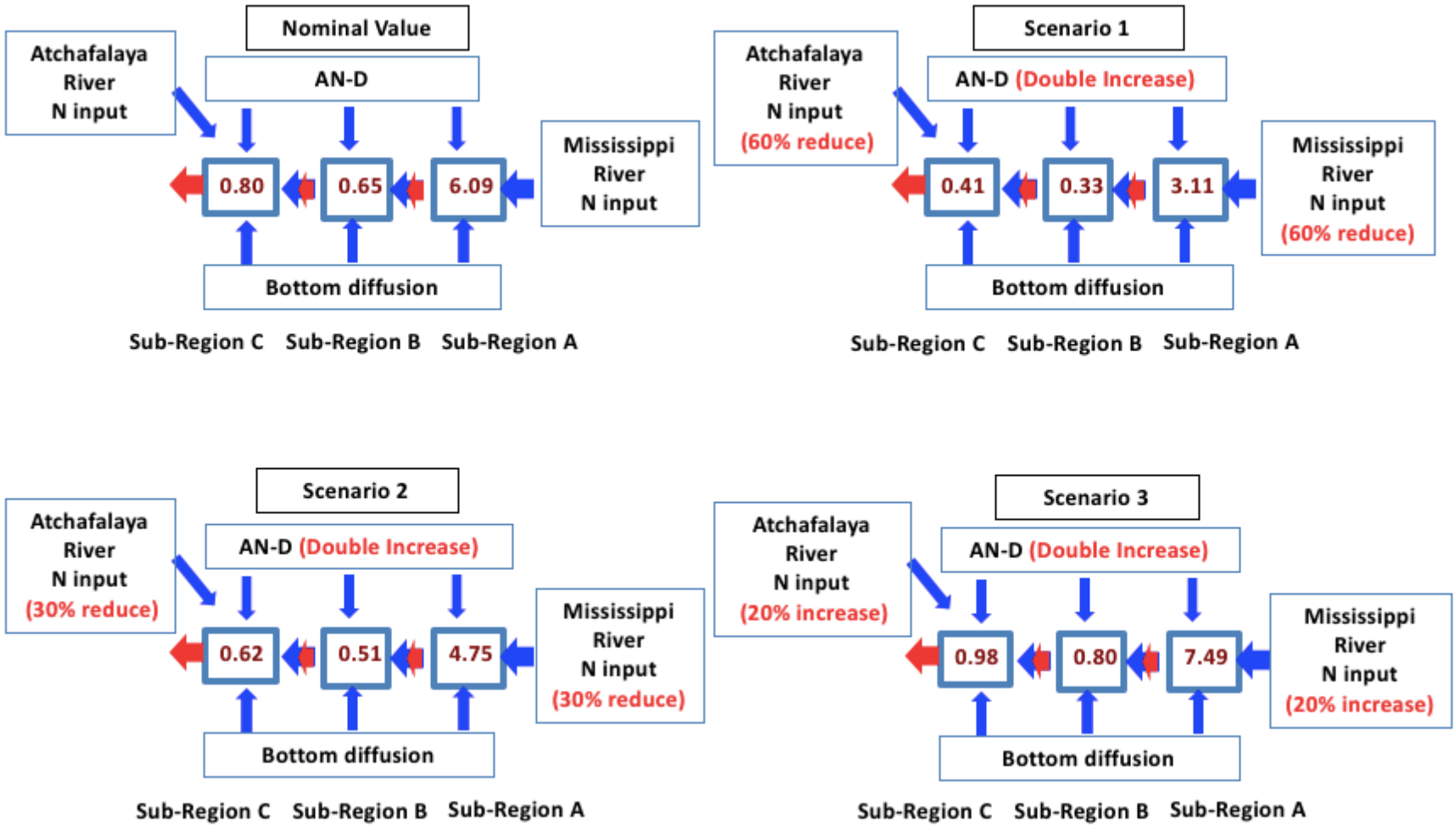

Figure 34. Representative Model scenario results based on MCH M5 (May 20 ~ 26, 2005) cruise. Each box number indicate rate of potential primary production (gC m^{-2} day^{-1}).

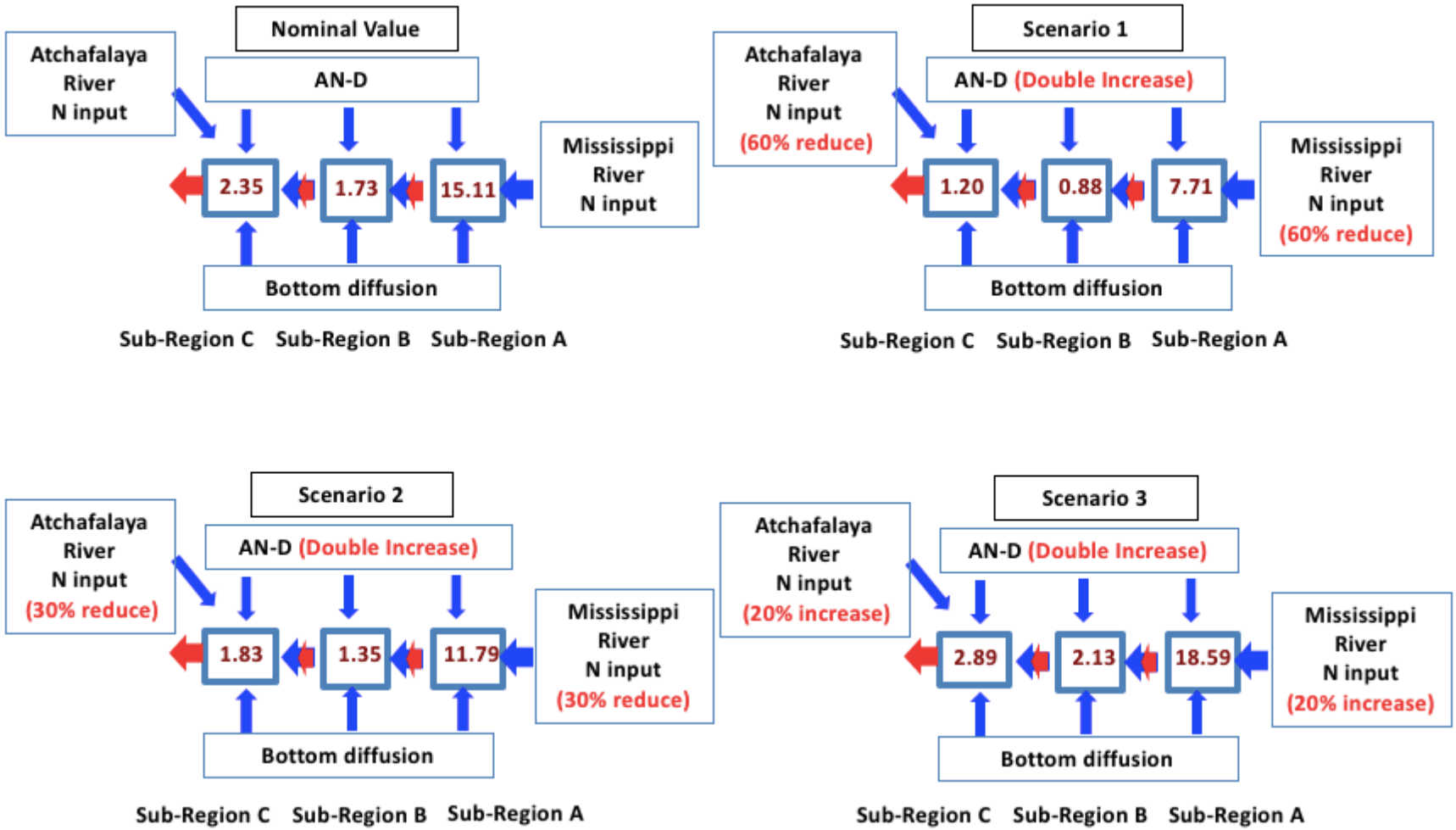

Figure 35. Representative Model scenario results based on MCH M8 (March 23 ~ 29, 2007) cruise. Each box number indicate rate of potential primary production (gC m^{-2} day^{-1}).

Table 11. Simulation results for selected model scenarios based on MCH M1 (April 5-7, 2004), as listed in Table 10. Biological production is calculated by our N-mass balance model. Also, oxygen demand is calculated by Redfield stoichiometry ratio (C: O_2 = 106: 138).

	F_{River}	$F_{AN\text{-}D}$	$F_{Bott/SGD}$	**Biological production**	**Oxygen demand**
Nominal Value	1.4×10^7 (~98 %)	1.4×10^5 (~1 %)	1.4×10^5 (~1 %)	Base line	
Scenario 1	5.6×10^6 (~93 %)	2.8×10^5 (~5%)	1.4×10^5 (~2%)	~45% decreased	~58% decreased
Scenario 2	9.8×10^6 (~96 %)	2.8×10^5 (~3%)	1.4×10^5 (~1%)	~22% decreased	~28% decreased
Scenario 3	1.7×10^7 (~97 %)	2.8×10^5 (~2%)	1.4×10^5 (~1%)	~17% increased	~21% increased

4.3.4 Means of checking methods in Gulf of Mexico (GOM)

From dawn to dusk, most of the organic matter in the ocean is produced or respired in situ by phytoplankton and bacteria. The DO concentration is enhanced by the phytoplankton production. Production occurs only during daylight, while respiration occurs during the whole day. This allows us to calculate net production and gross production. We modified equations 5 and 6 to estimate how much oxygen is used for regenerating nitrate for N uptake. The primary production equation includes light reactions which take place in sunlight; starting at Dawn) and dark reactions. To integrate oxygen changes between dawn and dusk for four Mississippi river plume regions, we used existing oxygen data from the 24-hour station measurements and calculated the net and gross primary production and respiration in the coastal GOM (Figure 36).

We used 1.25 as the carbon fixation primary production coefficient number based on the ratio 138 to 106 (O_2: C) and converted dissolved oxygen (DO) to carbon dioxide. We used a conversion number of 1.43 (coefficient number) to change O_2 unit as from ml/L to mg/m^2, when the sampling temperature was 20-degree. Each data set was integrated at 5 m depth intervals to estimate net and gross primary production (Figure 37). PP and organic carbon fluxes have rarely been estimated with continuous oxygen monitoring data. From equation 6, the regeneration of nitrate requires 36/138 of the total oxygen demand.

$$C_{106}\,(NH_3)_{16}\,H_3PO_4 + 138\,O_2 \rightarrow 106\,CO_2 + 16\,NO_3^- + H_3PO_4 + 122\,H_2O \quad \text{– Eq. 5.}$$

$$16\,NH_3 + 36\,O_2 \rightarrow 16\,NO_3 + 24\,H_2O \quad \text{– Eq. 6.}$$

This day-night difference represents uptake and regeneration with the stoichiometry between the two. Also, we suspect that there is loss of N from the system. The atomic ratio

between O_2 or C to DIN should be about 6.6; a higher value represents a loss of N. We focused on primary production and respiration within the euphotic zone equalized with an oxygen molar mass, which means that all carbon is produced by phytoplankton.

First, we calculated integrated primary production (IPP) using the difference between integrated O_2 values at dawn and dusk, while from dusk to the next dawn gives an estimate of the respiration. Thus, we integrated vertically to estimate IPP. The vertically integrated PP in MCH 24-hour continuously monitoring station was 3.22 ~ 5.71 gC m^{-2} day^{-1} during the 3 cruises near the Atchafalaya River and 2.71 gC m^{-2} day^{-1} near the Mississippi River, respectively (Figure 37 and Table 12). We compared the results from our N-mass balance Box model, which considered the layers above and below the pycnocline, and the two independent IPP (vertical and horizontal) results were very similar with its ranges (Table 12).

The MCH M8C vertical profiles for DO concentrations at dawn and dusk were very similar (parallel pattern) unlike the other MCH profiles. For this reason, we plotted salinity and DO concentrations as one-time series at each depth. Each depth is colored differently (blue at surface, red at 5m, orange at 10m, gray at 15m, and yellow at 20m depth). Secondly, we plotted the horizontal values at dawn and at dusk, which are shown in horizontal profiles (Figures 38 and 39).

In Figure 38, based on the salinity time series data, during cruise MCH M8C, there were two different water masses separated by a front that passed through the area at around 9:00 am. This water mass indicated that low salinity water from the coastal freshwater was replaced by higher salinity ocean water. Due to the existence of two different water masses, we plotted them separately (Figure 39 and Table 12). Apart from the MCH M8A data, we only have one-time series near the Mississippi River. We also integrated PP horizontally in the MCH M8A using DO concentration (Figure 40 and Table 12).

Using 24-hour continuous monitoring data we can estimate the gross production during the day from the net production from dawn to dusk and the mean respiration during the period from dusk to dawn of the next day. This assumes that respiration rate is constant throughout the 24-hour period. We compared the results of our organic carbon flux estimates from the double-layered N-mass balance model to with vertical and horizontal IPP estimates from DO data. The two-independent model (Vertical IPP and Horizontal IPP) results showed similar patterns of production (Table 13).

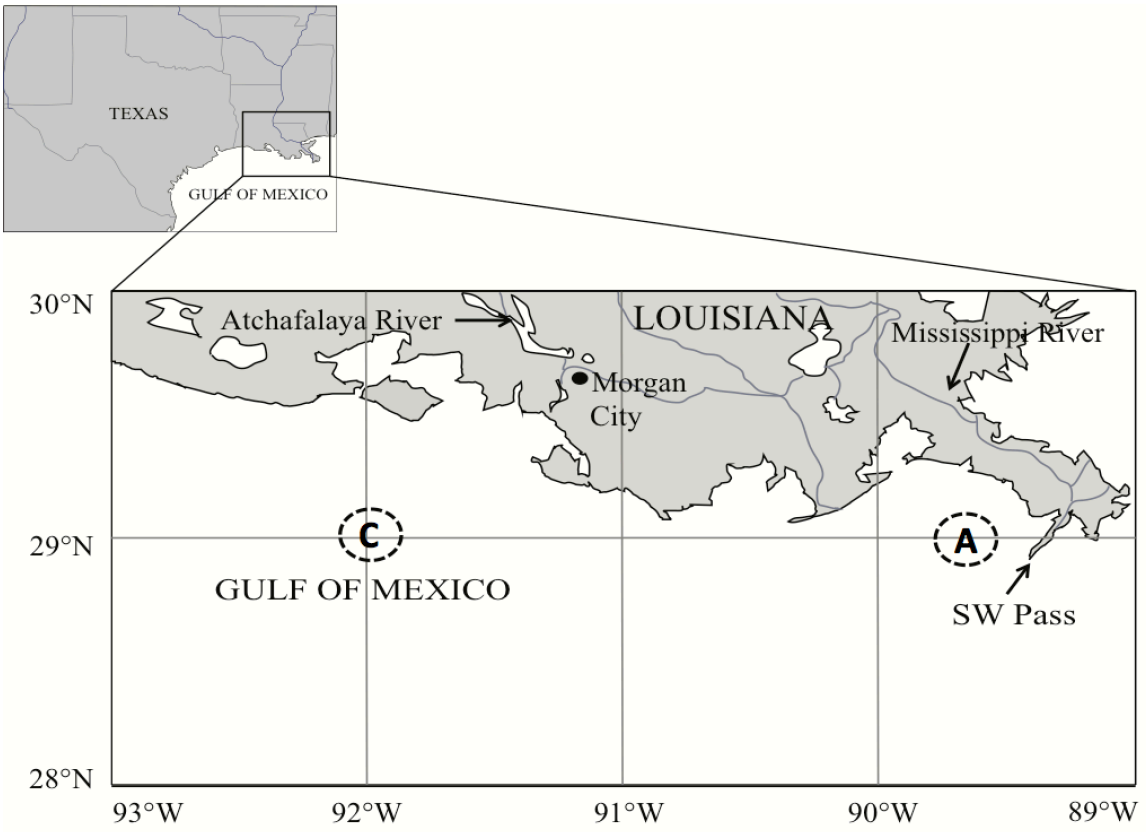

Figure 36. Dotted circles show the locations of 24-hour continuous monitoring stations during MCH M5C (May 24 ~ 25, 2005), M7C (August 23, 2005), M8A (March 23 ~ 24, 2007) and M8C (March 25 ~ 26, 2007), respectively. Station A is near the Mississippi River and C is near the Atchafalaya River.

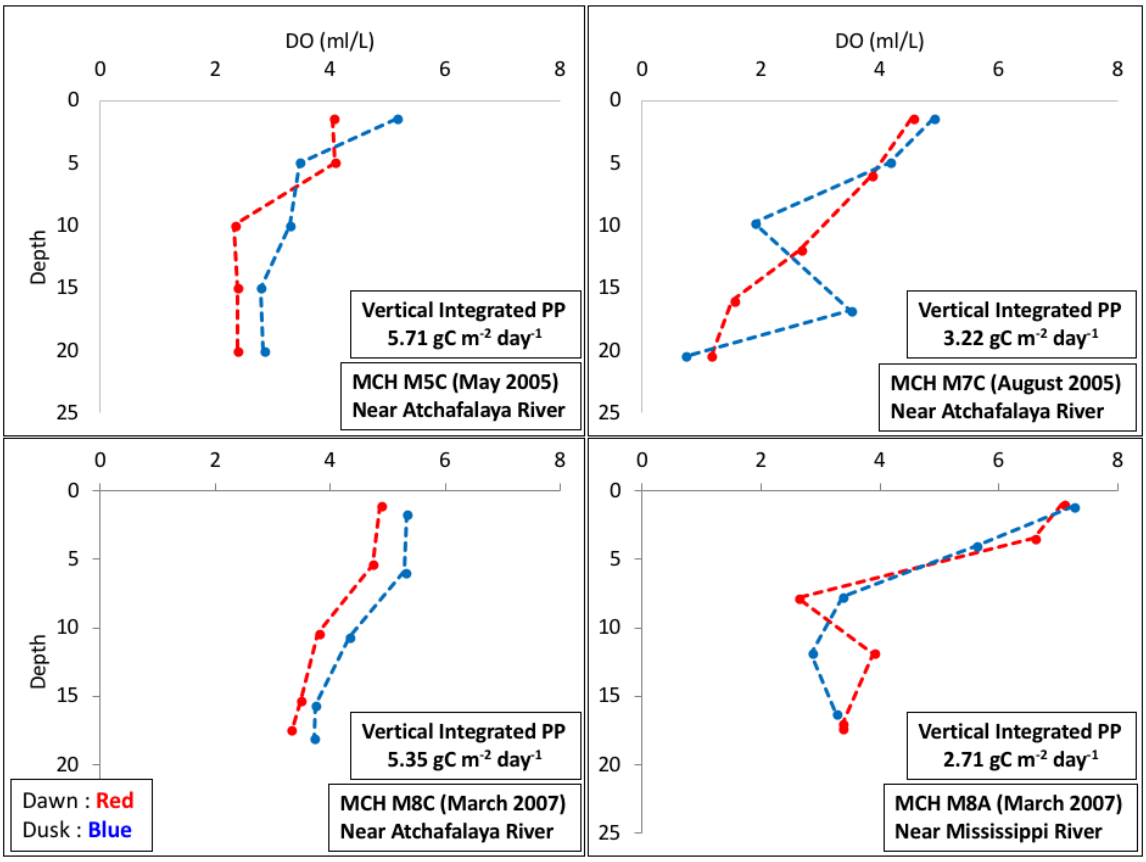

Figure 37. Vertical values at dawn and at dusk in MCH (M5 ~ M8), from which we integrated PP. Blue dot for dissolved oxygen data in dusk and red dot for dawn period.

Vertical integrated PP was calculated like this:

DO_d=1 – DO_d=5 = a O_2ml/L/day = 1.43*a mgO_2/L/day

= 1.43*a gO_2/m^3/day (d=5m) = 5*1.43*a g/m^2/day

= (5*1.43*a)/32 moles O_2/m^2/day = (5*1.43*1.25*a)/32 moles CO_2/m^2/day

= (5*1.43*1.25*12*a)/32 g CO_2/m^2/day

a=variable number

d=depth

Carbon fixation PP coefficient number= 1.25

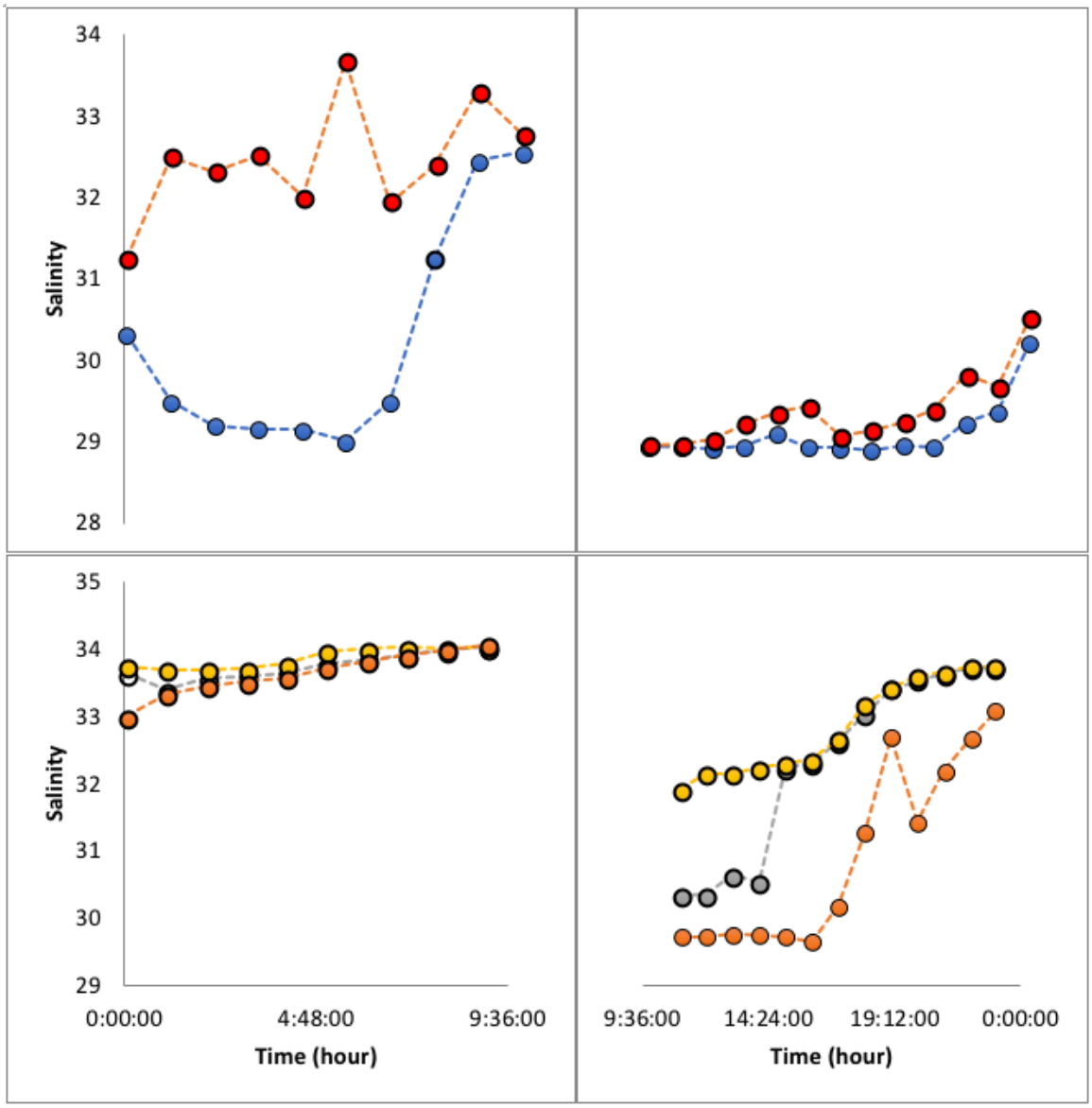

Figure 38. Salinity data during MCH M8C, which was close to the Atchafalaya River, were plotted for two different time periods during the 24-hour monitoring station time series. Each depth was plotted in a different color (Blue: Surface, Red: 5m, Orange: 10m, Gray: 15m, Yellow: 20m)

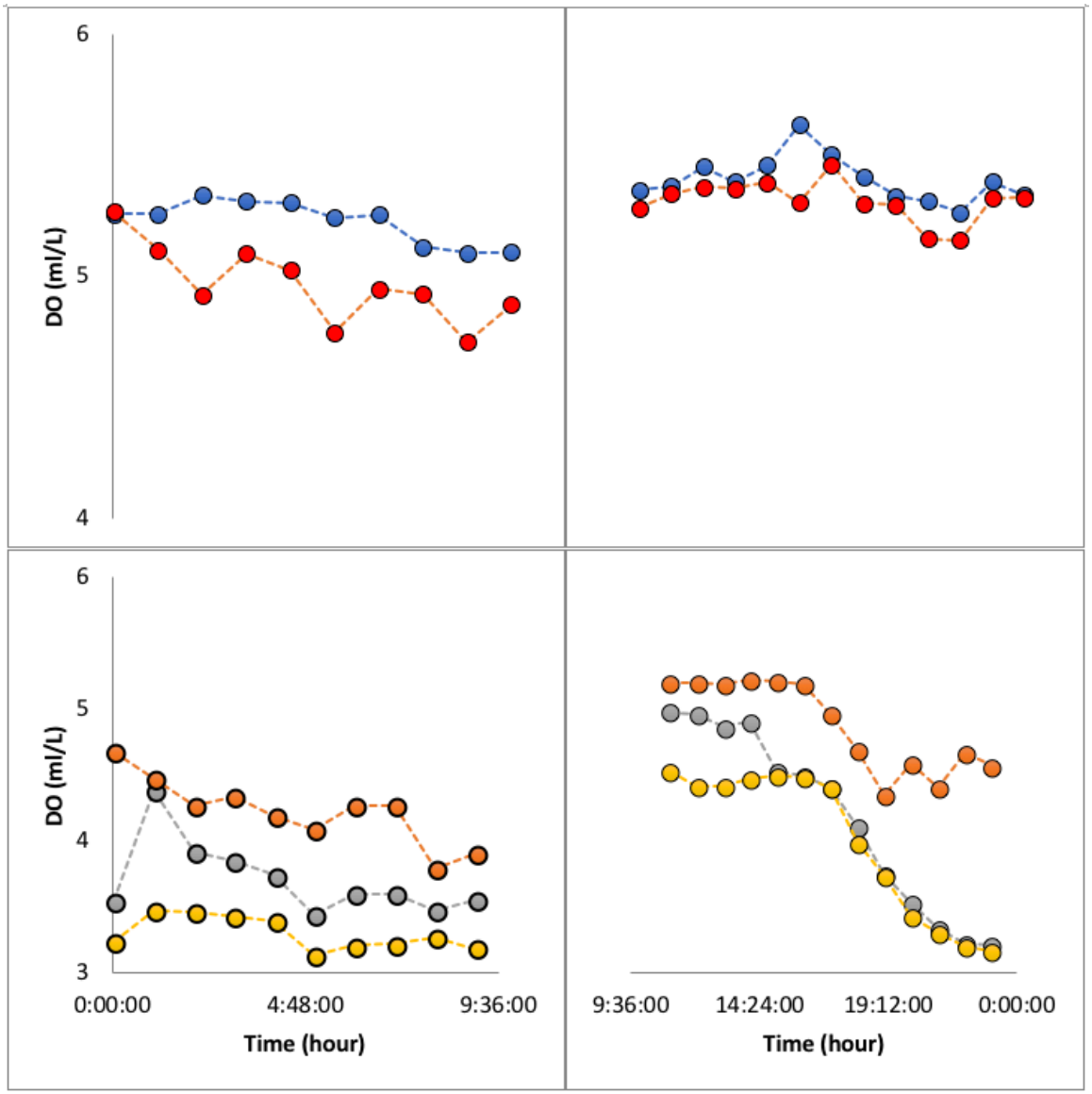

Figure 39. DO data during MCH M8C, close to the Atchafalaya River, were plotted for two different time periods during the 24-hour monitoring station time series. Each depth was plotted in a different color (Blue: Surface, Red: 5m, Orange: 10m, Gray: 15m, Yellow: 20m)

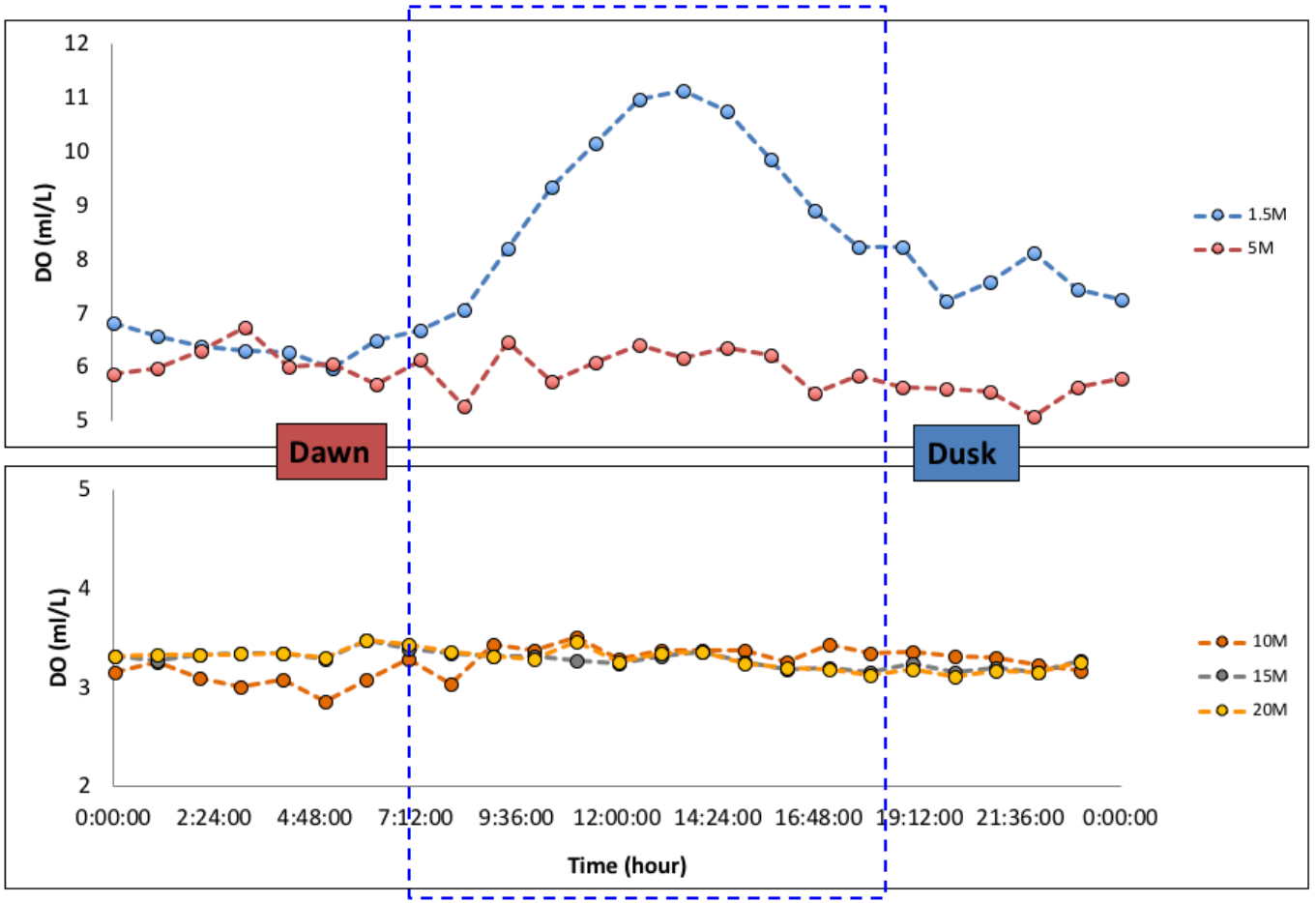

Figure 40. DO data in the time series at MCH M8A, close to the Mississippi River, plotted against time during the 24-hour monitoring station. Each depth was plotted in a different color (Blue: Surface, Red: 5m, Orange: 10m, Gray: 15m, Yellow: 20m).

Table 12. Two separate water masses moved close to the Atchafalaya River during the MCH M8C (March 2007) 24-hour continuous monitoring station. These two separate water masses, based on salinity changes, provide different estimates of net and gross primary production. During this cruise period, the low salinity water (< 30) might be discharging from the Atchafalaya River.

Salinity	Integrated PP (Each Water Masses)	Integrated PP (Dawn to Dusk)
> 30	0.5 gC m^{-2} day^{-1}	
		5.4 gC m^{-2} day^{-1}
< 30	5.6 gC m^{-2} day^{-1}	

Table 13. Different approaches of estimating primary production in the Northern Gulf of Mexico. Both vertical and horizontal integrated primary production (IPP) were estimates of net and gross primary production and respiration from integrated oxygen changes between Dawn and Dusk.

MCH Cruises	Integrated Primary Production (gC m^{-2} day^{-1})			
	Vertical	**Horizontal**	***Box Model**	**Previous findings**
M5C (May 2005)	5.7	5.1	4.2	****0.04-11.5 (Salinity 18~32)**
M7C (August 2005)	3.2	3.1	N/A	
M8A (March 2007)	2.7	5.1	5.7	
M8C (March 2007)-(a)	-2.4	N/A	2.3	
M8C (March 2007)-(b)	5.5	4.4		

* Estimate Gross Potential Biomass

** Lohrenz et al. (1998, 1999); Quigg et al. (2011)

M8C cruise has two different water masses, so was divided into (a) and (b) to calculate IPP individually.

4.3.5 An N-mass balance model in the Coastal Sea off Korea (CSK)

RC02 published their theoretical model, not only to explain hypoxia in the GOM but also more generally as an explanation of what affects production along river plumes. However, they did not quantify their model with nutrient data and no one has applied this model to another region. The coastal sea off Korea is another opportunity to test the RC02 hypothesis because we have data that include low salinity samples in this region. Currently, we have collected the historical data (Table 3) near the mid-western and southern parts of the coastal sea of Korea (Figure 4). Therefore, we examined and evaluated the theoretical model of RC02 in the southern and western ocean of Korea where freshwater with high terrestrial input mixes into the coastal ocean.

Around the mid-western and southern coastal area of Korea several major rivers discharge to the coastal sea (Lim et al., 2003, 2005, 2007, 2008; Kim et al., 2010, 2011). Conditions in the MCK near the Taean peninsula, where the two different water masses from Gyunggi Bay (Han River) and the Keum River mix together (Choi et al., 1998, 1999), are similar to the coastal GOM. However, the big differences between the CSK and the coastal GOM are the increasing AN-D inputs and nutrient inputs from groundwater discharge (Kim et al., 2010; Kim et al., 2011). In the CSK, the AN-D input might also be a more important source because the AN-D is fifteen times higher than in the GOM. Therefore, we compared how N input from AN-D controls carbon fluxes between the two regions through our N-mass balance model.

We used our N-mass balance model to estimate the PPP in the MCK and defined three different zones (Figures 41 and 42). Similar to the GOM region, the PPP rates were increased near the river mouth, and we set the boundaries of each zone based on our N-mass balance model results. Based on nutrient data, as was done for the GOM, we set the PPP rate of the brown zone at over 1.5 gC m^{-2} day^{-1} because of the high N sources from the river, AN-D, and benthic diffusion. We defined the green zone as having PPP rates between 0.3 to 1.5 gC m^{-2} day^{-1} and the blue zone as having rates of less than 0.3 gC m^{-2} day^{-1}.

Figures 41 and 42 shows that the boundaries of the three zones above and below the pycnocline layer were, roughly consistent. It seems that AN-D is consistently adding extra nitrogen to the surface ocean with the riverine N input. However, the brown zone in the upper layer in the MCK August 2008 cruise data was changed to the green zone below the pycnocline layer. This is due to the strong coastal tidal mixing. According to Lim et al. (2008), the physical mixing of freshwater from the Keum River and/or Gyunggi Bay with nearby coastal water mostly controls the spatial distribution patterns of nutrients and salinity. There is a strong tidal front off the Taean Peninsula during spring and summer. The tidal effects were felt not only close to the coastal region but also over the outer shelf of the MCK (Lim et al., 2008).

The AN-D input source is mainly coming from the China side of the East China Sea (ECS) and the boundaries of the green and blue zones were affected above and below the pycnocline. The offshore region, with low nutrient concentrations would normally be the boundary of the blue zone, however, over the outer shelf of the MCK, the upper layer was green zone but the lower layer was changed to the blue zone (Figures 41 and 42). This is also due to strong water mixing with different water masses in MCK region. In the blue zone offshore, four different water masses are mixed fast, and this affects how the zones are distributed above and below the pycnocline layer.

On the outer shelf of the MCK, the Yellow Sea Bottom Cold Water Mass (YSBCWM) brings high nutrient concentrations through upwelling, thus, this might affect our blue zone.

Based on MCK cruise data results, we can initially determine where the three different zones are in the MCK (Figure 43). We identified the brown zone close to the Keum River mouth and the green and blue zones further away from the coast of Korea. Through our scenario results, the AN-D is a considerable factor in the MCK as well as the riverine N input from the Keum river. We cannot apply our model to the Chinese side, owing to the lack of data from the Yellow River. However, we can assume that near the Yangtze river mouth, which has a large hypoxia zone during summer, there is a large brown zone and need to compare this with the GOM as well.

We also estimated the PPP in the SRE using our N-mass balance model and identified three different zones here as well (Figure 44). However, the area sampled in the SRE was considerably smaller than our other regions such as the GOM and the MCK and there were no benthic diffusion data. Due to these limitations, we compared our results in the SRE with those from a previous study to check the model sensitivity. Yang et al. (2005) measured PP rates in the SRE in February, August, and October 2001. They modified the ^{14}C method from Steeman-Nielsen (1952) and Parsons et al. (1984). Primary productivity ranged between 0.05 and 11 gC m^{-2} day^{-1}, and typically the highest productivity was found at salinities between 10 and 20. Also, this salinity range was affected by light limitation and low salinity water from river plume, which agrees with RC02's brown zone.

Using the N-mass balance model to estimate carbon fluxes in the SRE produces very similar productivity rates to Yang et al. (2005), despite the assumptions in our box model (Table

8). We only made calculations for the layer above the pycnocline, using equation 4, which has no benthic diffusion input term because there was no benthic diffusion data in the SRE. We defined the boundaries of the three zones in the SRE based on the MCK PPP rate; our model produced PPP rates in this region of 0.1 to 8 gC m^{-2} day^{-1} (Figure 44). Thus, in future we should collect the chlorophyll data to estimate the APP rate more accurately. This improves the agreement with the ^{14}C measurements.

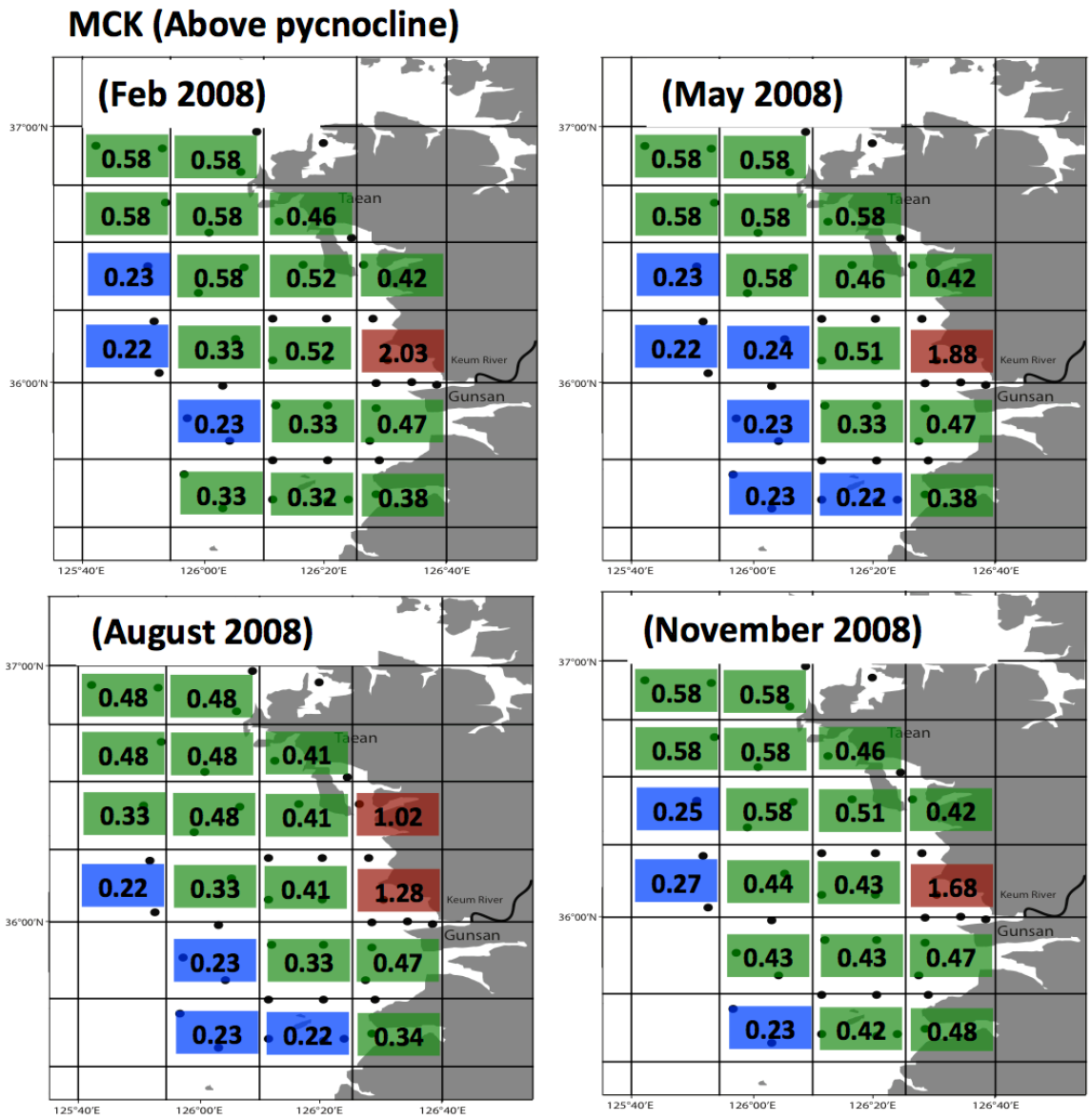

Figure 41. The distribution of the three zones off Mid-western Korea (MCK) based on the RC02 hypothesis applied to the N-mass balance model. Colors represent boxes found in each of the three zones above the pycnocline layer. (Unit: gC m^{-2} day^{-1})

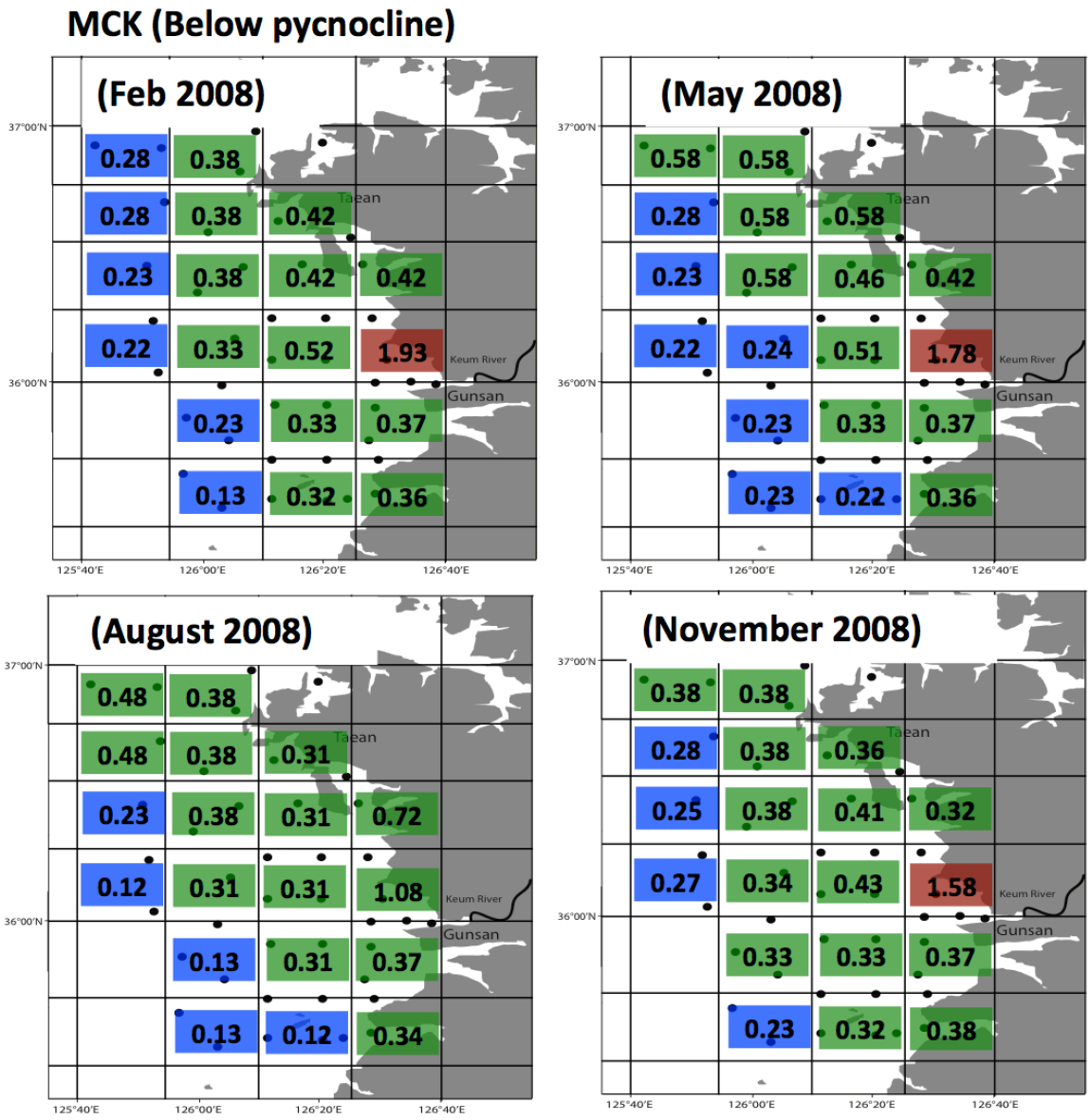

Figure 42. The distribution of the three zones off Mid-western Korea (MCK) based on the RC02 hypothesis applied to the N-mass balance model. Colors represent boxes found in each of the three zones below the pycnocline layer. (Unit: gC m^{-2} day^{-1})

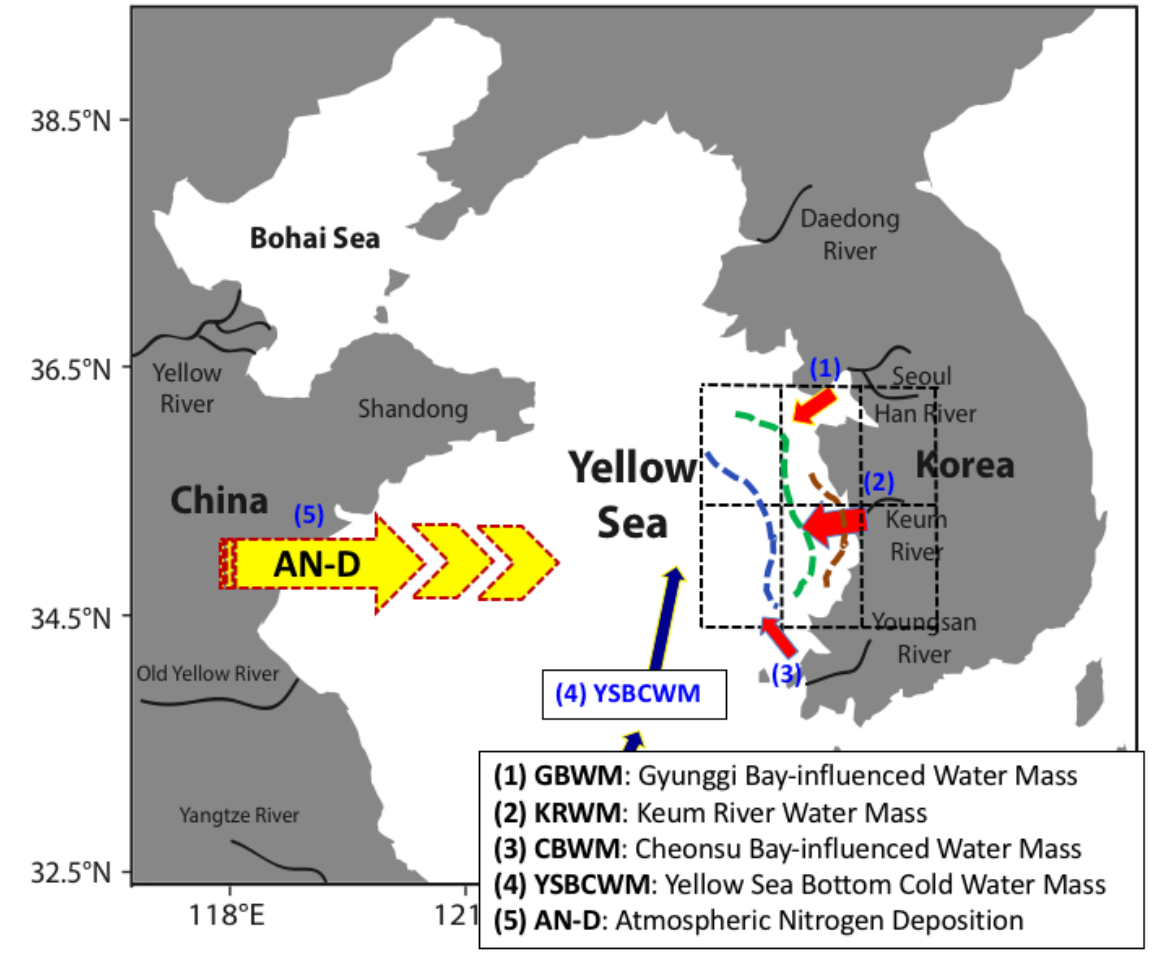

Figure 43. Representative Model scenario results based on MCK cruises data.

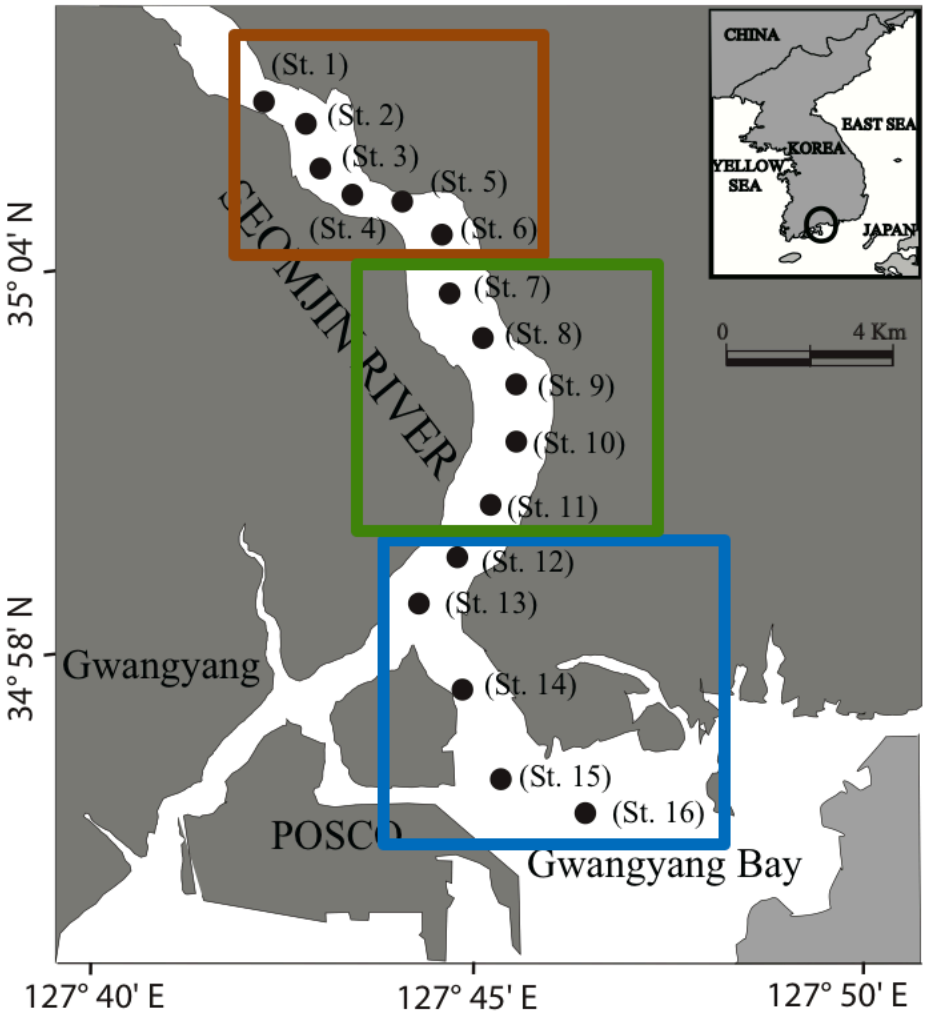

Figure 44. The boundaries of the three zones in the Seomjin River Estuary (SRE) based on our N-mass balance model. The range of PPP was 0.1 to 8 gC m^{-2} day^{-1}, which is similar to a previous study from Yang et al. (2005).

4.3.6 Model scenarios in Mid-western Coastal Sea off Korea (MCK)

Because of the lack of research on hypoxia scenario studies in Korea, we modified the various scenarios from the GOM (Table 10) based on our nominal values from our MCK data. We applied three scenarios to the MCK region. Figures 45 ~ 48 illustrate our calculated model scenario results. Each box number indicates the rate of PPP averaged over the area of each zone (gC m^{-2} day^{-1}). Similar to GOM results, riverine N input remains the major controlling factor, however, in this area, the AN-D source is a more critical source than in the GOM region (Table 14). The AN-D input source increased by 27% to 47% of total input under scenario 1. Also, based on our scenario 3 results, increases in the AN-D input source and riverine N input together will affect biological production by increasing carbon fluxes up to 25% and oxygen demand up to 32% if we fail to reduce riverine N input in future (Table 14). This indicates that AN-D input can be an important controlling factor in the MCK. In addition, the results showed that in the near future both AN-D flux and riverine N flux need to be considered as regards nitrogen management in not only the hypoxic zone but also the eutrophic zone. Thus, these model scenarios with consideration of AN-D input will be helpful in determining the direction of future coastal nutrient management or hypoxia management studies in the MCK.

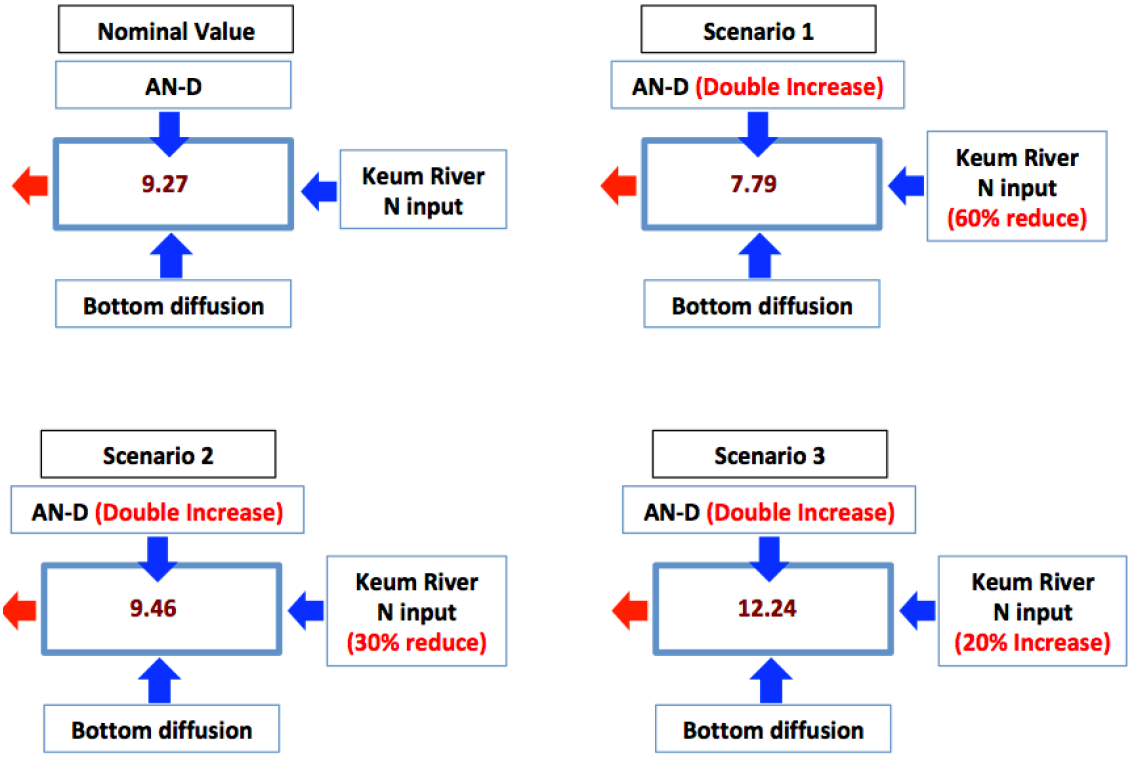

Figure 45. Representative Model scenario results based on the CSK February 2008 cruise. Each box number indicates the rate of potential primary production (gC m^{-2} day^{-1}).

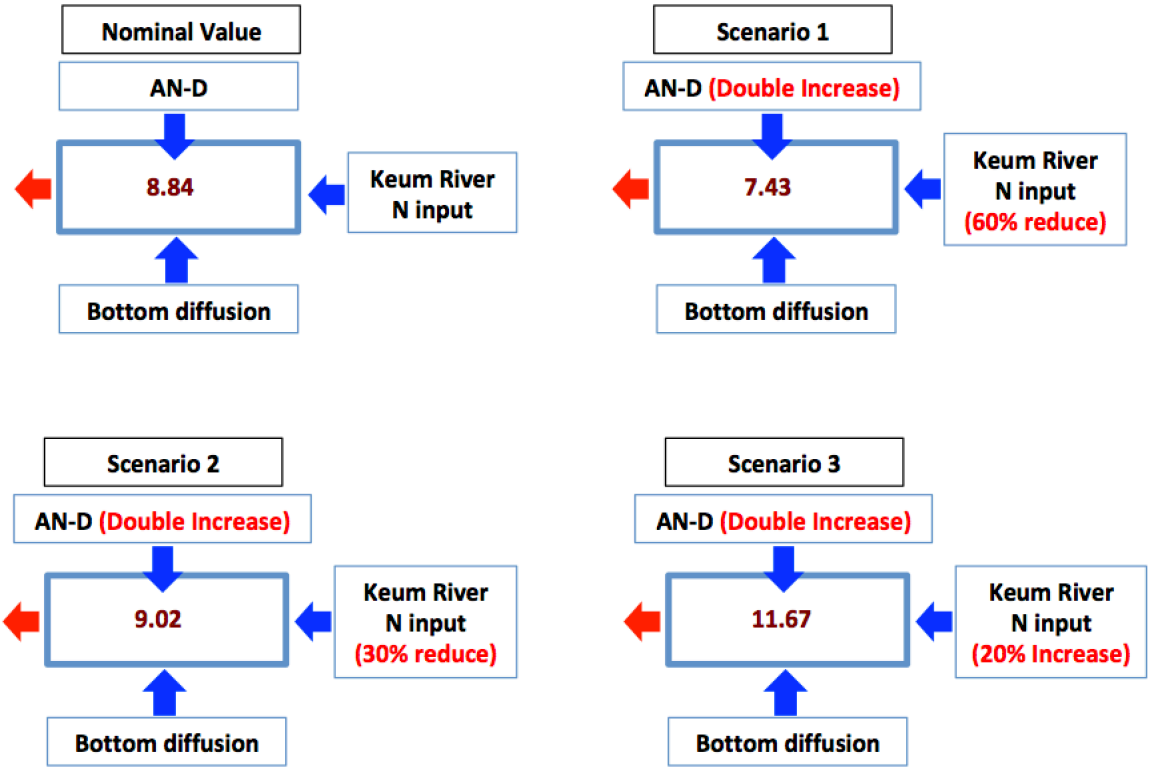

Figure 46. Representative Model scenario results based on the CSK May 2008 cruise. Each box number indicates the rate of potential primary production (gC m^{-2} day^{-1}).

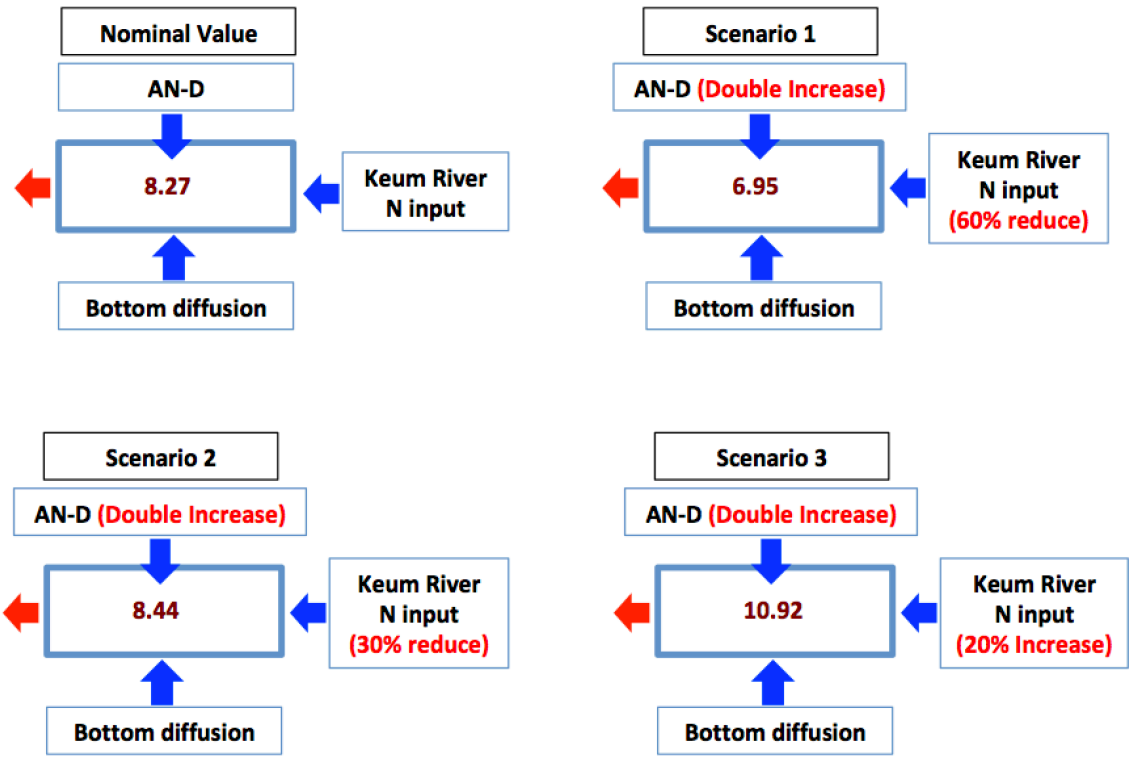

Figure 47. Representative Model scenario results based on the CSK August 2008 cruise. Each box number indicates the rate of potential primary production (gC m^{-2} day^{-1}).

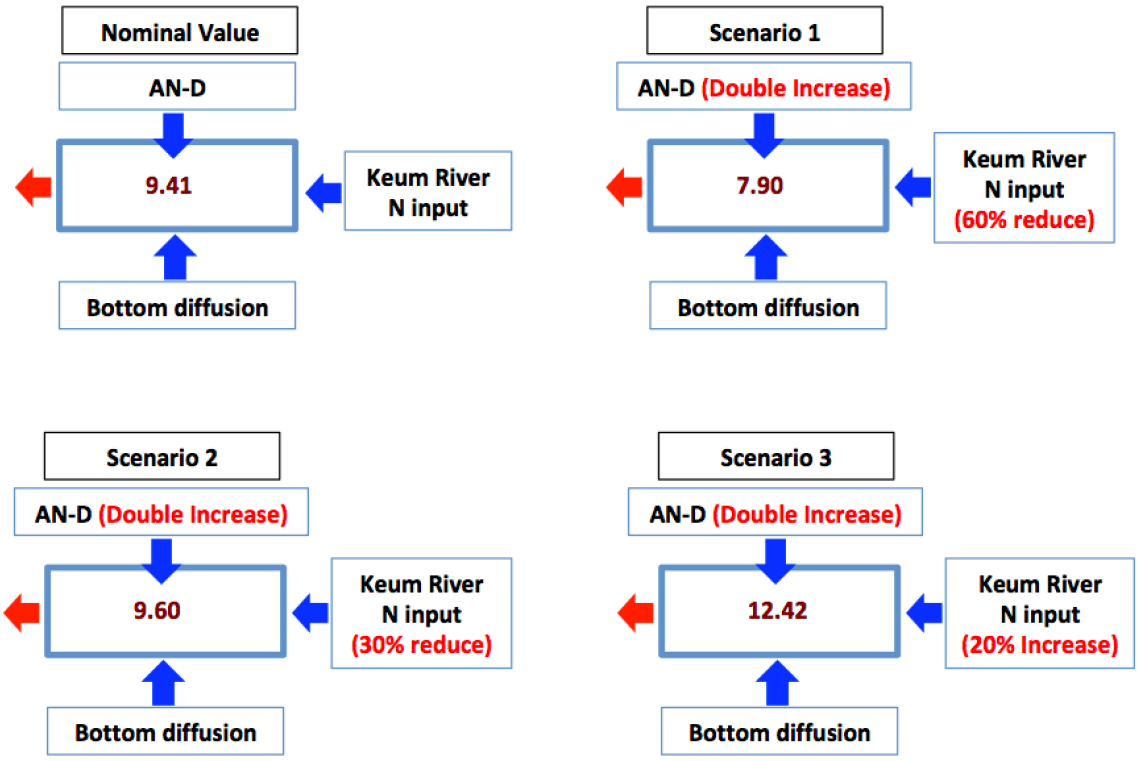

Figure 48. Representative Model scenario results based on the CSK November 2008 cruise. Each box number indicates the rate of potential primary production (gC m^{-2} day^{-1}).

Table 14. Simulation results for selected model scenarios based on CSK (February 2008) data, as explained in Table 10. Biological production is calculated by our N-mass balance model. Oxygen demand is calculated by the Redfield stoichiometry ratio (C: O_2 = 106: 138).

	F_{River}	$F_{AN\text{-}D}$	$F_{Bott/SGD}$	**Biological production**	**Oxygen demand**
Nominal Value	1.9×10^6 (~60%)	6.0×10^5 (~20%)	6.0×10^5 (~20%)	Base line	
Scenario 1	7.2×10^5 (~29%)	1.2×10^6 (~47%)	6.0×10^5 (~24%)	~13% decreased	~16% decreased
Scenario 2	1.3×10^6 (~41%)	1.2×10^6 (~39%)	6.0×10^5 (~20%)	~2% decreased	~2% decreased
Scenario 3	2.2×10^6 (~55%)	1.2×10^6 (~30%)	6.0×10^5 (~15%)	~25% increased	~32% increased

4.4 Discussion

4.4.1. Comparing the edges of the three zones using different methods

Most previous model studies were focused on predicting the hypoxia area in the GOM (Bierman et al., 1994; Justic et al., 1996, 2002, 2003; Scavia et al., 2004; Fennel et al., 2011, 2013). Especially, Justic et al., (1996; 2003) used a two-layer model incorporating vertical oxygen data, from station C6 only, to predict the size of the hypoxia area. However, in this study, our N-mass balance model used historical data from the LATEX shelf to, estimate potential carbon fluxes in the GOM, and calculated the overall oxygen demand from those carbon fluxes, which affects hypoxia condition.

In contrast with our model, traditional predictive models do not account for different nitrogen input sources such as AN-D and SGD. Fennel et al. (2011; 2013) used her simulation model to predict the size of the hypoxia region in the GOM. Her model was expanded to include oxygen concentration as well as a plankton model from Fasham et al. (1990). Her simulation model ignored AN-D input and did not estimate potential carbon fluxes or overall oxygen demand. Also, most of the model studies concluded that reducing riverine N input is the only solution to decrease the size of the hypoxia area in the GOM (Gulf of Hypoxia Task Force; Scavia et al., 2013; Hypoxia Action Goal Plan Report, 2005, 2008; Rabalais et al. 2009). According to our model results, AN-D is still a minor controlling factor in the GOM, however, in the CSK, the AN-D contributed more in the TN budget and may be a major controlling factor in the future. This indicates that AN-D should be considered as another input term for nutrient managements in Asia.

Based on the model calculation, we identified the boundaries of the RC02 three zones and compared them with the results of Lahiry (2007) (Figure 49). She used a DO/salinity relationship to define the edges of each zone for MCH M1, M2, and M3. Both sets of results showed a good

agreement near the Mississippi River for the boundaries of the brown and green zones. Typically, near the Atchafalaya River region, our sub-region C, our model produces both green and blue zones. However, in her MCH M1 results, brown and green zones exist (Figure 49). Thus, it seems that using the DO/salinity relationship to identify the three zones cannot cover the complex biological processes that occur in the region, although our method can cover this. Therefore, we believe that using our N-mass balance model results and nutrient/salinity relationships to differentiate the different zones is a more sensible way to look at biological processes in the GOM than the previous study from Lahiry (2007).

Again, our model considers different nitrogen input sources, which can estimate potential carbon fluxes. Through the potential carbon fluxes, we can estimate overall oxygen demand. Still our model cannot predict the size of the hypoxia area but can estimate the overall oxygen demand.

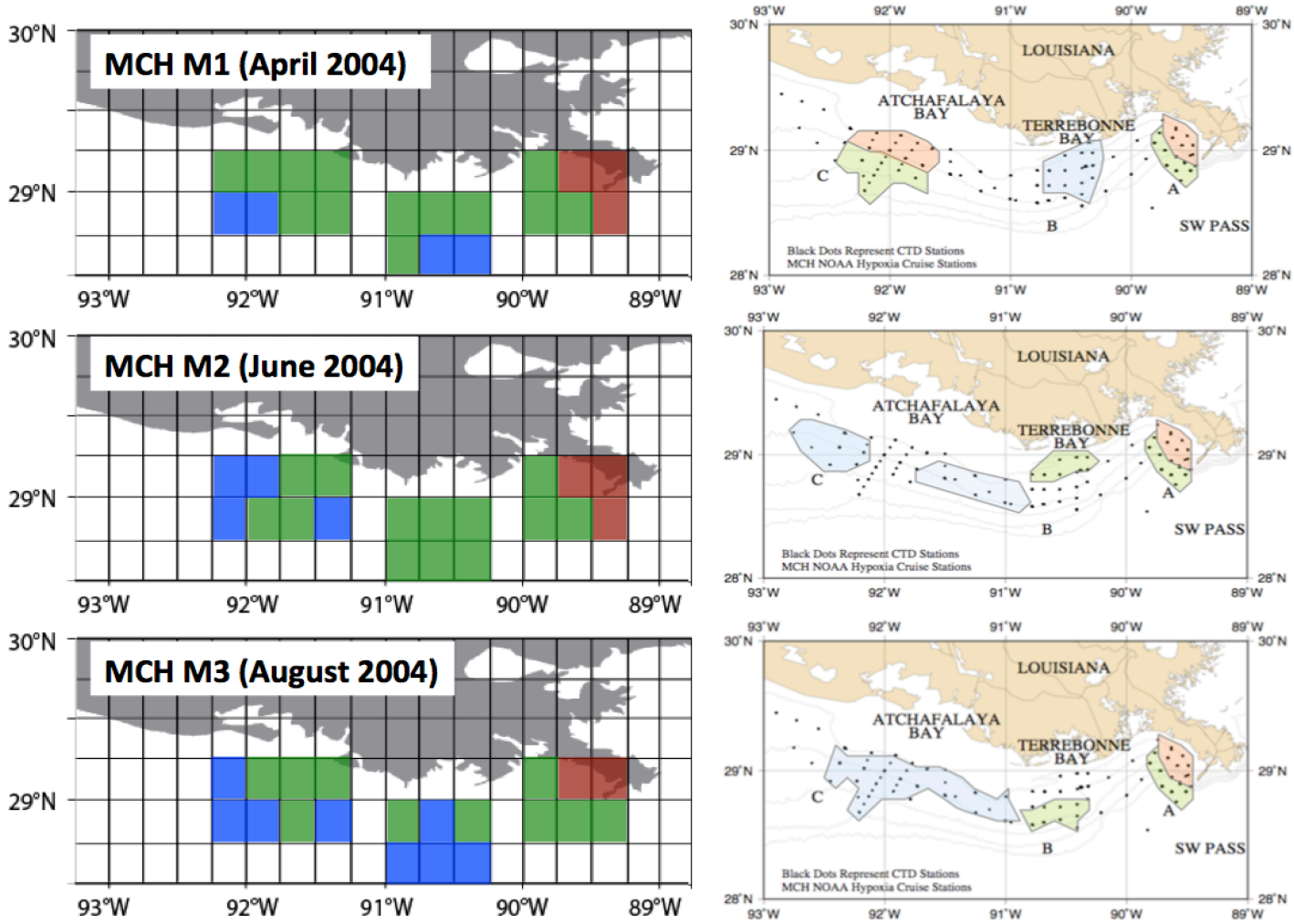

Figure 49. Comparison of the results of the three zone analysis from Lahiry (2007) and this study using the N-mass balance model. Areas shaded in three colors represent the Brown, Green and Blue zones respectively.

4.4.2. Comparing the Gulf of Mexico (GOM) and the Coastal Sea off Korea (CSK)

Both the GOM and CSK regions have different nitrogen inputs from AN-D, river input, and benthic fluxes. These different nitrogen input sources not only control coastal productivity but also reflect the different seasonal cycling in the two regions. In the GOM, the riverine N input source is consistently the dominant source that controls coastal productivity and eutrophication, while, in the MCK, AN-D is also becoming a critical controlling factor. The strong tidal mixing near the MCK, which results in a tidal front along the offshore region, may have an important role in the distribution of nutrients (Lim et al., 2008).

We evaluated our model and tested its sensitivity based on three different scenarios. As a result, we believe that using our N-mass balance model to separate different zones based on RC02 is appropriate not only for large-scale regions like the GOM and MCK but also at small scales such as river or estuary systems. The model also estimates primary production and carbon flux based on inclusion of AN-D data that has not been considered previously (e.g. Bierman et al., 1994; Kim et al., 2011). Our results agree well with previous ^{14}C measurements in the GOM (Quigg et al., 2011) and the MCK (Yang et al., 2005).

The results of these scenarios represent how the biological processes in these coastal regions are controlled by changes in individual sources of nutrients. Thus, we can initially predict with our model how reducing nitrogen input sources can help reduce coastal organic carbon fluxes and overall oxygen demand. We have only considered different input terms of our N-mass balance model, the other output terms such as water mixing rates and the residence time for each box need more detailed study in future work to calculate more realistic production changes in each box. This will require cooperative studies among different research fields, including the fields of atmospheric chemistry (AN-D), coastal ecology, marine biogeochemistry, and benthic biology. Also, our N-

mass balance model is necessary in order to find direct links between the atmosphere, ocean, and benthic sediment and biological production and global carbon fluxes in the future.

CHAPTER V

SUMMARY, CONCLUSIONS AND FUTURE RESEARCH

5.1 Research summary and conclusions

This study demonstrated that different nitrogen input sources can control carbon fluxes in two different regions, the coastal Gulf of Mexico (GOM) and the Coastal Sea off Korea (CSK). We estimated carbon fluxes using our N-mass balance model and determined where the edges of the three different zones described in RC02 are, both above and below the pycnocline layer.

We tested our three hypotheses as discussed in chapters III and IV using different methods. The first hypothesis was that the RC02 hypothesis is a good description of nutrient supply to coastal waters. As RC02 had not been tested previously with real data, we used data from a number of cruises in the GOM and around Korea. A linear relationship at low (< 25) salinities between salinity and nitrogen or silicate concentration defined the salinity range of the brown zone. The blue zone was defined as being the region where nutrient concentrations fell below 1 μM, while the green zone covered the salinity range between them. We found that it was possible to determine the boundaries of the zones using nutrient/salinity ratios in the Gulf of Mexico (Hypothesis 1-1) only with winter data west of the Mississippi delta. We believe this is due to low biological uptake and more stable nutrient concentrations in the coastal region in winter than in summer.

It was anticipated that different cruises would give different results for the positions of the boundaries of the brown, green and blue zones; this was confirmed for stations west of the Mississippi delta (Hypotheses 1-2, 1-3). In the NEGOM area, however, nutrient/salinity relationships did not work in either summer or winter owing to the lack of major nutrient inputs

from the Mississippi to the shelf east of the delta. This means that RC02 does not hold generally, or at least does not hold during the summer in the northern GOM, based on our data sets. We believe this is because the high productivity in the northern GOM during summer means that nutrient concentrations over the shelf are low, and that to sample the brown zone one needs to sample much closer to the river mouths; in other words, scales matter.

In addition, we applied this method to a region along the west coast of Korea and to a small-scale estuary on the Korean south coast, using the data given in Tables 2 and 3. From our results, we quantified each zones' salinity and nutrient concentrations based on observations (Tables 6 and 7). The results show that RC02 does hold in the coastal waters of Korea but confirms the need to think carefully about sampling scales. As the discharges of water and nutrients along the west coast and in the Seomjin River Estuary (SRE) are much smaller than those of the MARS, stations need to be closer together.

RC02 strictly applies only to the surface layer. Hypothesis 1-4 was tested to see whether we could find similar relationships below the pycnocline. Our results suggest that RC02 is applicable below the pycnocline, but not from nutrient/salinity relationships; it was necessary to use the box model for this.

The second hypothesis was that the Mississippi and Atchafalaya rivers have different nutrient concentrations that can be used to show which river supports production in different areas of the Texas-Louisiana shelf. We found that we can use a N-mass balance model to estimate potential production in each region and which river supports this production (Hypothesis 2-1). We determined the edges of each zone based on real nutrient data and that the boundaries of each zone vary from cruise to cruise. Also, we compared the edges of the three zones from the results of Chapter III, where we used nutrient/salinity relationships, and Chapter IV, based on the box model.

The comparison showed that our methodology is reasonable for determining the boundaries of the three zones both above and below the pycnocline, and this study is also the first time that changes in the three zones below the pycnocline layer have been identified. Using our N-mass balance model, we estimated potential coastal production, carbon fluxes, and oxygen demands across the northern Gulf of Mexico and off Korea (Hypothesis 2-2). The two regions had different productivity values; in the brown zone potential production in the GOM was >2 g C m^{-2} d^{-1}, but only 1.5 g C m^{-2} d^{-1} off the coast of Korea. The blue zone had < 0.1 g C m^{-2} d^{-1} in the GOM and < 0.3 g C m^{-2} d^{-1} in the Korean coastal region, while the green zone was between the two.

We also considered additional nitrogen sources such as AN-D, SGD, and benthic nutrient regeneration to estimate more accurate coastal carbon fluxes. The model results showed that in the northern GOM AN-D and SGD were only minimal sources of nitrogen, and that by far the largest source (97%) was the MARS. This was not the case in Korea, where deposition and groundwater discharge along the western coastline accounted for up to 20% each of the nitrogen inputs. Note that these estimates do not consider denitrification, which has not been measured directly in either region, and so our results are likely high. In addition, we compared productivity along the coastal GOM and CSK from our N-mass balance model result with previous results from ^{14}C measurements and also with a dawn-to-dusk oxygen balance model (Hypothesis 2-2). These three different methods of estimating coastal productivity showed very similar results, and our model may therefore be used for sensitivity studies.

This calibration result led us to test our third hypothesis that changes in the ratios of the AN-D and riverine N fluxes will affect carbon cycling in coastal waters in these regions (Hypothesis 3-1). We produced three different scenarios, two with reduced riverine nitrogen input, one with increased riverine input, and the results in the GOM indicate that riverine N input is still

the most important factor regardless of the ratios used. However, in the CSK, we need to consider not only riverine N input as a source but also AN-D and benthic diffusion. Thus, the AN-D is not important in GOM, but could be important in the CSK, where the model showed that doubling the AN-D input is equivalent to cutting the riverine N input by 30%. We believe that this consideration should help us for our future nutrient management.

In addition, we concluded from our results that RC02 may hold where we have a major nutrient source and that sampling scales are important. For instance, the CSK as sampled is probably too large a region because of the low river flow rates, while summer data within the GOM need to be taken closer to the river mouths.

5.2 Future research

In the future, we will also investigate the effects of light on APP and PPP in the brown and green zone using turbidity or PAR data. Therefore, we can compare the effects of changing light levels with both phytoplankton biomass and nutrient inputs. Also, SeaWiFs data can be compared with our N-mass balance model results to identify the edges of the three zone and estimate coastal productivity.

We also need to collect more AN-D and SGD data to estimate more accurate carbon fluxes and the interactions between each box, such as from the atmosphere to the surface box (AN-D factors) or benthic inputs to the bottom box (SGD factors), including any regenerated nitrogen. From this, we can develop a three-layer box model, which includes fluxes from the air to the sea surface, from the sea surface to subsurface, and from the subsurface to benthic region, to calculate a clearer estimate of coastal carbon fluxes. Although in our scenario results riverine N input was

still a significant factor in total N loads to the GOM, we should be aware that there might be some combined effects of minor different input sources such as SGD, AN-D, etc.

The CSK has different nitrogen input sources, but also different environmental conditions such as strong tidal mixing and fall blooms of phytoplankton in the coastal ocean. Due to these characteristics in the CSK, the monthly chlorophyll-a concentration in both regions (GOM and CSK) had a different seasonal pattern. Especially, in the CSK, the coastal chlorophyll-a concentration did not vary very much during the year and this indicates that the coastal carbon flux in the CSK can be supported throughout the year by AN-D input sources, unlike in the GOM where the river input controls productivity (Figures 50 and 51). Thus, it seems that we can initially identify three zones using satellite SeaWiFs data to estimate APP rate in the future. Further long-term experimental and modeling studies are recommended to confirm the quantitative impact of different nitrogen input sources to estimate not only coastal carbon fluxes but also primary production for nutrient management in the future work.

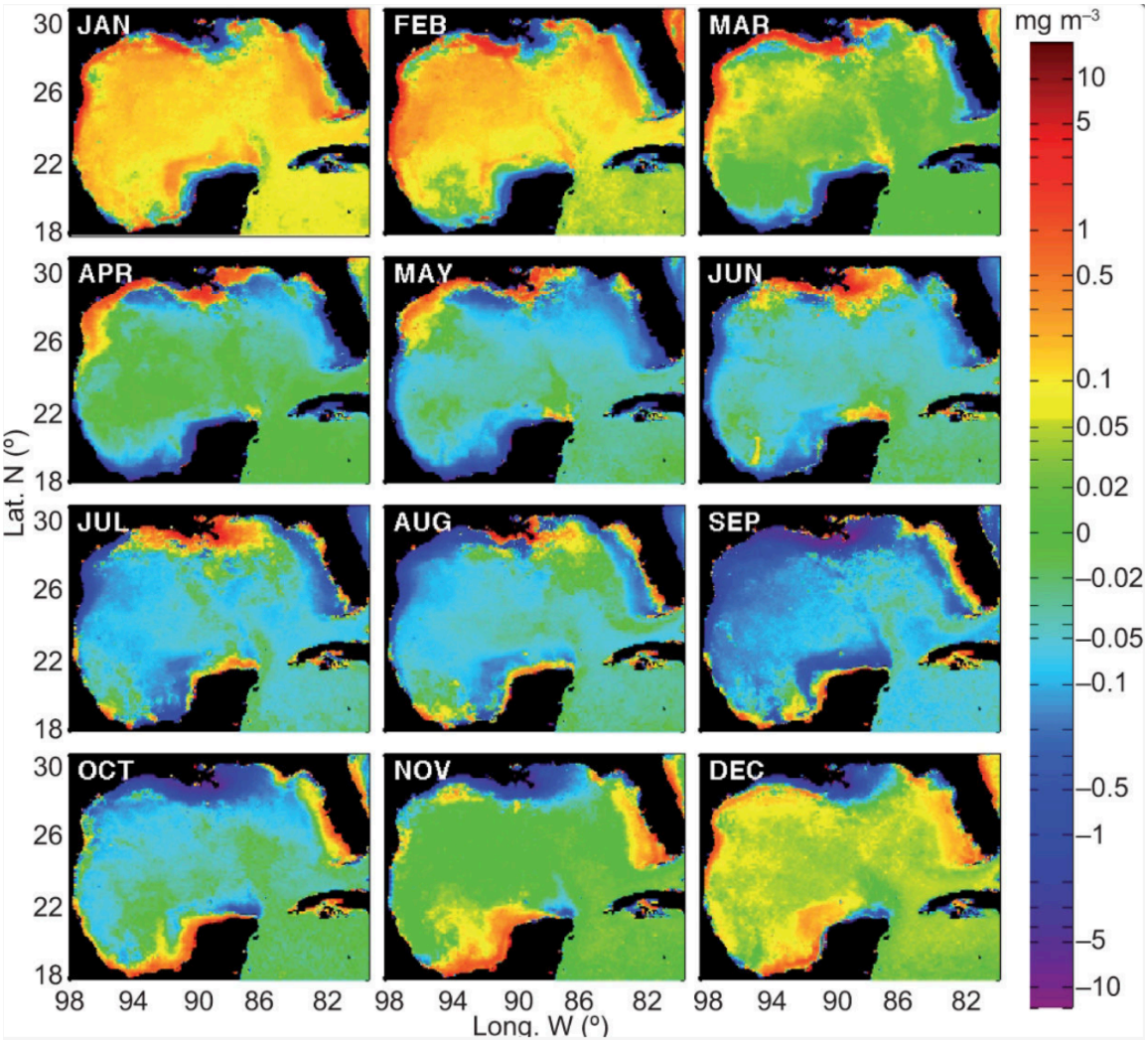

Figure 50. Long-term monthly means (1997 ~ 2012) of chlorophyll-a concentration in the Gulf of Mexico, [Jorge et al., 2014]. *Reprinted with permission of Atmósfera.*

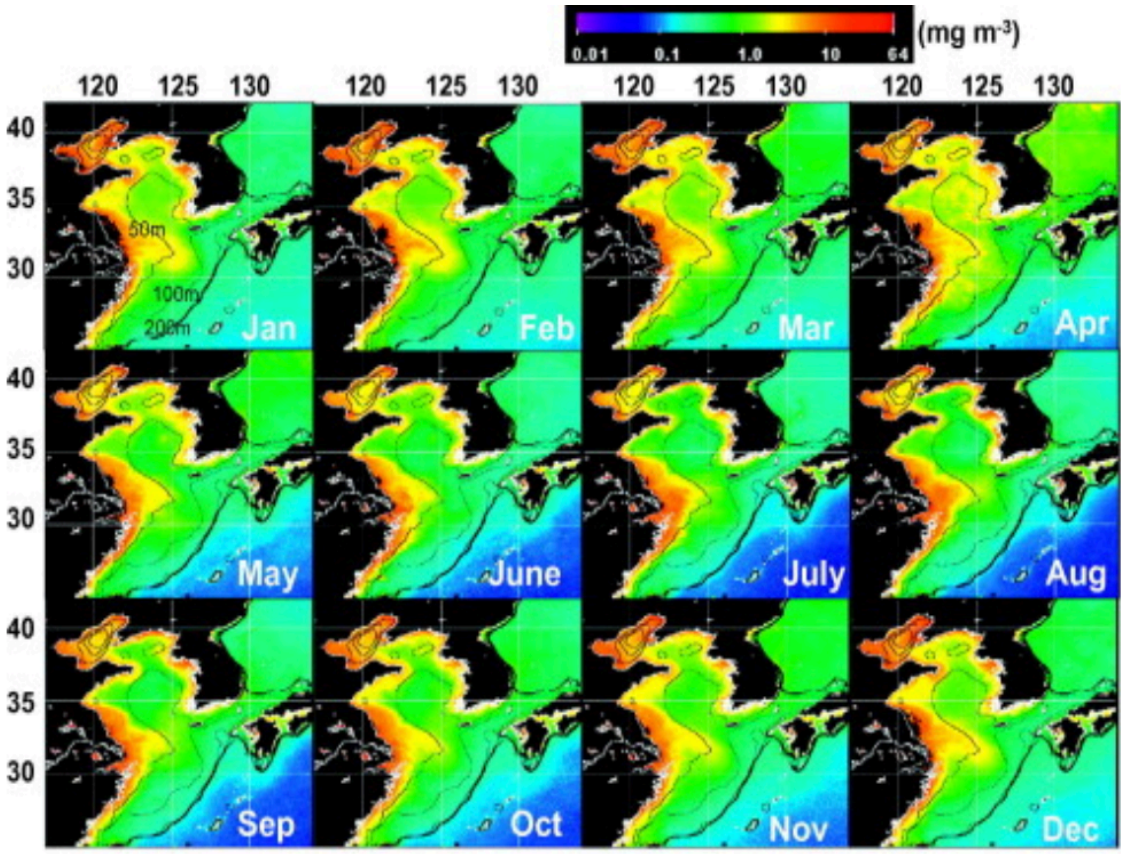

Figure 51. Monthly SeaWiFs chlorophyll-a concentration in East China sea and Yellow Sea during 10 years, [Yamaguchi et al., 2012]. *Reprinted with permission of Progress in Oceanography.*

REFERENCES

Anderson GC. 1969. Subsurface chlorophyll maximum in the northeast Pacific Ocean. Limnology and Oceanography. Vol.14(3). pp.386-391.

Anderson LA and Sarmiento JL. 1994. Redfield ratios of remineratlization determined by nutrient data analysis. Global Biogeochemical Cycles. Vol.8(1). pp.65-80.

Akimoto H. 2003. Global Air Quality and Pollution. Science. Vol.302(5651). pp. 1716-1719.

Alexander RB, Smith RA, Schwarz GE, Preston SD, Brakebill JW, Srinivasan R, Pacheco PA. 2000. In an assessment of nitrogen loads to US estuaries with an atmospheric perspective; Valigura, R., Alexander, R., Castro, M. S., Greening, H., Meyers, T., Paerl, H., Turner, R. E. Eds.; Coastal and Estuarine Studies; American Geophysical Union: Washington, DC, 2000.

Alexander RB, Smith RA, Schwarz GE, Boyer EW, Nolan JV, and Brakebill JW. 2008. Differences in phosphorus and nitrogen delivery to the Gulf of Mexico from the Mississippi river basin. Environmental Science and Technology. Vol.42. pp.822-830.

Baron JS, Rueth HM, Alexander MW, Nydick KR, Allstott EJ, Minear JT, and Moraska B. 2000. Ecosystem responses to nitrogen deposition in the Colorado front range. Ecosystems. Vol. 3. pp. 352-368.

Bashkin VN, Park SU, Choi MS, and Lee CB. 2002. Nitrogen budgets for the Republic of Korea and the Yellow Sea region. Biogeochemistry. Vol.57/58. pp. 387-403.

Bauer JE, Cai WJ, Raymond PA, Bianchi TS, Hopkinson CS, and Regnier PAG. 2013. The changing carbon cycle of the coastal ocean. Nature. Vol.504. pp. 61-70.

Belabbassi L, Chapman P, Nowlin WD, Jochens AE, and Biggs DC. 2005. Summertime nutrient supply to near-surface waters of the northeastern Gulf of Mexico: 1998, 1999, and 2000. Gulf of Mexico Science. Vol. 2. pp. 137-160.

Belabbassi L. 2006. Examination of the relationship of river water to occurrences of bottom water with reduced oxygen concentrations in the northern Gulf of Mexico. Texas A & M University. Ph.D. Dissertation.

Behera SN, Sharma M, Aneja VP, and Balasubramanian R. 2013. Ammonia in the atmosphere: a review on emission sources, atmospheric chemistry and deposition on terrestrial bodies. Environmental Science Pollution Research. Vol.20(11). pp. 8092-8131.

Bianchi TS, DiMarco SF, Cowan Jr JH, Hetland RD, Chapman P, Day JW, and Allison MA. 2010. The Science of hypoxia in the Northern Gulf of Mexico: A review. Science of the total Environment. Vol.408(7). pp.1471-1484.

Bierman VJ, Hinz SC, Wiseman JR. WJ, Rabalais NN, and Turner RE. 1994. A Preliminary Mass Balance Model of Primary Productivity and Dissolved Oxygen in the Mississippi River Plume/Inner Gulf Shelf Region. Estuaries. Vol.17(4). pp.886-899.

Boyle E, Collier R, Dengler AT, Edmond JM, NG AC, and Stallard RF. 1974. On the chemical mass-balance in estuaries. Geochimica et Cosmochimica Acta. Vol.38. pp.1719-1728.

Boynton WR, Garber JH, Summers R, and Kemp WM. 1995. Inputs, transformations, and transport of nitrogen and phosphorus in Chesapeake Bay and selected tributaries. Estuaries. Vol.18. pp. 285-314.

Bode A, and Dortch Q. 1996. Uptake and regeneration of inorganic nitrogen in coastal waters influenced by the Mississippi River: spatial and seasonal variations. Journal of Plankton Resources. Vol.18. pp.2251-2268.

Castro MS, and Driscoll C. 2002. Atmospheric Nitrogen Deposition to Estuaries in the Mid-Atlantic and Northeastern United states. Environmental Science and Technology. Vol. 36. pp.3242-3249.

Castro MS, Driscoll CT, Jordan TE, Reay WG, Boynton WR, Seitzinger SP, Styles RV, Cable JE. 2002. In An assessment of nitrogen loads to United States estuaries with an atmospheric perspective; Valigura, R., Alexander, R., Castro, M. S., Greening, H., Meyers, T., Paerl, H., Turner, R. E. Eds.; Coastal and Estuarine Studies; American Geophysical Union.

Cattaldo T, Jeandel C, Dehairs F, Candaudap F, and Metzl N. 2006. Dissolved barium in the Southern Ocean: conservative vs. non-conservative behavior as constrained by a multiple end-member mixing model. Journal of Food and Agriculture Organization of the United Nations.

Chen N, Hong H, Huang Q, and Wu J. 2011. Atmospheric nitrogen deposition and its long-term dynamics in a southeast China coastal area. Journal of Environmental Management. Vol.92 (6). pp.1663-1667.

Cho KR, Reid O, and Nowlin Jr WD. 1998. Objectively mapped stream function fields on the Texas-Louisana shelf based on 32 months of moored current meter data. Journal of Geophysics Research. Vol.103(C5). pp. 10377-10390.

Choi HY, Lee SH, and Oh IS. 1998. Quantitative Analysis of the Thermal Front in the Mid-Eastern Coastal Area of the Yellow Sea. Journal of the Korean Society of Oceanography [The Sea]. Vol.3. pp.1-8.

Choi HY, Lee SH, and Yoo KY. 1999. Salinity Distribution in the Mid-eastern Yellow Sea during the High Discharge from the Keum River Weir. Journal of the Korean Society of Oceanography [The Sea]. Vol.4, pp.1-9.

Cornell S, Rendell A, and Jickells T. 1995. Atmospheric inputs of dissolved organic nitrogen to the oceans. Nature. Vol.376. pp.243-246.

Dagg MJ, Ammerman JW, AMON RMW, Gardner WS, Green RE, Lohrenz SE. 2007. A review of water column processes influencing hypoxia in the northern Gulf of Mexico. Estuaries Coasts. Vol.30. pp.735-752.

De Boer AM, Watson AJ, Edwards NR, and Oliver KIC. 2010. A multi-variable box model approach to the soft tissue carbon pump. Climate of the past. Vol.6. pp.827-841.

Desmit X, Ruddick K, and Lacroix G. 2015. Salinity predicts the distribution of chlorophyll a spring peak in the southern North Sea continental waters. Journal of Sea Research. Vol.103. pp.59-74.

Diaz RJ, and Rosenberg R. 1995. Marine benthic hypoxia: A review of its ecological effects and the behavioural responses of benthic macrofauna. Oceanography Marine Biology. Ann. Rev. Vol.33. pp.245-303.

Diaz RJ, and Rosenberg R, 2008. Spreading dead zones and consequences for marine ecosystems. Science, Vol.321(5891). pp.926-9.

DiMarco SF, Chapman P, Walker N, and Hetland RD. 2010. Does local topography control hypoxia on the eastern Texas-Louisiana shelf? Journal of Marine Systems. Vol.80(1). pp.25-35.

Doney SC, Mahowald N, Lima L, Feely RA, Mackenzie FT, Lamarque JF, and Rasch PJ. 2007. Impact of anthropogenic atmospheric nitrogen and sulfur deposition on ocean acidification and the inorganic carbon system. Proceedings of the National Academy of Science. Vol.104. pp.14580-14585.

Dortch Q, and Whitledge TE. 1992. Does nitrogen or silicon limit phytoplankton in the Mississippi River plume and nearby regions? Continental Shelf Research. Vol.12. pp.1293-1309.

Duce RA, LaRoche J, Altierl K, Arrigo KR, Baker AR, Capone DG, Cornell S, Dentener F, Galloway J, Ganeshram RS, Geider RJ, Jickells T, Kuypers MM, Langlois R, Liss PS, Liu SM, Middelburg JJ, Moore CM, Nickovic S, Oschlies A, Pedersen T, Prospero J, Schlitzer R, Seitzinger S, Sorensen LL, Uematsu M, Ulloa O, Voss M, Ward B, and Zamora L. 2008. Impacts of Atmospheric Anthropogenic Nitrogen on the Open Ocean. Science. Vol.320. pp. 893-897.

Duxbury AC. and McGary NB. 1965. Local changes of salinity and nutrients off the mouth of the Columbia river. University of Washington.

Emery WJ. and Meincke J. 1986. Global water masses: summary and review. Oceanologica Acta. Vol.9. pp.383-391.

Emery WJ. 2003. Water types and water masses. Ocean Circulation/Water Types and Water Masses. pp. 1556-1567.

Fasham MJR, Ducklow HW, and Mckelvie SM. 1990. A nitrogen-based model of plankton dynamics in the oceanic mixed layer. Journal of Marine research. Vol.48. pp.591-639.

Feng Y. 2012. Statistical and realistic numerical model investigations of anthropogenic and climatic factors that influence hypoxic area variability in the Gulf of Mexico. Texas A & M University. Ph.D. Dissertation.

Fennel K, Hetland R, Feng Y, and DiMarco SF. 2011. A coupled physical-biological model of the Northern Gulf of Mexico shelf: model description, validation and analysis of phytoplankton variability. Biogeosciences. Vol.8. pp.1881-1899.

Fennel K, Hu J, Laurent A, Marta-Almeida M, and Hetland R. 2013. Sensitivity of hypoxia predictions for the northern Gulf of Mexico to sediment oxygen consumption and model nesting. Journal of Geophysical Research: Oceans, Vol.118. pp.990-1002.

Fisher DC, and Oppenheimer M. 1991. Atmospheric nitrogen deposition and the Chesapeake Bay estuary. Ambio. Vol. 20. pp. 102-108

Forrest DR, Hetland RD, and DiMarco SF. 2011. Multivariable statistical regression models of the areal extent of hypoxia over the Texas–Louisiana continental shelf Environmental. Research. Letters. Vol.6(4).

Foster P. 1973. Ultraviolet absorption/salinity correlation as an index of pollution in inshore sea waters. New Zealand Journal of Marine and Freshwater Research. Vol.7(4). pp.369-379.

Green RE, Gould JR. RW, and Ko DS. 2008. Statistical models for sediment/detritus and dissolved absorption coefficients in coastal waters of the northern Gulf of Mexico. Continental Shelf Research. Vol.28(10). pp.1273-1285.

Goolsby DA, Battaglin WA, Lawrence GB, Artz RS, Aulenbach BT, Hooper RP, Keeney DR, and Stensland GJ. 1999. Flux and Sources of Nutrients in the Mississippi-Atchafalaya River Basin. NOAA Coastal Ocean Program Decision Analysis Series. No. 17.

Goolsby DA. 2000. EOS, Trans. Am. Geophysics. Union. Vol.29. pp.321.

Gulf Hypoxia Action Plan 2005 Report. Mississippi River Gulf of Mexico Watershed Nutrient Task Force.

Gulf Hypoxia Action Plan 2008 Report. Mississippi River Gulf of Mexico Watershed Nutrient Task Force.

Hakanson L, and Eklund JM. 2010. Relationships between chlorophyll, salinity, phosphorus, and nitrogen in lakes and marine areas. Journal of Coastal Research. Vol. 26. pp.412-423.

Hameedi J, Paerl H, Kennish M, and Whitall D. 2007. Nitrogen deposition in U.S. coastal bays and estuaries. EM: Air & Waste management Association's Magazine. pp.19-25.

Harrison PJ, Yin KD, Lee JH, W Gan JP, and Liu HB. 2008. Physical–biological coupling in the Pearl River Estuary. Continental Shelf Research. Vol. 28. pp.1405–1415, doi: org/10.1016/j.csr.2007.02.011.

He CH, Wang X, Liu X, Fangmeler A, Christie P, and Zhang F. 2010. Nitrogen deposition and its contribution to nutrient inputs to intensively managed agricultural ecosystems. Ecological Application. Vol.20(1). pp.80-90.

Hetland RD, and DiMarco SF. 2008. How does the character of oxygen demand control the structure of hypoxia on the Texas-Louisiana continental shelf? Journal of Marine Systems. Vol.70. pp.49-62.

IPCC. 2014. Climate Change 2014: Synthesis Report. Contribution of Working Groups I, II and III to the Fifth Assessment Report of the Intergovernmental Panel on Climate Change [Core Writing Team, R.K. Pachauri and L.A. Meyer (eds.)]. IPCC, Geneva, Switzerland, 151 pp.

Iwata T, Shinomura Y, Natori Y, Igarashi Y, Sohrin R, and Suzuki Y. 2005. Relationship between salinity and nutrients in the sub-surface layer in the Suruga Bay. Journal of Oceanography. Vol.61. pp.721-732.

Jaworski NA, Howarth RW, and Hetling LJ. 1997. Atmospheric deposition of nitrogen oxides onto the landscape contributes to coastal eutrophication in the northeast united states. Environmental Science and Technology. Vol.31. pp.1995-2004.

Johnson AG, Glenn CR, Burnett WC, Peterson RN, and Lucey PG. 2008. Aerial infrared imaging reveals large nutrient-rich groundwater inputs to the ocean. Geophysical Research Letters. Vol.35(15). L15606.

Jorge ZH, Rosario RC, and Andriana MJ. 2014. The response of the Gulf of Mexico to wind and heat flux forcing: What has been learned in recent years? Atmósfera. Vol. 27. pp. 317-334.

Justic D, Rabalais NN, and Turner RE. 1996. Effects of climate change on hypoxia in coastal waters; A doubled CO2 scenario for the northern Gulf of Mexico. Limnology and Oceanography. Vol.41(5). pp.992-1003.

Justic D, Rabalais NN, and Turner RE. 2002. Modeling the impacts of decadal changes in riverine nutrient fluxes on coastal eutrophication near the Mississippi River Delta. Ecological Modelling. Vol. 152. pp.33-46.

Justic D, Rabalais NN, and Turner RE. 2003. Simulated responses of the Gulf of Mexico hypoxia to variations in climate and anthropogenic nutrient loading. Journal of Marine Systems. Vol.42. pp. 115-126.

Justic D, Bierman VJ, Scavia D, and Hetland RD. 2007. Forecasting Gulf's Hypoxia: The Next 50 Years? Estuaries and Coasts. Vol.30(5). pp.791-801.

Kanakidou M, Myriokefalitakis S, Daskalakis N, and Fanourgakis G. 2016. Past, Present, and Future Atmospheric Nitrogen Deposition. American Meteorological Society. Vol.73(5). pp.2039-2047.

Knee KL, Street JH, Paytan A, Grossman EE, and Boehm AB. Nutrient inputs to the coastal ocean from submarine groundwater discharge a groundwater-dominated system: Relation to land use (Kona coast, Hawaii, U.S.A.). Limnology and Oceanography. Vol. 53(3). pp.1105-1122.

Kim G, Kim JS, and Hwang DW. 2011. Submarine groundwater discharge from oceanic islands standing in oligotrophic oceans: Implications for global production and organic carbon fluxes. Limnology and Oceanography. Vol.56(2). pp. 673-682.

Kim JS, Lee MJ, Kim J, and Kim G. 2010. Measurement of Temporal and Horizontal Variations in 222Rn Activity in Estuarine Waters for Tracing Groundwater Inputs. Ocean Science Journal. Vol. 45(4). pp.197-202.

Kim TW, Lee K, Najjar RG, Jeong HD, and Jeong HJ. 2011. Increasing N abundance in the northwestern Pacific Ocean due to atmospheric nitrogen deposition. Science. Vol.334. pp.505-509.

Lahiry S. 2007. Relationships between nutrients and dissolved oxygen concentrations on the Texas-Louisiana shelf during spring-summer of 2004. Texas A & M University. MS. Thesis.

Lawrence GB, Goolsby DA, Battaglin WA, and Stensland GJ. 2000. Atmospheric nitrogen in the Mississippi River Basin-emissions, deposition and transport. Science of The Total Environment. Vol.248(2-3). pp.87-100.

Laurent A, Fennel K, Hu J, and Hetland RD. 2012. Simulating the effects of phosphorus limitation in the Mississippi and Atchafalaya River plumes. Biogeosciences, Vol.9. pp.4797-4723.

Lee YH, and Yang JS. 1997. 500-days continuous observation of nutrients, chlorophyll suspended solid and salinity in the Keum Estuary, Korea. The Journal of the Korean Society of Oceanography. Vol.2. pp. 1-7.

Lee J, Park KT, Lim JH, Yoon JE, and Kim IN. 2018. Hypoxia in Korean coastal waters: A case study of the natural Jinhae Bay and artificial shihwa bay. Frontiers in Marine Science. Vol.5. pp.1-19.

Li Y, Nowlin WD, and Reid RO. 1996. Mean hydrographic fields and their inter-annual variability over the Texas-Louisiana continental shelf in spring summer and fall. Journal of Geophysics Research. Vol.102. pp.1027-1049.

Lim D, Um IK, Jeon SK, Yoo JM, and Jung HS. 2003. Physichemical Characteristics of Coastal Pesudo-Estuarine Environment Formed During the Summer Flood season in the South Coast of Korea. Journal of the Korean Society of Oceanography [The Sea]. Vol.8(2). pp.151-163.

Lim D, Lee WJ, Jang MC, Lee J, Lee W, Chang M, Hwang KC, and Shin K. 2005. Spatial and Temporal Distribution of Inorganic Nutrients and Factors Controlling Their Distributions in Gwangyang Bay. Ocean and Polar Research. Vol. 27(4). pp. 359-379.

Lim D, Kim YO, Kang MR, Jang PK, Shin K, and Jang M. 2007. Variability of Water Quality and Limiting Factor for Primary Production in Semi-enclosed Masan Bay, South Sea of Korea. Ocean and Polar Research. Vol. 29(4). pp. 349-366.

Lim D, Kang MR, Jang PG, Kim SY, Jung HS, Kang YS, and Kang US. 2008. Water Quality Characteristics Along Mid-Western Coastal Area of Korea. Ocean and Polar Research. Vol. 30(4). pp. 379-399.

Liss PS. 1976. Conservative and non-conservative behaviour of dissolved constituents during estuarine mixing. In: Burton, J. D.; Liss, P. S. ed., Estuarine chemistry. London, Academic Press. pp.93-130.

Liu SM, Zhang J, Chen SZ, Chen HT, Hong GH, Wei H, and Wu QM. 2003. Inventory of nutrient compounds in the Yellow Sea. Continental Shelf Research. Vol. 23. pp. 1161-1174.

Liu X, Xu W, Du E, Pan Y, and Goulding K. 2016. Reduced nitrogen dominated nitrogen deposition in the United States, but its contribution to nitrogen deposition in China decreased. PNAS Letter. Vol.113.

Loder TC, and Reichard RP. 1981. The Dynamics of Conservative Mixing in Estuaries. Estuaries. Vol. 4(1). pp.64-69.

Lohrenz SE, Wiesenburg DA, Arnone RA, and Chen XG. 1998. What controls primary production in the Gulf of Mexico? In: Sherman K, Kumpf H, Steidinger K (ed) The Gulf of Mexico Large Marine Ecosystem: Assessment, sustainability and management. Blackwell Science, Malden, MA. pp.151-170.

Lohrenz SE, Fahnenstiel GL, Redalje DG, Lang GA, Dagg MJ, Whitledge TE, and Dortch Q. 1999. Nutrients, irradiance, and mixing as factors regulating primary production in coastal waters impacted by the Mississippi River plume. Continental Shelf Research. Vol.19. pp.1113-1141.

Luo XS, Tang AH, Shi K, Wu LH, Li WQ, Shi WQ, Shi XK, Erisman JW, Zhang FS, and Liu XJ. 2014. Chinese coastal seas are facing heavy atmospheric nitrogen deposition. Environmental Research Letters. Vol.9. pp.1-10.

Mamayev OI. 1975. Temperature-Salinity analysis of world ocean waters. Elsevier Oceanography Series. #11. Elsevier Scientific Pub. Co., Amsterdam. pp. 374.

Milliman JD and Meade RH. 1983. World-wide delivery of river sediment to the oceans. The Journal of Geology. Vol.91(1). pp.1-21.

Nixon SW. 1981. Remineralization and nutrient cycling in coastal marine ecosystems. In: Neilson, B, and Cronin, L. (Eds.), Estuaries and Nutrients. Humana Press, Clifton, New Jersey, pp. 111-138.

Nipper M, Sanchez Chavez JA, Tunnell Jr. JW. 2004. "Marsh Island," "Calcasieu Lake," and "General Facts about the Gulf of Mexico." GulfBase: Resource Database for Gulf of Mexico Research.

Nunnally. C, Quigg. A, DiMarco. S, Chapman. P, and Rowe. G. 2014. Benthic-Pelagic Coupling in the Gulf of Mexico Hypoxic Area: Sedimentary enhancement of hypoxic conditions and near bottom primary production. Continental Shelf Research. Vol.85. pp. 143-152.

Parsons TR, Maita Y, and Lalli CM. 1984. A manual of chemical and biological methods for seawater analysis. Pergamon Press 173pp.

Paerl HW, Dennis RL, and Whitall DR. 2002. Atmospheric Deposition of Nitrogen: Implications for Nutrient Over-Enrichment of Coastal Waters. Estuaries. Vol.25(4B). pp.677-693.

Park MO, Kim SS, Kim SG, Kwon J, Lee SM, and Lee YW. 2012. Factors controlling temporal-spatial variations of marine environment in the Seomjin River Estuary through 25-hour continuous monitoring. Journal of the Korean Society for Marine Environment and Energy. Vol.15(4). pp.314-322.

Park MJ, Savenije HHG, Cai H, Jee EK, and Kim NH. 2017. Progressive change of tidal wave characteristics from the eastern Yellow Sea to the Asan Bay, a strongly convergent bay in the west coast of Korea. Ocean Dynamics. Vol. 67. pp. 1137-1150.

Park YH. 2017. Analysis of characteristics of Dynamic Tidal Power on the west coast of Korea. Renewable and Sustainable Energy Reviews. Vol. 68. pp. 461-474.

Pujo-Pay M, Conan P, Joux F, Oriol L, Naudin JJ, and Cauwet G. 2006. Impact of phytoplankton and bacterial production on nutrient and DOM uptake in the Rhone River plume (NW Mediterranean). Marine Ecology Progress Series. Vol.315. pp.43-54.

Qureshi NA. 1995. The role of fecal pellets in the flux of carbon to the sea floor on a river-influenced continental shelf subject to hypoxia. Louisiana State University. Ph.D. Dissertation

Quigg A, Sylvan J, Gustafson A, Fisher T, Oliver R, Tozzi S, and Ammerman J. 2011. Going west: nutrient limitation of primary production in the northern Gulf of Mexico and the importance of the Atchafalaya River. Aquatic Geochemistry. Vol.17. pp.519-544.

Rabalais NN, and Smith LE. 1995. The effects of bottom water hypoxia on benthic communities of the southeastern Louisiana continental shelf. New Orleans, Louisiana, U.S. Minerals Management Service, Gulf of Mexico OCS Region: 105.

Rabalais NN, and Turner RE. 2001. Hypoxia in the Northern Gulf of Mexico: Description, causes and change, pp. 1–36. In N. N. Rabalais and R. E. Turner (eds.), Coastal Hypoxia: Consequences for Living Resources and Ecosystems. Coastal and Estuarine Studies 58.

Rabalais NN, Turner RE, and Scavia D. 2002. Beyond science into policy: gulf of Mexico hypoxia and the Mississippi river. Bioscience. Vol.52(2). pp.129-142.

Rabalais NN, Turner RE, Sen Gupta BK, Boesch DF, Chapman P, and Murrell MC. 2007. Hypoxia in the northern Gulf of Mexico: Does the science support the plan to reduce, mitigate, and control hypoxia? Estuaries Coastal. Vol.30. pp.753-772.

Rabalais NN, Turner RE, Justic D, Diaz RJ. 2009. Global change and eutrophication of coastal waters. ICES. Journal of Marine Science. Vol.66. pp.1528–1537

Redalje DG, Lohrenz SE, and Fahnenstiel GL. 1994. The relationship between primary production and the vertical export of particulate organic matter in a river impacted coastal ecosystem. Estuaries. Vol.17. pp.829-838.

Redfield AC. 1934. On the proportions of organic derivatives in seawater and their relation to the composition of plankton. In: James John-stone Memorial Volume (R.J. Daniel, Ed.). pp.176-192.

Redfield AC, Kethchum BH, and Richards FA. 1963. The influence of organisms on the composition of seawater. In: The Sea Vol.2 (M.N. Jill, Ed.). pp.26-77.

Riemann B, Simonsen P, and Stensgaard L. 1989. The carbon and chlorophyll content of phytoplankton from various nutrient regimes. Journal of Plankton Research. Vol.11(5). pp. 1037-1045.

Robertson DM, and Saad DA. 2014. SPARROW Models Used to Understand Nutrient Sources in the Mississippi/Atchafalaya River Basin. Journal of Environmental Quality. Vol.42. pp. 1422-1440.

Rowe GT. 2001. Seasonal hypoxia in the bottom water off the Mississippi River Delta. Journal of Environmental Quality. Vol.30. pp.281-290.

Rowe GT, and Chapman P. 2002. Hypoxia in the northern Gulf of Mexico: some nagging questions. Gulf Mexico Science. Vol.20. pp.153-160.

Rowe GT, Kaegi MEC, Morse JW, Boland GS, and Briones EGE. 2002. Sediment community metabolism associated with continental shelf hypoxia, northern Gulf of Mexico. Estuaries. Vol. 25(6), pp.1097–1106.

Ruddick K, and Lacroix G. 2006. Hydrodynamics and meteorology of the Belgian coastal zone.

Scavia D, Justic D, and Bierman VJ. 2004. Reducing Hypoxia in the Gulf of Mexico: Advice from Three Models. Estuaries. Vol.27(3). pp.419-425.

Scavia D, Evans MA, and Obenour DR. 2013. A scenario and forecast model for Gulf of Mexico hypoxic area and volume. Environmental Science and Technology Vol.47. pp.10423–10428.

Sigman DM and Hain MP. 2012. The Biological Productivity of the Ocean. Nature Education. Vol.3. pp.1-16.

Steeman-Nielsen. 1952. The use of radioactive carbon (C-14) for measuring organic production in the sea. Journal of marine Science. Vol.18. pp.117-140

Sylvan JB, Dortch Q, Nelson DM, Maier Brown AF, Morrison W, Ammerman JW. 2006. Phosphorus limits phytoplankton growth on the Louisiana shelf during the period of hypoxia formation. Environmental Science and Technology Vol.40(24). pp.7548– 7553.

Tang CH, Wong, CK, Lie AAY, and Yung YK. 2015. Size structure and pigment composition of phytoplankton communities in different hydrographic zones in Hong Kong's coastal seas. Journal of the Marine Biological Association of the United Kingdom. Vol.95. pp.885–896, doi: 10.1017/s0025315415000223

Tan SC, Li J, Che H, Chen B, and Wang H. 2017. Transport of East Asian dust storms to the marginal seas of China and the southern North Pacific in spring 2010. Atmospheric Environment. Vol. 148. pp. 316-328.

Turner RE, and Rabalais NN. 1994. Changes in the Mississippi River nutrient supply and offshore silicate-based phytoplankton community responses. In Dyer, K.R and R. J Orth(eds.). Changes in Fluxes in Estuaries: Implications from Science to management Proceedings of

ECSA22/ERF Symposium. International Symposium Series. Olsen and Olsen. Gredensborg. Denmark:147-150.

Turner RE, Rabalais NN, and Justic D. 2006. Predicting summer hypoxia in the northern Gulf of Mexico: Riverine N, P, and Si loading, Marine. Pollution. Bull., Vol.52. pp.139–148.

Tyrrell T. 1999. The relative influences of nitrogen and phosphorus on oceanic primary production. Nature. Vol.400. pp.525-531.

Wade TL, and Sweet ST. 2008. Final Report Coastal Bend Bays and Estuaries Program (CBBEP): Atmospheric Deposition Study. 48pp.

Wang H, Dai M, Liu J, Kao SJ, Zhang C, Cai WJ, Wang G, Qian W, Zhao M, and Sun Z. 2016. Eutrophication-Driven Hypoxia in the East China Sea off the Changjiang Estuary. Environmental Science & Technology. Vol.50. pp.2255-2263.

Wu ML, Hong YG, Yin JP, Dong JD, and Wang YS. 2016. Evolution of the sink and source of dissolved inorganic nitrogen with salinity as a tracer during summer in the Pearl River Estuary. Scientific Reports. Vol.6. 36638.

Yang SR, Song HS, Kim KC, Park C, and Moon CH. 2005. Changes in environmental factors and primary productivity in the seomjin river estuary. Journal of the Korean Society of Oceanography [The Sea]. Vol.10. pp.164-170.

Yang JS and Ahn TY. 2008. The analysis of the correlation between groundwater level and the moving average of precipitation in Kuem river watershed. The Journal of Engineering Geology. Vol.18. pp.1-6.

Yamaguchi H, Kim HC, Son YB, Kim SW, Okamura K, Kiyomoto Y, and Ishizaka J. 2012. Seasonal and summer interannual variations of SeaWifs chlorophyll a in the Yellow Sea and East China Sea. Progress in Oceanography. Vol.105. pp.22-29.

Yeo HG, and Kim JH. 2002. SPM and fungal spores in the ambient air of west Korea during the Asian dust (Yellow sand) period. Atmospheric Environment. Vol. 36. pp. 5437-5442.

Ye F, Ni Z, Xie L, Wei G, and Jia G. 2015. Isotopic evidence for the turnover of biological reactive nitrogen in the Pearl River Estuary, south China. Journal of Geophysical Research: Biogeosciences. Vol.120. pp.661–672.

Zhang L, Jacob DJ, Knipping EM, Kumar N, Munger JW, Carouge CC, Donkelaar Av, Wang YX, and Chen D. 2013. Nitrogen deposition to the United States: distribution, sources, and processes. Atmos. Chem. Phys. Vol.12. pp. 4539-4554.

Zhao Y, Zhang L, Pan Y, Wang Y, Paulot F, and Henze DK. 2015. Atmospheric nitrogen deposition to the northwestern Pacific: seasonal variation and source attribution. Atmos. Chem. Phys. Vol.15. pp.10905-10924.